

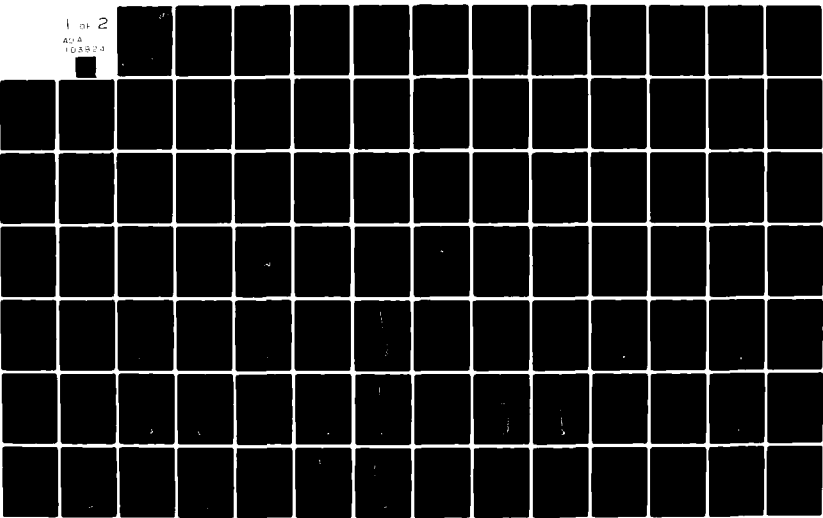
AD-A103 824

NAVAL UNDERWATER SYSTEMS CENTER NEWPORT RI  
SHIPBOARD POWERLINE TRANSFORMERS: H EMISSION CHARACTERISTICS, E-ETC(U)  
JAN 81 L J DALSASS  
UNCLASSIFIED NUSC-TM-801173

F/G 20/14

NL

1 of 2  
424  
108924



ADA103824



LEVEL  
14

DTIC

NUSC - TM-801173



## Shipboard Powerline Transformers: H Emission Characteristics, EMI Models, and a Test Procedure That Utilizes Simulated Input Signals.

(12) 102

(11) Louis J. Dalsass  
Submarine Electromagnetic  
Systems Department

(1) This is memo

(11) 1 January 1981

DMG FILE COPY

406068

NUSC  
Naval Underwater Systems Center  
Newport, Rhode Island • New London, Connecticut

DISTRIBUTION STATEMENT A  
Approved for public release  
Distribution Unlimited

81 7 10 113

Enclosure (1) to  
NUSC Ltr. Ser.  
1343-197

ATTC



## NAVAL UNDERWATER SYSTEMS CENTER

HEADQUARTERS  
NEWPORT, RHODE ISLAND 02840

NEWPORT, R. I. 02840  
AREA CODE 401  
841 - EXT.  
AUTOVON 948 + EXT.

NEW LONDON, CONN. 06320  
AREA CODE 203  
442 - 0771 - EXT.  
AUTOVON 636 + EXT.

IN REPLY REFER TO:  
343:DSD:lrk  
3912  
Ser. 1343-197

From: Commanding Officer  
To: Commander, Naval Sea Systems Command, Naval Sea Systems Command Headquarters, (H. DeMatta, Code 61R4); Washington, DC 20362  
Commander, Naval Electronics Systems Command (J. Cauffman, Code 614), Washington, DC 20360  
Subj: Electromagnetic Compatibility (EMC) R&D Program Output; forwarding of NUSC Technical Memorandum 801173

Ref: (a) Submarine "Below-Decks" EMC R&D Program (P.E. 62543N)

Encl: (1) NUSC TM 801173 entitled "Shipboard Powerline Transformers: H Emission Characteristics, EMI Models, and a Test Procedure that Utilizes Simulated Input Signals"  
(2) Transformer EMI Model Task: Remaining work  
(3) Leakage Reactance Transformer Tests

1. The reference (a) program has as one of its objectives to validate electro-magnetic interference (EMI) models that can be utilized both manually as well as in the computer controlled EMC prediction program that is presently being developed at NUSC.

2. The enclosed Technical Memorandum documents the effort required to develop a new test procedure and to validate a shipboard powerline transformer radiated EMI model useful in the 5 kHz to 50 kHz frequency band. This range of frequencies is particularly important because it includes the VLF communications frequency band. Since typical VLF receivers and couplers have nanovolt sensitivities, they can be extremely susceptible to radiated electromagnetic interference (EMI). This model will improve the accuracy of EMC predictions required to ensure the compatibility of "below-decks" electrical/electronic equipment. The transformer leakage magnetic field model considers the following factors:

- a. The distance from the center of the transformer to a field location ( $R$ )
- b. The shielding effectiveness (S.E.) of the transformer case
- c. The current spectrum of the input (powerline) harmonics
- d. Model limitations (such as endcaps, seams, and gratings)
- e. The transformer vertical half distance ( $R_o$ )

In summary, the model behaves as follows:

- a. At distances close to the transformer ( $R < 2.5 R_o$ ), the magnetic field falls off at a  $1/R^3$  rate.
- b. At distances greater than  $2.5 R_o$ , the magnetic field falls off at a  $1/R^2$  rate.

343:DSD:lrk  
3912  
Ser. 1343-197

Subj: Electromagnetic Compatibility (EMC) R&D Program Output; forwarding

The test procedure developed to conduct the transformer model measurements had the following characteristics:

- a. Utilized a broadband noise generator to simulate the effects of powerline harmonics in the 5 kHz to 50 kHz frequency range
- b. Utilized a Fast Fourier Transform (FFT) Analyzer to rapidly complete the number of spectrum averages required to ensure accurate data
- c. Utilized magnetic field normalization to compensate for transformer current variations (these variations were caused by impedance changes and harmonic distortion effects created by the magnetic core)

3. The transformer EMI modeling effort is nearing completion. There are, however, several unresolved questions on the most accurate transformer distance model and fundamental frequency model to utilize. Mr. L. Dalsass has begun the tasks described in enclosures (2) and (3), which are expected to resolve these ambiguities. A final report is expected during the first quarter of FY82.

*J.T. Fine*

W. S. ADAMS  
By direction

Copy to: (w/encl)

NAVSEA 61R4 (H. DeMattia, extra copy)  
61433 (G. Rees)  
61434 (R. Peterson)  
NAVELEX 51024 (S. Caine)  
NOSC Code 8105 (Dr. J. Rockway)  
Code 9234 (E. Kamm, J. Henry)  
UPENN (Dr. R. Showers, N00140-81C-BB63)  
DTIC  
NAVMAT 08D17  
NAVMAT 08

## ABSTRACT

Harmonics of the powerline fundamental frequency (60/400 Hz) can be generated whenever nonlinear loads are connected to the power distribution system. In some cases, these currents can be the source of radiated magnetic field emissions that adversely affect shipboard equipment. In this memorandum, the magnetic fields from shipboard power transformers were determined using an offline broadband generator as a source of controlled powerline harmonics at frequencies up to 50 kHz. Normalizing the flux density,  $B$ , by the harmonic current spectral density in the primary winding,  $I$ , was found to be an effective method to compensate for impedance changes and harmonic distortion caused by the transformer magnetic core.

It was shown that between 5 and 50 kHz the magnetic fields from transformers rated at 200 W to 5 kVA depend on the distance from the center of the transformer to the field point, the shielding effectiveness of the case, and the current spectrum of the input harmonics. In this frequency band, a transformer surface not containing seams or openings behaves similar to an ideal shielding boundary with respect to frequency ( $f^{-1/2}$  dependence). At a distance close to the transformer, the magnetic fields are proportional to  $1/R^3$  (dipole source); at greater distances they are proportional to  $1/R^2$ . The transition occurs between regions where the leakage inductance and internal conductor-generated magnetic fields, respectively, are dominant.

*R squared, R cubed  
S to the minus 1/2 power*

## ADMINISTRATIVE INFORMATION

This memorandum was funded under NUSC Project No. A51000, "Submarine Electromagnetic Compatibility R&D Program," Principal Investigator, D. S. Dixon, Code 343. The sponsoring organization is Naval Electronics Systems Command; Mr. J. Cauffman, of Code 3041, is Program Manager. The Technical Agent is Mr. H. DeMatta, Code 61R4, of the Naval Sea Systems Command.

Accession For	
NTIS GRA&I	<input checked="" type="checkbox"/>
DTIC TAB	<input type="checkbox"/>
Unannounced	<input type="checkbox"/>
Justification	
<i>Per Mr. on file</i>	
Distribution/	
Availability Codes	
Dist	Avail and/or Special
A	

## TABLE OF CONTENTS

	Page
ABSTRACT . . . . .	i
ADMINISTRATIVE INFORMATION . . . . .	i
LIST OF ILLUSTRATIONS . . . . .	v
INTRODUCTION . . . . .	1
DISCUSSION . . . . .	2
A. Transformer Magnetic Fields . . . . .	2
B. Transformer Models . . . . .	3
C. Magnetizing Inductance . . . . .	4
D. Leakage Inductance . . . . .	5
E. Instrumentation . . . . .	5
F. Transformer Test Models . . . . .	7
G. Data Analysis . . . . .	8
H. Broadband Input Characteristics . . . . .	9
I. Magnetic Field Measurements/Calculations . . . . .	9
J. Discussion of Probe Separation Geometry . . . . .	11
K. Comparison of Normalized Transformer Magnetic Fields (B/I) at 25 kHz . . . . .	12
L. Effect of Internal Conductors on Transformer Leakage Fields . . . . .	13
M. Open-Circuited Secondary Winding (Effect on Inversion) . . . . .	15
N. Data Summary and Analysis . . . . .	15
O. Comments on Transformer Shielding Models (5 to 50 kHz) . . . . .	20
P. Comparison of Transformer Leakage Fields Versus Frequency . . . . .	22
Q. High Frequency Leakage Field Model . . . . .	23
R. Relationship of Primary-Current Spectrum I(f) to Susceptor-Coupled EMI . . . . .	24
S. Leakage Field Versus Distance Models . . . . .	26
T. EMI Implications of the Test Results . . . . .	28

TABLE OF CONTENTS (Cont'd)

	Page
CONCLUSIONS . . . . .	30
ACKNOWLEDGMENTS . . . . .	31
REFERENCES . . . . .	89

## LIST OF ILLUSTRATIONS

Figure		Page
1	Deltec Corporation DT25T5 200 W Transformer Shown in Relation to a Coordinate System Referenced to its Symmetry Axes . . . . .	33
2	General Electric 9T51Y13 3 kVA Transformer Shown in Relation to a Coordinate System Referenced to its Symmetry Axes . . . . .	34
3	Jefferson Electric 5 kVA Transformer, Serial 12438, Shown in Relation to a Coordinate System Referenced to its Symmetry Axes . . . . .	35
4	Horizontal Section of the Test Probe Showing Some Construction Details . . . . .	36
5	Series-Induced Open-Circuit Probe Voltage for a 1-Gauss Magnetic Field at Frequencies Up to 100 kHz . . . . .	36
6	Approximate Transformer Equivalent Circuit for a Turns Ratio ( $n$ ) of 1:1 . . . . .	37
7	Hysteresis Loop for a Typical Transformer Lamination and Transformer Magnetizing Inductance Model . . . . .	38
8	Block Diagram of Wide-Band Measurement System Used to Measure Transformer Magnetic Fields . . . . .	39
9	Circuit Diagram of Break-In Box Used in the Wide-Band Instrumentation System . . . . .	40
10	Approximate Transfer Equivalent Circuits With an Assumed Turns Ratio of Unity, $n = 1:1$ . . . . .	41
11	Diagram for Adding or Subtracting Decibels (Courtesy of General Radio Co., West Concord, MA) . . . . .	42
12	Comparison of Flux Density at 25 kHz at Different Locations in the Leakage Field of Transformers Normalized to 1 A of Primary-Winding Current With a Short-Circuited Secondary Winding . . . . .	43
13	Input Voltage and Current Spectral Densities for a 200 W Transformer . . . . .	44
14	Probe Voltage Versus Frequency Plots as a Function of Probe Distance From the Top Surface of the DT25T5 200 W Transformer as the Probe Was Moved Along the Vertical Coordinate Axis Shown in Figure 1 . . . . .	45
15	Normalized Flux Density at the Top Surface of the 200 W Transformer (Center of Laminations) . . . . .	46

## LIST OF ILLUSTRATIONS (Cont'd)

Figure		Page
16	Probe Voltage Versus Frequency Plots as a Function of Probe Distance From the Top Surface of the DT25T5 Transformer as the Probe Was Moved Along a Vertical Axis Intersecting the Edge of the Lamination Stack . . . . .	47
17	Normalized Flux Density at the Top Surface of the 200 W Transformer (Edge of Laminations) . . . . .	48
18	Probe Voltage Versus Frequency Plots as a Function of Probe Distance From the Side of the DT25T5 200 W Transformer as the Probe Was Moved Along the Horizontal Axis Shown in Figure 1 . . . . .	49
19	Normalized Flux Density at the Side of the 200 W Transformer . . . . .	50
20	Probe Voltage Versus Frequency Plots as a Function of Probe Distance From the Primary-Side Endcap of the DT25T5 200 W Transformer as the Probe Was Moved Along the Horizontal Axis Intersecting the Endcap Shown in Figure 1 . . . . .	51
21	Normalized Flux Density at the Primary Endcap of the 200 W Transformer . . . . .	52
22	Probe Voltage Versus Frequency Plots as a Function of Probe Distance From the Secondary Side Endcap of the DT25T5 200 W Transformer . . . . .	53
23	Normalized Flux Density at the Secondary Endcap of the 200 W Transformer . . . . .	54
24	Probe Voltage Versus Frequency Plots as a Function of Probe Distance From the Secondary Side Endcap of the DT25T5 200 W Transformer (Open-Circuited Secondary) . . . . .	55
25	Input Voltage and Current Spectral Densities for a 3 kVA Transformer . . . . .	56
26	Probe Voltage Versus Frequency Plots as a Function of Probe Distance From the Top Surface of a 3 kVA GE 9T51Y13 Transformer as the Probe Was Moved Along a Vertical Axis Intersecting the Narrow Seam in the Transformer Cover Shown in Figure 2 . . . . .	57
27	Normalized Flux Density at the Top Surface of the 3 kVA Transformer Above the Narrow Seam in the Cover . . . . .	58
28	Probe Voltage Versus Frequency Plots as a Function of Probe Distance From the Top Surface of a 3 kVA GE 9T51Y13 Transformer as the Probe Was Moved Along a Vertical Axis Intersecting the Center of the Lamination Stack Shown in Figure 2 . . . . .	59

## LIST OF ILLUSTRATIONS (Cont'd)

Figure		Page
29	Normalized Flux Density at the Top Surface of the 3 kVA Transformer Above the Center of the Lamination Stack . . . . .	60
30	Probe Voltage Versus Frequency Plots as a Function of Probe Distance From the Top Surface of a 3 kVA GE 9T51Y13 Transformer (Open-Circuited Secondary) . . . . .	61
31	Probe Voltage Versus Frequency Plots as a Function of Probe Distance From the Side of the 3 kVA GE 9T51Y13 Transformer as the Probe Was Moved Along the Horizontal Axis Shown in Figure 2 . . . . .	62
32	Normalized Flux Density at the Side of the 3 kVA Transformer . . . . .	63
33	Probe Voltage Versus Frequency Plots as a Function of Probe Distance From the Side of a 3 kVA GE 9T51Y13 Transformer (Open-Circuited Secondary) . . . . .	64
34	Probe Voltage Versus Frequency Plots as a Function of Probe Distance From the I/O Endcap of a 3 kVA GE 9T51Y13 Transformer as the Probe Was Moved Along the Horizontal Axis Shown in Figure 2 . . . . .	65
35	Normalized Flux Density at the I/O Endcap of the 3 kVA Transformer . . . . .	66
36	Probe Voltage Versus Frequency Plots as a Function of Probe Distance From the I/O Endcap of a 3 kVA GE 9T51Y13 Transformer (Open-Circuited Secondary) . . . . .	67
37	Probe Voltage Versus Frequency Plots as a Function of Probe Distance From the Endcap Opposite the I/O Endcap of the 3 kVA GE 9T51Y13 Transformer as the Probe Was Moved Along the Horizontal Axis Shown in Figure 2 . . . . .	68
38	Normalized Flux Density at the Endcap Opposite the I/O Endcap of the 3 kVA Transformer . . . . .	69
39	Input Voltage and Current Spectral Densities for a 5 kVA Transformer . . . . .	70
40	Probe Voltage Versus Frequency Plots as a Function of Probe Distance From the Top Surface of the Jefferson Electric 12438 Transformer as the Probe Was Moved Along a Vertical Axis Intersecting the Center of the Seam Nearest the Endcap Shown in Figure 3 . . . . .	71
41	Normalized Flux Density at the Top Surface of the 5 kVA Transformer Above the Seam Nearest the Endcap . . . . .	72

## LIST OF ILLUSTRATIONS (Cont'd)

Figure	Page
42 Probe Voltage Versus Frequency Plots as a Function of Probe Distance From the Top Surface of the Jefferson Electric 12438 Transformer as the Probe Was Moved Along a Vertical Axis Intersecting the Center of the Seam Nearest the Endcap (Open-Circuited Secondary) . . . . .	73
43 Probe Voltage Versus Frequency Plots as a Function of Probe Distance From the Top Surface of the Jefferson Electric 12438 Transformer as the Probe Was Moved Along a Vertical Axis Intersecting the Center of the Seam Nearest the Center of the Case Shown in Figure 3 . . . . .	74
44 Normalized Flux Density at the Top Surface of the 5 kVA Transformer Above the Seam Nearest the Center of the Case . . . . .	75
45 Probe Voltage Versus Frequency Plots as a Function of Probe Distance From the Side of the Jefferson Electric 12438 Transformer as the Probe Was Moved Along the Horizontal Axis Shown in Figure 3 . . . . .	76
46 Normalized Flux Density at the Side of the 5 kVA Transformer . . . . .	77
47 Probe Voltage Versus Frequency Plots as a Function of Probe Distance From the Side of the Jefferson Electric 12438 Transformer (Open-Circuited Secondary) . . . . .	78
48 Probe Voltage Versus Frequency Plots as a Function of Probe Distance From the Endcap of the Jefferson Electric 12438 Transformer (Side With Open Grating) Shown in Figure 3 . . . . .	79
49 Normalized Flux Density at the Endcap (Open Grating) of the 5 kVA Transformer . . . . .	80
50 Comparison of the Maximum Leakage Flux Density From a 200 W, a 3 kVA, and a 5 kVA Transformer in Units of Decibels Relative to 1 Gauss Normalized to 1 A of Primary-Winding Current (B/I) Versus Frequency With the Location of the Respective Transformer Surface Identified at the Right . . . . .	81
51 Comparison of the Leakage Flux Density From a 200 W, a 3 kVA, and a 5 kVA Transformer in Units of Decibels Relative to 1 Gauss Normalized to 1 A of Primary-Winding Current (B/I) Versus Frequency With the Location of the Respective Transformer Surface Identified at the Right . . . . .	82
52 Normalized Flux Density at the Top Surface of a 200 W Transformer Versus Spacing . . . . .	83

## LIST OF ILLUSTRATIONS (Cont'd)

Figure	Page
53 Normalized Flux Density at the Side of a 200 W Transformer Versus Spacing . . . . .	84
54 Normalized Flux Density at the Primary Endcap of a 200 W Transformer Versus Spacing . . . . .	85
55 Normalized Flux Density at the Top Surface Seam of a 3 kVA Transformer Versus Spacing . . . . .	86
56 Normalized Flux Density at the Endcap Opposite the I/O Endcap of the 3 kVA Transformer Versus Spacing . . . . .	87
57 Normalized Flux Density at the Side of the 5 kVA Transformer Versus Spacing . . . . .	88

SHIPBOARD POWERLINE TRANSFORMERS: H EMISSION CHARACTERISTICS,  
EMI MODELS, AND A TEST PROCEDURE THAT  
UTILIZES SIMULATED INPUT SIGNALS

INTRODUCTION

Power-system related electromagnetic interference (EMI) is a frequent cause of performance degradation for equipment operating on both submarines and surface ships. In many cases, the interference is caused by magnetic fields generated by such common powerline emitters as cables, switchboards, or transformers, which inductively couple into low-level input circuitry found in various very low frequency (VLF) or sonar receiver subsystems.

The most likely sources of such magnetic fields at sonar/VLF frequencies are the powerline harmonics generated by nonlinear loading of the power distribution system. This loading occurs if equipments containing power supply rectifiers or other pulsing loads are connected to the power line.

Because the harmonic amplitudes vary in unpredictable ways due to changing load conditions, equipment connections, etc., they are usually unsuitable as exciting sources for tests on power devices requiring controlled harmonic inputs. The objectives of this memorandum are to report on test results for the magnetic fields generated by power transformers excited from an offline source at frequencies up to 50 kHz. The tests employed a wide-band calibrated Gaussian noise source and a power-amplifier driver that allowed broadband testing of the transformers (to be accomplished simultaneously) at frequencies from 5 through 50 kHz.

For these measurements, the driver-output spectrum was neither filtered nor shaped, in effect supplying approximately the same input-voltage spectral density to the transformer under test. The effects on the leakage fields, due to changes in input amplitude could, however, be observed by adjusting the power-amplifier output.

## DISCUSSION

## A. TRANSFORMER MAGNETIC FIELDS

The leakage fields surrounding magnetic devices, such as transformers, possess aspect symmetries that depend on the orientation of the primary and secondary windings.<sup>1,2</sup> The magnetic fields generated from the power transformers under test were measured by moving an air-cored magnetic probe to different locations in the transformer's external leakage field. To permit acceptable spatial resolution of the field "pattern", a probe with small cross-sectional area was used to approximate a localized point sensor.

Magnetic-flux density measurements were taken along all principal symmetry axes (relative to the lamination core) of the transformers as well as near physical features of the transformers that might contribute to large stray field components. These measurement points included field points adjacent to seams and gratings in the transformer case and input/output (I/O) connectors for both open-circuited and short-circuited secondary winding conditions.

In these tests, the probe "sensed" the normal or perpendicular component of the leakage field, i.e., the plane of the probe was parallel to the transformer enclosure. Figures 1 through 3 illustrate the three test transformers, which ranged from 200 W to 5 kVA, respectively. The normal component of the leakage field is parallel to the Cartesian coordinate axes shown in the figures.

Figure 4 shows details of the probe construction. The transmission line to the probe is a twisted shielded pair to prevent EMI from coupling into the line conductors by undesired magnetic and common-mode electric fields. The maximum open-circuit voltage induced in such an air-cored probe that is placed in a uniform sinusoidal magnetic field is given by

$$|e| = NA\omega B = KfB . \quad (1)$$

From equation (1),

$$K = 2\pi NA , \quad (2)$$

where

$|e|$  = the maximum induced voltage (volts),

$N$  = the total number of turns on the probe,  
 $A$  = the cross-sectional area of the probe ( $\text{meters}^2$ ),  
 $\omega$  = the angular frequency (radians/second) ( $2\pi f$ ),  
 $f$  = the frequency of the magnetic field (Hz), and  
 $B$  = the magnetic field flux density (webers/meter $^2$ ).

The constant,  $K$ , of the probe was determined from Helmholtz-coil measurements using a calibrated 5.5-in. (14-cm) loop antenna as a reference. The results are shown in figure 5.

Field patterns were determined for probe locations from the transformer case to approximately 12 in. (30 cm) distant. This separation corresponds to limitations caused primarily by (1) low probe sensitivity and (2) driver-output limitations.

## B. TRANSFORMER MODELS

An approximate power-transformer equivalent circuit is shown in figure 6. For simplicity, a unity ratio (1:1) of primary to secondary turns has been assumed. The circuit model parameters are defined as

$L_m$  = magnetizing inductance (henrys),  
 $L_p$  = primary leakage inductance (henrys),  
 $L_s$  = secondary leakage inductance (henrys),  
 $R_c$  = core-loss resistance from eddy-current/hysteresis contributions (ohms),  
 $R_{cu}, R_{cu'}$  = copper conductor losses (ohms),  
 $C_s$  = shunt capacitance (farads), and  
 $R_l$  = load resistance (ohms).

The magnetizing inductance,  $L_m$ , provides the flux linkages that couple the primary and secondary windings of the transformer. In addition to flux confined to the laminations which supply useful power conversion, the leakage components  $L_p$  and  $L_s$  are also present. Magnetic fields from transformers couple to external circuits because of the following factors:

1. Leakage field coupling inductances,  $L_p$  and  $L_s$ , and

2. Currents flowing in the powerline conductors, both internal and external to the transformer.

### C. MAGNETIZING INDUCTANCE

The variation with frequency of magnetizing inductance of a tape-wound or stamped-core transformer can be complex and dependent on such factors<sup>3,4</sup> as

1. The magnetic characteristics of the core,
2. The winding parameters,
3. The core dimensions,
4. The lamination thickness and resistivity, and
5. The input frequency.

For example, the magnetic characteristics referred to in 1, above, include the alloy composition as well as the process used to anneal the transformer core. Factors detrimental to achieving high core permeability include residual stresses from operations such as drilling bolt holes for fasteners, machining, and routine handling of the core material.

Figure 7a shows the hysteresis loop behavior for Magnesil, a silicon-iron alloy commonly used for transformer cores. For a transformer constructed utilizing a UI magnetic core, as shown in figure 7b, the magnetizing inductance can be approximated by

$$L_m = \frac{N^2 A \mu_{av} \mu_0}{l}, \quad (3)$$

where

$L_m$  = the magnetizing inductance (henrys),

$A$  = the core cross-sectional area (meters<sup>2</sup>),

$\mu_{av}$  = the average relative permeability (see figure 7a),

$\mu_0$  = the permeability of free space, equal to  $4\pi \times 10^{-7}$  henrys/meter, and

$l$  = the mean centerline length of the lamination (meters).

#### D. LEAKAGE INDUCTANCE

In addition to the mutual flux that couples the primary and secondary windings in a magnetic-cored power conversion device, a smaller leakage flux component confined primarily to an air path is also present. Because the leakage path is through the air, this inductance can be viewed as being equivalent to an air-core inductor.<sup>5</sup>

As a general rule, the leakage inductance depends on the following variables:

1. The spacing between the primary and secondary windings,
2. The amount of coil "build",
3. The winding widths, and
4. The number of primary/secondary turns.

#### E. INSTRUMENTATION

##### Leakage Field Measurements

Figure 8 is a block diagram of the instrumentation for a wide-band noise system employing a fast Fourier transform (FFT) processor and display system. The objective of the measurement system is to utilize the speed and ease of operation of a digital-based spectrum analyzer in conjunction with a wide-band Gaussian noise source to provide an automated broadband analysis capability.

Remarkable improvements in speed with subsequent improvements in efficiency are possible with broadband digital-based measurement systems relative to sinusoidal testing. This last factor becomes an important consideration in the evolution of equipment data for inclusion in computer-based data banks such as those needed for the electromagnetic compatibility (EMC) R&D program.

##### Wide-Band Driver

Figure 9 is a circuit diagram of the junction box used to monitor the line currents and voltages supplied to the transformer under test. Toroids  $L_2$ ,  $L_3$ , and  $L_4$  are used to sense the differential line currents  $I_1$ ,  $I_2$ , and  $I_3$ .  $T_1$ ,  $T_2$ , and  $T_3$  are stepdown transformers used to monitor the input

voltage. Since our tests were conducted on single-phase transformers, only input lines A and B were monitored. Transformer power ratings ranged from 0.2 to 5 kVA.

### FFT Spectrum Analysis

A Nicolet 446 spectrum analyzer was employed for I/O analysis of the broadband transformer magnetic fields. The availability of FFT instruments with highly automated user controls has simplified greatly the wide-band testing of components and systems. In particular, the Nicolet 446 analyzer has front-panel controls that automate all of the operations needed to perform sampling, filtering, and analog-to-digital (A/D) conversion of the input signal.

The operation of these FFT analyzers relies on the approximation of a Fourier integral representing the signal spectrum by a discrete transform,<sup>6</sup>

$$F(\omega) = \int_{-\infty}^{+\infty} f(t)e^{j\omega t} dt \quad (4)$$

$$c(i) = \sum_{k=0}^{N-1} f(k\Delta t)e^{j2\pi ki/N}, \quad (5)$$

$$i = 0, 1, 2, \dots, N-1,$$

where  $f(t)$  is the input signal.

A total of  $N^2$  terms are required to evaluate the transform coefficients,  $c(i)$ , in equation (5). A large reduction in the number of required operations is possible with instruments using modern FFT algorithms. This results in considerable simplification in instrument hardware and lower cost and weight.

### Spectrum Averaging

The transform coefficient,  $c^2(i)$ , is a measure of the signal power at the  $i$ -th frequency element. For a data record  $T$  seconds long, where  $T$  is greater than the transform period,  $T_s$ , spectral averaging of the  $n = T/T_s$  individual spectral estimates is accomplished on the Nicolet unit. Averaging is advantageous because of the lower statistical variance of the spectral amplitudes.

For most of our tests, 64 averages provided sufficient accuracy and also kept the averaging time within reasonable limits.

#### FFT Analyzer Bandwidths

The Nicolet 446 is classified as a 400-line analyzer providing 400 frequency-resolution elements irrespective of the size of the analysis band. For operation in the 0 to 50 kHz frequency range employed in our tests, the resolution-element bandwidth,  $\alpha$ , which is the baseline width of a single frequency, is

$$\alpha = \frac{\text{Analysis band (Hz)}}{\text{Number of frequency elements}} = \frac{50 \times 10^3}{4 \times 10^2} = 125 \text{ Hz} . \quad (6)$$

The noise bandwidth, BW, for the Nicolet 446 analyzer is given by<sup>7</sup>

$$BW = 1.5\alpha = 187.5 \text{ Hz} .$$

The conversion of the measured data from a 187.5 bandwidth to a 1 Hz bandwidth can be accomplished simply by the bandwidth correction

$$\text{dBV//}\sqrt{1} = \text{dBV//}\sqrt{187.5} - 22.7 \text{ dB} ,$$

(i.e., a 10 log BW correction factor) where  $\text{dBV//}\sqrt{1 \text{ Hz}}$  = volts in decibels relative to a 1 Hz bandwidth.

#### F. TRANSFORMER TEST MODELS

##### Open-Circuited Secondary (No Load)

A power transformer with an open-circuited secondary can be approximated by the model shown in figure 10a. In this case, the secondary leakage reactance does not appear in the circuit model since current is not being drawn by the secondary circuit. The primary exciting current needed to supply the flux linkages in the core of most transformers is usually less than 10 percent of full-load current at a fundamental frequency of 60 or 400 Hz.

##### Short-Circuited Secondary

To facilitate supplying a power transformer with full rated current from a power-amplifier driver, a short-circuited secondary was used as a test load. This represents a loading condition of the worst case that a transformer is

likely to encounter in operation. However, the input voltage that is required (for this short-circuited secondary test) is normally only a small fraction of rated voltage, typically 10 to 15 V for a design input of 100 V. The net effect is to reduce the driver power requirements.

Since the magnetizing current (exciting current) is small, < 10 percent of full-load current, an approximate short-circuited model that neglects the magnetizing inductance, as shown in figure 10b, applies in this case.

#### G. DATA ANALYSIS

The transformer leakage magnetic fields are converted by magnetic induction to a voltage at the terminals of the test probe. Then the probe voltage is amplified and fed to the Nicolet 446 FFT analyzer. A family of curves of probe voltage spectral density as a function of the separation distance from the transformer were plotted using a Tektronix 4662 interactive digital plotter. The vertical axis of each spectral plot is in decibels relative to 1 volt (dBV). The horizontal scale extends from approximately 1 Hz to 50 kHz. As noted earlier, the noise analysis bandwidth for this 50 kHz analysis range is 187 Hz. Voltage spectra (loop antenna output) were obtained for a 200 W Deltec Corporation DT25T5 transformer, a 2 kVA General Electric 9T51Y13 transformer, and a 5 kVA Jefferson Electric transformer.

The measurement-system noise floor with the broadband source disconnected from the transformer is labelled "ambient" on each plot. For the majority of the measurements that were taken, the ambient line is significantly lower than the probe voltage and could be neglected. However, in a few cases, at extreme distances from the transformers and at high frequencies (> 35 kHz), the resulting low probe output voltage approached the ambient. In those cases, a numerical correction was required to remove the ambient-noise contamination.

If  $V_s(f)$  and  $V_a(f)$  are, respectively, the signal and ambient-voltage spectral densities at a frequency of  $f$  Hz, the actual probe voltage,  $V'_s(f)$ , can be calculated, because  $V_s(f)$  and  $V_a(f)$  are uncorrelated, as

$$V'_s = \sqrt{V_s^2 - V_a^2} . \quad (7)$$

The decibel chart in figure 11 simplifies the calculation of  $V'_s$ , given the amplitudes  $V_s$  and  $V_a$ . For example, if the measured probe voltage,  $V_s$ , at

a particular frequency is 6.8 dB above the ambient, the actual voltage,  $V_s'$ , would be 1 dB less. The 1 dB is the result of contamination of the probe voltage by the presence of the additional ambient noise. A noise correction, indicated by an asterisk (\*), was applied whenever differences between probe voltage and ambient were less than 7 dB.

#### H. BROADBAND INPUT CHARACTERISTICS

The input exciting voltage to the transformer under test was supplied by a broadband pseudorandom noise generator (Hewlett Packard Model 3722A) and a McIntosh power-amplifier driver (see figure 8).

The Gaussian noise approximates a flat voltage spectral density for input frequencies from 1 Hz to 50 kHz. Spectra of the input exciting voltage and primary current were measured with both open- and short-circuited secondary windings. For the short-circuited case, operation at full-rated broadband root-mean-square (rms) current was possible only with the 200 W transformer, because of a 300 W power-amplifier driver limitation. The (rms broadband) input voltage and primary winding current levels are labelled adjacent to each plot.

#### I. MAGNETIC FIELD MEASUREMENTS/CALCULATIONS

The voltage induced in an air-cored test probe by a magnetic field is given by equation (1). The factor K, the gain of the probe, is a function of the probe capture area, NA. For input frequencies less than the resonance frequency, a well-designed probe will have a linear variation of output voltage with frequency, as shown in figure 5, where a 1-gauss exciting field was used to calibrate the probe. Table 1 is a listing of probe output voltages [in decibels ( $20 \log_{10} Kf$ )] at selected frequencies of 5, 15, 25, 35, and 50 kHz. These data points were obtained from figure 5.

Table 1. Probe Output for 0 dBG Field Strength

Frequency (kHz)	5	15	25	35	50
Probe Output (dBV)	-15.9	-6.4	-1.9	0.98	4.08

The probe voltage,  $V_p$ , from equation (1), is

$$V_p = KfB . \quad (8)$$

After subtraction of the preamplifier gain and conversion to decibels ( $20 \log_{10}$ ), equation (8) becomes

$$V_p = V_s(\text{dB}) - G_A(\text{dB}) = Kf(\text{dB}) + B(\text{dB}) , \quad (9)$$

where

$V_s(\text{dB})$  = amplified probe voltage (decibels), and

$G_A(\text{dB})$  = preamplifier gain (decibels).

From equation (9),

$$B(\text{dB}) = dBG = V_s(\text{dB}) - G_A(\text{dB}) - Kf(\text{dB}) , \quad (10)$$

where  $dBG$  = flux density in decibels relative to 1 gauss.

Equation (10) can be normalized on a per-unit-current basis ( $B/I$ ) to account for differences in transformer exciting current spectral density as

$$B/I = B(\text{dB}) - I(\text{dB}) = V_s(\text{dB}) - G_A(\text{dB}) - Kf(\text{dB}) - I(\text{dB}) . \quad (11)$$

A computer program written for an HP-25C calculator was used to evaluate  $B/I$  from equation (11), given  $V_s$ ,  $G_A$ ,  $Kf$ , and  $I$  as input parameters. The values of  $V_s$  and  $I$  were obtained from the spectral plots at discrete frequencies of 5, 15, 25, 35, and 50 kHz. The selection of these frequencies was arbitrary to a certain extent, but the intent was to include sample frequencies applicable to the sonar and VLF radio bands. It should be noted, however, that the leakage fields at other frequencies are equally accessible.

An Ithaco preamplifier was used to amplify the probe output voltage. A gain ( $G_a$ ) of 30 dB was used in all probe measurements. Values of  $G_a$ ,  $Kf$ , and  $I$  were written into HP-25C storage registers 1, 2, and 3, respectively, as input entries for calculation of ( $B/I$ ). A listing of the program steps needed to implement the calculation of  $B/I$  from equation (11) is given below:

1. Initial entries, store in registers:
  - a. Amplifier gain ( $G_a$ ),
  - b. Probe factor ( $Kf$ ), see table 1, and

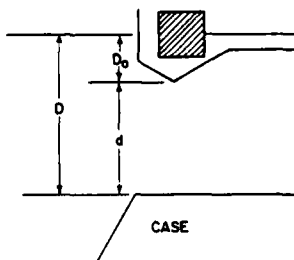
- c. Current spectral density ( $I$ ).
2. Steps:
- a. Enter the amplified probe voltage ( $V_s$ ),
  - b. Recall (contents of) register 1,
  - c. Subtract step b from step a,
  - d. Recall register 2,
  - e. Subtract step d from the results of step c,
  - f. Recall register 3, and
  - g. Subtract step f from step e.

#### J. DISCUSSION OF PROBE SEPARATION GEOMETRY

It was noted earlier that the air-cored probe was protected by a polyurethane potting compound. The separation distance,  $d$ , in the  $V_s$  spectral plots is the distance from the flat lower surface of the probe head to the transformer case. The mid-plane of the probe, corresponding to the center of the air-cored loop, was spaced an additional 1.72 cm.

The total distance,  $D$ , from the transformer case to the center of the loop is

$$D = d + D_0 , \quad (12)$$



where  $d$  and  $D_0$  are in cm, and  $D_0 = 1.72$  cm.

Comparisons of the leakage magnetic-field variation with distance were made in some cases by converting from absolute separation distance,  $D$ , to the parameter  $D/D_0$ , which is the ratio of  $D$  to the initial separation value,  $D_0$ .

K. COMPARISON OF NORMALIZED TRANSFORMER  
MAGNETIC FIELDS (B/I) AT 25 kHz

The flux density, normalized to 1 A of primary current (B/I), was calculated using the probe voltage spectral plots and equation (11). B/I was determined at frequencies of 5, 15, 25, 35, and 50 kHz. As previously discussed, these frequencies were selected to provide sufficient coverage in the sonar/VLF bands but at the same time limit the data analysis and subsequent summaries to manageable proportions. Values of B/I at any other frequency in the band can, of course, also be determined using this procedure.

Figure 12 shows the results of this calculation at 25 kHz for the Deltec Corporation 200 W, General Electric 3 kVA, and Jefferson Electric 5 kVA transformers. The bar graph summarizes the comparative magnitude of leakage fields for a probe position corresponding to  $d = 0$ .

For the Deltec DT25T5 and General Electric (GE) 9T51Y13 transformers, the largest contributions originate at the top surface at the center of the lamination stack. In each case, the laminations are fully exposed, as shown in figures 1 and 2.

The absence of shielding over the laminations resulted in the highest measured values of B/I that were observed. The situation is different in the case of the 5 kVA transformer, which employs a steel panel over the lamination stack. The magnetic field at the top surface is more than 50 dB lower than for the other two smaller units. At the seams in the top surface of the 5 kVA transformer, flux penetrates through the gaps to the exterior of the enclosure. However, the resulting magnetic fields at both the center and end seams are still less than for fully exposed laminations because the narrow gaps permit only a small percentage of the available flux lines to escape confinement.

The enclosure surfaces of the Deltec DT25T5 and GE 9T51Y13 transformers that contribute the largest exterior magnetic fields are (1) the top surface over the core stack, (2) the sides, and (3) the endcaps. In the case of the 5 kVA transformer, the shielding effectiveness of the enclosure generally inhibits the leakage fields except in the vicinity of seams and openings.

L. EFFECT OF INTERNAL CONDUCTORS ON  
TRANSFORMER LEAKAGE FIELDS

As stated in an earlier section of this memorandum, the leakage fields from transformers are generated by the following sources:

1. The leakage inductance contributed by the primary and secondary windings, and
2. The internal conductors connected to the primary and secondary windings.

The magnitude of the external magnetic field contributed by the leakage inductance would be expected to decrease as the separation distance from the transformer enclosure increases. This "fall-off" with distance can be interpreted as resulting from flux spreading at greater distance, in effect leaving reduced numbers of flux lines per unit area at those locations.

At some transformer surfaces where the fields are relatively low, an inversion in the distance relationship would occur. That is, at an intermediate spacing (nominally 4 to 6 cm), the field would begin to increase with increasing distance. At some further distance, the field decreases once again.

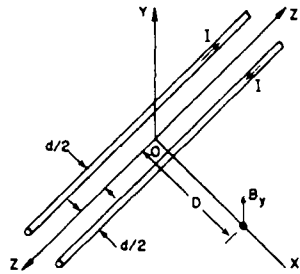
Numerous examples of this inversion are found in the test results, which are shown in figures 13 through 57. This inversion, however, did not occur at high field strength locations, such as the tops of the Deltec DT25T5 and GE 3 kVA transformers. The explanation is that the magnetic fields generated by the power conductors, internal to the transformer, are much smaller than the leakage fields in the vicinity of the exposed laminations. However, they become comparable to the smaller fields originating at the side and endcaps.

An examination of several of the transformers showed that the reason for the inversion was that the internal conductors of the transformers were inadequately twisted and not shielded. At some surfaces, usually close to the conductors (I/O endcaps), these conductor sources become more significant contributors to the external field than the magnetic core leakage inductances. It is interesting to note that all three transformers tested showed inversion effects at one or more surfaces.

An estimate of the magnetic field generated by the transformer's internal conductors can be made by assuming a parallel wire-pair model. For this

radiator model, the conductor spacing is assumed to be equal to the approximate net displacement of the actual conductors. The flux-density component,  $B_y$ , per ampere of exciting current,  $I$ , is given approximately by<sup>8</sup>

$$\frac{B_y}{I} = \frac{\mu_0 d}{2\pi D^2}, \quad D \gg d. \quad (13)$$



where

$D$  = the coordinate of the field point relative to the center of the wire pair (meters),

$d$  = the conductor spacing (meters),

$B_y$  = the component flux density perpendicular to the loop area formed by the conductors (webers/meter<sup>2</sup>), and

$\mu_0$  = the magnetic permeability of free space ( $4\pi \times 10^{-7}$  henrys/meter).

Values of  $d$  and  $D$  were approximated as  $d = 0.25$  in.  $\approx 0.007$  meter and  $D = 10$  cm = 0.1 meter.

The parameter  $D$  is the sum of the distances from the conductor pair to the transformer case ( $\approx 6$  cm) and from the case to the external field point ( $\approx 4$  cm), for a total of 10 cm. From equation (13),

$$\frac{B_y}{I} = \frac{4\pi \times 10^{-7} \times 0.007}{2\pi(0.1)^2} = 1.4 \times 10^{-7} \left( \frac{\text{webers}}{\text{meter}^2} \right) \text{ per ampere}.$$

Since 1 gauss =  $10^{-4}$  webers/meter<sup>2</sup>,

$$\frac{B_y}{I} = 1.4 \times 10^{-3} \text{ G/A} = 57.1 \text{ dBG/A}.$$

This value of  $B_y/I$  also must be reduced by the shielding effectiveness of the transformer enclosure. For example, figure 23a shows the results obtained for  $B/I$  from the secondary endcap of a 200 W DT25T5 transformer versus the field separation ratio  $D/D_0$ . At a frequency of 5 kHz and a separation parameter of  $D/D_0 \approx 6.0$ ,  $B/I = -70.1$  dBG/A. Beyond this distance, the field begins

to increase after continuously decreasing at closer distances to the endcap. An additional example is given in figure 35a, which shows B/I at the I/O endcap of the GE 9T51Y13 3 kVA transformer. At a frequency of 5 kHz and  $D/D_0 \approx 5.0$ ,  $B/I \approx -67.0$  dBG/A.

Although the calculation above is based on estimates of conductor spacing and an uncertain shielding effectiveness of the endcaps, nevertheless, B/I is not inconsistent with the onset of the inversion effects that were observed.

#### M. OPEN-CIRCUITED SECONDARY WINDING (EFFECT ON INVERSION)

Further evidence of the role the current-carrying internal conductors play in the leakage-field inversion effects can be demonstrated in tests in which the transformer secondary winding is open circuited. In this instance, no current is being conducted by the secondary winding and only a small amount of exciting current flows in the primary.

The results of the open-circuit tests are presented in the Data Summary and Analysis section of this memorandum, where the field-inversion effects are discussed in further detail.

Corrective procedures that could counteract the inversion effects, however, were not attempted. This, for example, would include modification of the transformers, such as by retwisting and shielding of the internal conductors.

#### N. DATA SUMMARY AND ANALYSIS

The purpose of this section is to provide a brief description and discussion of the test data and the results of the flux-density (B/I) calculations at various locations relative to the transformer enclosure. The leakage fields (B/I) are obtained by applying equation (11) (which was programmed on the HP-25C calculator) to the probe data obtained from each figure.

All figures are grouped with the probe-data figure number identified first, followed by the B/I results that are observed from it. A brief description of probe location and some commentary on the results of the analysis complete the summary.

The plots of B/I as a function of the normalized spacing ratio,  $D/D_0$ , show the distance dependence of the leakage fields at the extreme ends of the frequency band. B/I at intermediate frequencies of 15, 25, and 35 kHz are tabulated below the plot in each figure. The parameter d can be converted to the spacing ratio,  $D/D_0$ , as discussed elsewhere in this memorandum.

Deltec DT25T5 200 W Transformer

1. Figure 13, Description. The input source levels of voltage and current spectral densities used for the DT25T5 transformer tests are shown in figure 13.

2. Figures 14 and 15.

a. Description. The probe was located at the top surface of the transformer on a vertical axis intersecting the center of the lamination stack (see figure 1). Figure 14 is the amplified probe voltage versus frequency and spacing plots at the above location. Figure 15 shows the flux density per ampere of primary exciting current (B/I) as a function of spacing at this location.

b. Comments. B/I is "normal". The leakage fields decrease continuously with increasing distance from the transformer surface. The highest fields are generated at this location.

3. Figures 16 and 17.

a. Description. The probe remains on the top surface but has been moved to a vertical axis which now intersects the outside edge of the laminations. Figure 16 is the amplified probe voltage versus frequency and spacing plots. Figure 17 shows the normalized flux densities (B/I) corresponding to figure 16.

b. Comments. B/I is "normal". The leakage fields decrease continuously with distance from the surface.

4. Figures 18 and 19.

a. Description. The probe is now at the side of the transformer along the horizontal axis shown in figure 1. Figure 18 is the amplified probe voltage versus frequency and spacing at this location. Figure 19 shows B/I versus spacing.

b. Comments. B/I decreases rapidly within a short distance (10 cm) from the surface. Ambient noise limited the measurements to a maximum of 10 cm separation. B/I is "normal".

5. Figures 20 and 21.

a. Description. The probe is at the primary endcap along a horizontal axis (see figure 1). Figure 20 is the amplified probe voltage versus frequency and spacing plots. Figure 21 shows the corresponding B/I versus spacing.

b. Comments. The magnetic fields from the primary endcap surface are comparable to the fields at the side. B/I is "normal".

6. Figures 22, 23, and 24.

a. Description. The probe is at the secondary endcap along a horizontal axis. Figure 22 is the amplified probe voltage versus frequency and spacing plots. Figure 23 shows the flux density (B/I) versus spacing corresponding to figure 22.

b. Comments. The leakage fields decrease from  $d = 0$  ( $D/D_0 = 1$ ) to  $d = 6$  cm ( $D/D_0 = 4.5$ ), increase for  $d > 6$  cm to 12 cm ( $D/D_0 = 8.1$ ), then decrease once again to  $d = 18$  cm ( $D/D_0 = 11.6$ ). This inversion is the result of the magnetic fields generated by the secondary-winding conductors. The primary endcap surface, by comparison, is normal. Figure 24 shows the amplified probe voltage versus frequency plots for an open-circuited secondary winding. Note that the spacing dependence is normal in this case, unlike the results of figure 22 for a shorted secondary winding.

GE 9T51Y13 3 kVA Transformer

1. Figure 25, Description. The input source levels of voltage and current spectral densities used for the GE 9T51Y13 3 kVA transformer are shown in figure 25.

2. Figures 26 and 27.

a. Description. The probe is at the top surface along a vertical axis that intersects the narrow seam in the cover (see figure 1). Figure 26 is the amplified probe voltage versus frequency and spacing. Figure 27 shows the flux densities per ampere of primary exciting current (B/I) versus spacing.

b. Comments. B/I is "normal". The highest fields are generated at this location over the seam.

3. Figures 28, 29, and 30.

a. Description. The probe remains at the top surface but has been moved along a vertical axis intersecting the center of the lamination stack. Figure 28 shows the amplified probe voltage versus frequency and spacing plots. Figure 29 shows the normalized flux densities (B/I) versus spacing.

b. Comments. The leakage fields decrease from  $d = 0$  ( $D/D_0 = 1$ ) to  $d = 2$  cm ( $D/D_0 = 2.2$ ), increase for  $d > 2$  cm to  $d = 6$  cm ( $D/D_0 = 4.5$ ), then decrease continuously to  $d = 24$  cm ( $D/D_0 = 15.1$ ). Figure 30 shows the amplified probe voltage versus frequency and spacing plots for an open-circuited secondary winding. Note that the spacing dependence is normal in this case, unlike the results of figure 28 with a shorted secondary. It is interesting that the flux density at this location has been depleted by the shunting of flux lines through the adjacent seam in the transformer cover (see figure 2).

4. Figures 31, 32, and 33.

a. Description. The probe is now at the side of the transformer along the horizontal axis shown in figure 2. Figure 31 shows the amplified probe voltage versus frequency and spacing plots. Figure 32 shows the normalized flux densities (B/I) versus spacing at this location.

b. Comments. The leakage fields decrease from  $d = 0$  to  $d = 6$  cm ( $D/D_0 = 4.5$ ), increase for  $d > 6$  cm to  $d = 14$  cm ( $D/D_0 = 9.2$ ), then decrease continuously to  $d = 20$  cm ( $D/D_0 = 12.8$ ). Figure 33 shows the results for an open-circuited secondary winding. The amplified probe voltage is normal in this case.

5. Figures 34, 35, and 36.

a. Description. The probe is located at the I/O endcap along the horizontal axis shown in figure 2. Figure 34 is the amplified probe voltage versus frequency and spacing plots. Figure 35 shows the normalized flux densities (B/I) versus spacing.

b. Comments. The leakage fields decrease from  $d = 0$  to  $d = 4$  cm ( $D/D_0 = 3.4$ ), increase for  $d > 4$  cm to  $d = 12$  cm ( $D/D_0 = 8.1$ ), then slowly decrease to  $d = 24$  cm (see figure 34). It should be noted that the magnetic

field at 24 cm is greater than at 4 cm. At a spacing of 4 cm, an unusually rapid decrease of the field occurs at frequencies below 10 kHz. This change is the largest observed in this spacing interval and appears to be due to field cancellation effects resulting from the phasing of the leakage and conductor fields. At a spacing of 4 cm, the probe voltage (figure 34) shows an abrupt decrease with frequency to a null-like minimum at 7300 Hz. Figure 36 shows the amplified probe voltage for an open-circuited secondary. No inversion or interference effects are present.

6. Figures 37 and 38.

a. Description. The probe is located at the endcap opposite the I/O endcap along the horizontal axis (see figure 2). Figure 37 is the amplified probe voltage versus frequency and spacing plots. Figure 38 shows B/I versus spacing.

b. Comments. B/I is "normal". Note that no field inversion occurs at this endcap, which is located some distance away from the I/O conductors.

Jefferson Electric 12438 5 kVA Transformer

1. Figure 39, Description. The input source levels of voltage and current spectral densities used for the Jefferson Electric 12438 5 kVA transformer are shown in figure 39.

2. Figures 40, 41, and 42.

a. Description. The probe is located at the top surface of the transformer along a vertical axis intersecting the center of the seam nearest the endcap (see figure 3). Figure 40 shows the amplified probe voltage versus frequency and spacing at this location. Figure 41 shows B/I versus spacing.

b. Comments. The leakage fields decrease from  $d = 0$  to  $d = 4$  cm ( $D/D_0 = 3.4$ ), increase for  $d > 4$  cm to  $d = 8$  cm ( $D/D_0 = 4.7$ ), then remain approximately constant out to 22 cm. Figure 42 shows the corresponding results for an open-circuited secondary winding. The amplified probe voltage is "normal". The leakage fields decrease with increasing distance from the transformer in contrast to the shorted-secondary winding results shown in figure 40.

3. Figures 43 and 44.

a. Description. The probe is still at the top surface but has been moved to the center of the seam nearest the center of the cover (see figure 3). Figure 43 is the amplified probe voltage versus frequency and spacing plots at this location. Figure 44 shows the flux densities (B/I) versus spacing at this location.

b. Comments. The leakage fields are normal, decreasing with increasing distance from the transformer.

4. Figures 45, 46, and 47.

a. Description. The probe is located at the side of the transformer on the horizontal axis shown in figure 3. Figure 45 shows the amplified probe voltage versus frequency and spacing plots. Figure 46 shows the normalized flux densities (B/I) versus spacing.

b. Comments. The leakage fields decrease from  $d = 0$  to  $d = 10$  cm ( $D/D_0 = 6.9$ ) and increase for  $d > 10$  cm. The test data were limited to 16 cm. Note that at 16 cm the leakage fields are approximately the same magnitude as at  $d = 0$ . Figure 47 shows the results at this location for an open-circuited secondary winding. No inversion occurs in this case.

5. Figures 48 and 49.

a. Description. The probe is located at an endcap surface of the transformer (side with open grating) along a horizontal axis (see figure 3). Figure 48 is the amplified probe voltage versus frequency and spacing plots. Figure 49 shows B/I versus spacing at this location.

b. Comments. The leakage fields (B/I) are normal.

0. COMMENTS ON TRANSFORMER SHIELDING MODELS (5 TO 50 kHz)

The external leakage fields at the surface of a transformer depend on the source strength of the internal fields and the shielding or attenuation that occurs at the enclosure interface. For practical transformer cases containing seams, gaps, complex shapes, and endcaps, no simple solution is possible.

For simple shielding enclosures, such as sheets and cylinders, a high-frequency shielding effectiveness (SE) can be calculated. This provides some insight into the relevancy of various parameters that need to be considered.

In the case of a cylindrical enclosure, a particularly simple expression can be used for both longitudinal and transverse magnetic field components. The shielding effectiveness (SE) in this case is<sup>9</sup>

$$\text{SE in decibels} = 20 \log_{10} \frac{a \exp(d/\delta)}{2\sqrt{2} \mu_r \delta}, \quad (14)$$

where

$a$  = the outer radius of the enclosure (meters),

$d$  = the enclosure thickness (meters),

$\mu = \mu_r \mu_0$  = the magnetic permeability (henrys/meter),

$\delta$  = the skin depth (meters)  $\sqrt{2/\omega \sigma \mu}$ ,

$\sigma$  = the conductivity of the enclosure (siemens), and

$\omega = 2\pi f$  (radians/second).

Equation (14) is valid provided that  $\mu \gg 1$ , which corresponds to an enclosure constructed of a ferromagnetic metal, typically steel. From equation (14) and the definition of the skin depth,  $\delta$ , the frequency dependence of the shielding effectiveness is approximately proportional to the square root of frequency. Over the 5 to 50 kHz frequency range considered in this memorandum, approximately 10 dB of additional shielding would be expected under these assumptions. Returning briefly to the results in figure 12, the transformer characteristic that is the dominant factor influencing the exterior magnetic field at frequencies from 5 to 50 kHz is the shielding effectiveness of the case. In fact, the 200 W transformer was a more serious EMI offender than the 5 kVA unit. For instance, the flux density over the top surface of the Deltec DT25T5 transformer lamination stack is 16 dB more than the highest emission from any surface of the larger 5 kVA transformer. Compared to the top surface of the GE 9T51Y13 3 kVA, the DT25T5 flux density is 18 dB higher.

The conclusion that can be drawn from figure 12 is that an effective transformer shielding enclosure should be constructed of a high-quality steel

alloy with a minimum of seams and openings. Since the strongest fields were over the magnetic core, a cover panel that encloses the stack is essential to reduce the possibility of magnetic-field coupling to nearby circuits and cables.

The next section compares the leakage fields from the test transformers as a function of the input exciting frequency. The results show that the simple shielding effectiveness model, above, is adequate to account for the falloff of the leakage fields with frequency that was observed in most cases.

#### P. COMPARISON OF TRANSFORMER LEAKAGE FIELDS VERSUS FREQUENCY

The leakage fields,  $B/I$ , at the surfaces of the transformers were determined at input frequencies of 5, 15, 25, 35, and 50 kHz. The procedure required the same steps used in obtaining the leakage field versus spacing plots.

The upper two sets of data points in figure 50 show the  $B/I$  versus frequency plot for the top surfaces of the Deltec DT25T5 and GE 9T51Y13 transformers over the lamination stacks. As noted earlier, the highest fields occurred at this location. A susceptor located in proximity with this surface would require the most protection against magnetic-field coupled EMI.

Superimposed on the two sets of data points is a line with a -10 dB per decade slope. The data shown are very accurately represented by this falloff line for frequencies within the 5 to 50 kHz band. Therefore, the normalized transformer leakage fields can be expressed as  $B/I \approx f^{-1/2}$ .

The lower curve in figure 50 is the maximum leakage field generated by the 5 kVA Jefferson Electric transformer. This field originates at the seam that is located at the side of the transformer. The  $B/I$  data also follow the same falloff with frequency slope. However, the excursions from the -10 dB/decade slope line are somewhat greater in this case.

It should be noted that for the DT25T5 and 9T51Y13 transformers, the shielding is within the magnetic-core structure of the transformer, which can be considered a relatively homogenous shielding geometry. This is not the case at the seam in the 5 kVA transformer since flux lines there will emerge distorted from the effects of the reluctance discontinuity at the boundary.

Therefore, it would be expected that external fields at those locations would normally depart to a greater extent from a simple shielding approximation, although in this instance the agreement is still good.

Figure 51 shows the results from the transformer endcap surfaces. These are identified as follows:

1. Primary winding endcap on the Deltec DT25T5,
2. I/O endcap on the GE 3 kVA unit, and
3. Side of the Jefferson Electric 5 kVA unit.

The leakage fields in this case, also, attenuate approximately as the inverse square root of frequency ( $f^{-1/2}$ ). An interesting feature of the Deltec DT25T5 data is the large departure from the -10 dB/decade line at a frequency of 5 kHz. At this endcap surface, the conductor-generated fields and leakage-inductance fields are comparable in magnitude. This results in the inverted magnetic field versus distance characteristic, as noted earlier. At frequencies above 5 kHz, the data points are closer to the -10 dB/decade falloff line.

Figure 55 shows the results for the opposite endcaps. The leakage fields at these locations also decrease at a -10 dB/decade rate. In summary, these results show that, at frequencies from 5 to 50 kHz, most panels of a transformer case can be considered as ideal shielding boundaries. Enclosure surfaces that contain narrow seams and are not regions of maximum leakage field, however, should not be included because of field distortion effects occurring at those locations. Also, the sides of the transformer, if not a maximum leakage-field surface, should be avoided because of the sensitivity of the normal component of magnetic field with respect to probe angle.

#### Q. HIGH FREQUENCY LEAKAGE FIELD MODEL

The results of the previous section suggest that the leakage field at most enclosure surfaces can be expressed by

$$(B/I)_f \text{ in dB} = (B/I)_{f_0} \text{ in dB} - 10 \log_{10} f/f_0 , \quad (15)$$

where

$(B/I)_f$  is the perpendicular component of leakage flux density relative to one ampere of primary current at a frequency of  $f$  Hz (decibels),

$(B/I)_{f_0}$  = the normalized flux density, B/I, evaluated at  $f_0$  Hz, and

$f_1, f_0$  = the compared frequencies,  $f_0 < f$ .

Equation (15) can also be written as

$$(B/I)_f = (B/I)_{f_0} (f/f_0)^{-1/2}, \quad f_0 < f. \quad (16)$$

If  $(B/I)_{f_0}$  is taken to be the value of B/I at the lowest frequency in the band, 5 kHz in this case,  $(B/I)_f$  at any frequency between 5 and 50 kHz is expressible as

$$(B/I)_f = C(f/f_0)^{-1/2}, \quad f_0 < f, \quad (17)$$

with  $C = (B/I)_{f_0}$ .

The conversion of the normalized values of B/I, in equation (17), above, to absolute values of B(f) and I(f) presumes that for some input range of exciting currents the variables B and I can be linearized, e.g., increasing the primary current by 6 dB results in a corresponding 6 dB increase in the leakage field. A limited amount of testing involving changes in the input amplitude of the broadband noise generator suggested this to be a reasonable first approximation. Equation (16) then becomes

$$B(f) = CI(f)(f/f_0)^{-1/2}. \quad (18)$$

#### R. RELATIONSHIP OF PRIMARY-CURRENT SPECTRUM $I(f)$ TO SUSCEPTOR-COUPLED EMI

The noise voltage coupled into a susceptible circuit that is located in the leakage field of the transformers can be obtained by substituting the flux density results of equation (18) into equation (1). The maximum open-circuit voltage is given by

$$|e| = |\partial\phi/\partial t| = NA\omega B \quad (19)$$

$$\begin{aligned} &= 2\pi f NACI(f)(f/f_0)^{-1/2} \\ &= 2\pi NACI(f)(f_0 f)^{1/2}, \quad f_0 < f, \end{aligned} \quad (20)$$

with

$\partial\phi/\partial t$  = the time rate of change of flux leakages coupling into the susceptor loop area,

$|e|$  = maximum open-circuit voltage,

$\omega = 2\pi f$ ,

B = the equivalent sinusoidal exciting flux density,

NA = the capture area of the susceptor, and

C =  $(B/I)_{f_0}$ .

In equation (20), the coupling voltage depends on the primary-winding current spectrum, I(f). This spectrum variation can be continuous, such as that used in the broadband tests, or it can be discrete, as from powerline harmonics generated as the result of using various nonlinear loads.

The behavior of the coupling voltage with respect to the current spectrum, I(f), in either case, can be examined for specific threshold envelopes. The selected spectral envelopes are

1.  $I(f) = f^{-1} = 1/f$ ,
2.  $I(f) = f^{-1/2}$ , and
3.  $I(f) = f^{-1/2} + \alpha$ , where  $\alpha$  = positive constant.

For  $I(f) = 1/f$ , equation (20) becomes

$$|e| = 2\pi NACf_0^{1/2}f^{-1/2}. \quad (21)$$

If there is no EMI problem at the baseband frequency  $f_0$ , it is also unlikely at higher frequencies, since the maximum open-circuit voltage decreases at a -10 dB/decade rate throughout the band.

For  $I(f) = f^{-1/2}$ ,

$$|e| = 2\pi NACf_0^{1/2}. \quad (22)$$

The maximum open-circuit voltage is constant for all frequencies, therefore no EMI problem is likely to occur.

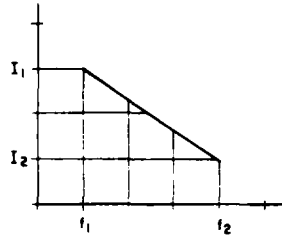
For  $I(f) = f^{-1/2} + \alpha$ ,  $\alpha$  = positive constant,

$$|e| = 2\pi NACf_0^{1/2}f^\alpha. \quad (23)$$

In this case, the susceptor voltage increases continuously with frequency, creating a potentially serious EMI problem. The severity of the coupling depends on the constant,  $\alpha$ , which is a measure of how much slower the

current spectrum decreases relative to a -10 dB/decade rate. For discrete powerline harmonics, this is equivalent to the condition

$$\left| \frac{I_2 - I_1}{f_2 - f_1} \right| < 10 \text{ dB/decade ,} \quad (24)$$



where

$I_2$  = the rms current amplitude in dB at a frequency of  $f_2$  Hz,

$I_1$  = the rms current amplitude in dB at a frequency of  $f_1$  Hz, and

$f_2, f_1$  = the frequencies in Hz,  $f_2 \gg f_1$ .

The quantity  $(I_2 - I_1)/(f_2 - f_1)$  represents the slope of the line connecting the peaks of the spectral components that are being compared.

#### S. LEAKAGE FIELD VERSUS DISTANCE MODELS

The leakage field versus distance plots discussed earlier were converted, based on a conversation with R. Showers, of the University of Pennsylvania, to a coordinate system whose origin was taken as the approximate center of the primary/secondary windings. This change was equivalent to an axis translation from the surface of the transformer case to a point near the transformer center approximately equal to one-half the vertical height of the unit away. From figures 1, 2, and 3, those distances for the Deltec DT25T5, GE 9T51Y13, and Jefferson Electric units are 6.1, 5.6, and 7.9 cm, respectively.

The basis for this change is that it relates the leakage fields to a frame of reference located at the source of the fields. Clearly this is only valid for the magnetic fields generated by the primary and secondary leakage inductances. Transformer surfaces where the leakage field contained large contributions from internal conductors are excluded in this analysis.

The distances,  $R$ , of the field points from the approximate source center that were used are

1. For the Deltec DT25T5 transformer,

$$R = d + D_0 + R_0 = d + 7.8 \text{ cm} , \quad (25)$$

since  $D_0 = 1.72 \text{ cm}$  and  $R_0 = 6.1 \text{ cm}$ .

2. For the GE 9T51Y13 transformer,

$$R = d + D_0 + R_0 = d + 7.3 \text{ cm} , \quad (26)$$

since  $D_0 = 1.72 \text{ cm}$  and  $R_0 = 5.6 \text{ cm}$ .

3. For the Jefferson Electric transformer,

$$R = d + D_0 + R_0 = d + 9.6 \text{ cm} , \quad (27)$$

since  $D_0 = 1.72 \text{ cm}$  and  $R_0 = 7.9 \text{ cm}$ .

The parameters  $d$  and  $D_0$  are defined as  $d$  = the probe distance measured from the surface of the transformer and  $D_0$  = the probe loop center spacing for  $d = 0$ .

Figure 52 shows  $B/I$  as a function of distance from the top surface of the Deltec DT25T5 transformer measured relative to the center,  $R$ . The plotted points are the results for the extreme ends of the band, i.e., at 5 and 50 kHz.  $B/I$  at frequencies of 15, 25, and 35 kHz are shown in the adjoining table (figure 52b).

At the surface of this transformer, the flux density decreases very rapidly with separation distance ( $1/R^3$ ). At a distance approximately equal to 2.5 times the distance  $R_0$ , the leakage field begins to decrease at a slower rate ( $1/R^2$ ). This behavior is defined as

$$\begin{aligned} \text{for } R < 2.5R_0, B/I \text{ is proportional to } 1/R^3 , \\ \text{for } 2.5R_0 > R < 5R_0, B/I \text{ is proportional to } 1/R^2 , \end{aligned} \quad (28)$$

where  $R_0$  is the transformer vertical half-distance, which is equal to 6.1 cm for the Deltec DT25T5 transformer.

Figures 53 and 54 are the results from the side and primary endcap surfaces, respectively, of the Deltec DT25T5 transformer. The agreement between all three orthogonal surfaces is excellent. The relation shown in equation (28) is valid for all three sides of the transformer.

Figures 55, 56, and 57 are the results from the top, endcap opposite the I/O connector, and side, respectively, of the GE 9T51Y13 transformer. The same expression used for the Deltec DT25T5 transformer is valid for this transformer, also, i.e.,

for  $R < 2.5R_0$ ,  $B/I$  is proportional to  $1/R^3$ ,

for  $2.5R_0 > R < 5R_0$ ,  $B/I$  is proportional to  $1/R^2$ ,

where  $R_0$  is the transformer half-distance, which is equal to 5.6 cm.

Because of the relatively low emissions from the Jefferson Electric 5 kVA transformer, some field-inversion effects were present at all surfaces other than the side seam and an endcap. The maximum leakage field from this transformer was generated at the side seam.

#### T. EMI IMPLICATIONS OF THE TEST RESULTS

Combining the results above and equation (18), the leakage flux density from the transformers can be expressed as

$$B(f, R) = \left(\frac{B}{I}\right)_{f_0, R_0} I(f) \left(\frac{f}{f_0}\right)^{-1/2} \left(\frac{R_0}{R}\right)^3, \quad R_0 < R < 2.5R_0, \quad (29)$$

$$B(f, R) = \left(\frac{B}{I}\right)_{f_0, R_0} I(f) \left(\frac{f}{f_0}\right)^{-1/2} \left(\frac{1}{2.5}\right)^3 \left(\frac{1}{R^2}\right), \quad 2.5R_0 < R < 5R_0. \quad (30)$$

The coefficients in equation (30) are obtained by inserting  $R = 2.5R_0$  into equation (29). The parameters in equations (29) and (30) are

$R$  = the distance from the field point to the center of the transformer in the same units as  $R_0$ ,

$R_0$  = the distance from the case to the center of the transformer,

$f$  = the input harmonic frequency (Hz),

$f_0$  = the frequency of the lower band edge,  $f_0 = 5$  kHz,

$I(f)$  = the input harmonic primary current, and

$\left(\frac{B}{I}\right)_{f_0, R_0}$  = the normalized perpendicular component of flux density per ampere of primary current at the enclosure surface,  $R = R_0$  at 5 kHz.

The absolute magnitudes of leakage field given by equations (29) and (30) require as inputs the parameters  $R$ ,  $f$ ,  $I(f)$ , and  $(B/I)_{f_0, R_0}$ . Factors that influence the value of  $(B/I)_{f_0, R_0}$  include the shielding effectiveness of the enclosure, kVA rating, and details of the transformer design. The leakage fields along the three orthogonal axes require values of  $(B/I)_{f_0, R_0}$  for the tops, sides, and the endcap locations. If, as in most EMI applications, the worst case or largest magnetic field is of primary concern, only one parameter is needed. The appropriate value of  $(B/I)_{f_0, R_0}$  is taken at the location corresponding to the highest emitting surface. At the present time,  $(B/I)_{f_0, R_0}$  must be determined by a test similar to the procedure described in this memorandum. In this case, however, the process is simply a single measurement at a frequency of 5 kHz taken in direct contact with the transformer enclosure,  $R = R_0$ .

In the future, it appears likely that  $(B/I)_{f_0, R_0}$  can be obtained by calculation based on the specific characteristics of a given transformer design. This capability would permit estimates of the leakage-field strengths from transformers to be predicted with improved confidence. It would, subsequently, add to the effectiveness of various protective-margin calculations used to assess shipboard equipment compatibility. These would include a wide variety of interactions, such as cabinet-to-cabinet, cabinet-to-cable, and cabinet-to-connector, where magnetic fields at frequencies up to 50 kHz have been known to be a major source of performance degradation in shipboard systems.

In examining equations (29) and (30), it should be noted that, at close distances to the transformer,  $R < 2.5R_0$ , the leakage inductance behaves similar to a magnetic dipole with respect to the magnetic-field dependence on the separation distance,  $1/R^3$ .

This inverse  $R^3$  relationship leads to a rapid decrease of magnetic-field strength within a short distance from the enclosure surface. The significance of the limiting distance,  $R = 2.5R_0$ , in equations (29) and (30) is that it appears to represent the distance from the transformer case where the internal conductor-generated magnetic fields become comparable in magnitude to the leakage fields. For  $R > 2.5R_0$ , they exceed the leakage fields and decrease at a slower rate,  $1/R^2$ , given by equation (13) for a conductor line pair.

## CONCLUSIONS

The leakage magnetic fields from power transformers were studied using a broadband Gaussian noise generator to simulate the effects of powerline harmonics at frequencies from 5 to 50 kHz. Normalizing the magnetic fields to 1 A of primary current ( $B/I$ ) proved to be an effective method of compensating for current variations resulting from the effects of impedance changes and harmonic distortion by the transformer magnetic core.

A program was written for the HP-25C calculator to compute the flux densities generated by the transformers in the vicinity of the tops, sides, and endcaps of several transformers ranging from 200 W to 5 kVA in power rating. In addition, the magnetic fields at seams, gratings, and I/O connector were included in the analysis.

It was shown that the leakage magnetic fields from transformers rated at 200 W to 5 kVA could be modeled accurately from 5 to 50 kHz. The model contains terms that depend on the following factors:

1. The distance from approximately the center of the transformer to the field point,  $R$ ,
2. The shielding effectiveness of the case, and
3. The current spectrum of the input harmonics.

At distances close to the transformer enclosure,  $R < 2.5R_0$ , the fields are inverse  $R^3$ ; at greater distances, the inverse  $R^2$  relationship applies. The limit,  $R = 2.5R_0$  (where  $R_0$  is the half-distance of the transformer), represents a transition between regions where the leakage inductance and internal conductor-generated magnetic fields, respectively, are dominant.

At some transformer surfaces, the magnetic fields "inverted", increasing with greater separation distance from the case. Within this inversion distance, spacing a susceptor to reduce EMI is counterproductive, resulting instead in higher magnetic-field coupled noise voltages.

TM 801173

#### ACKNOWLEDGMENTS

The author is grateful to Robert Sniegoski, of Code 343, for valuable help in obtaining the test results and to Ms. Bonnie Wardle, Code 343, for help with the illustrations.

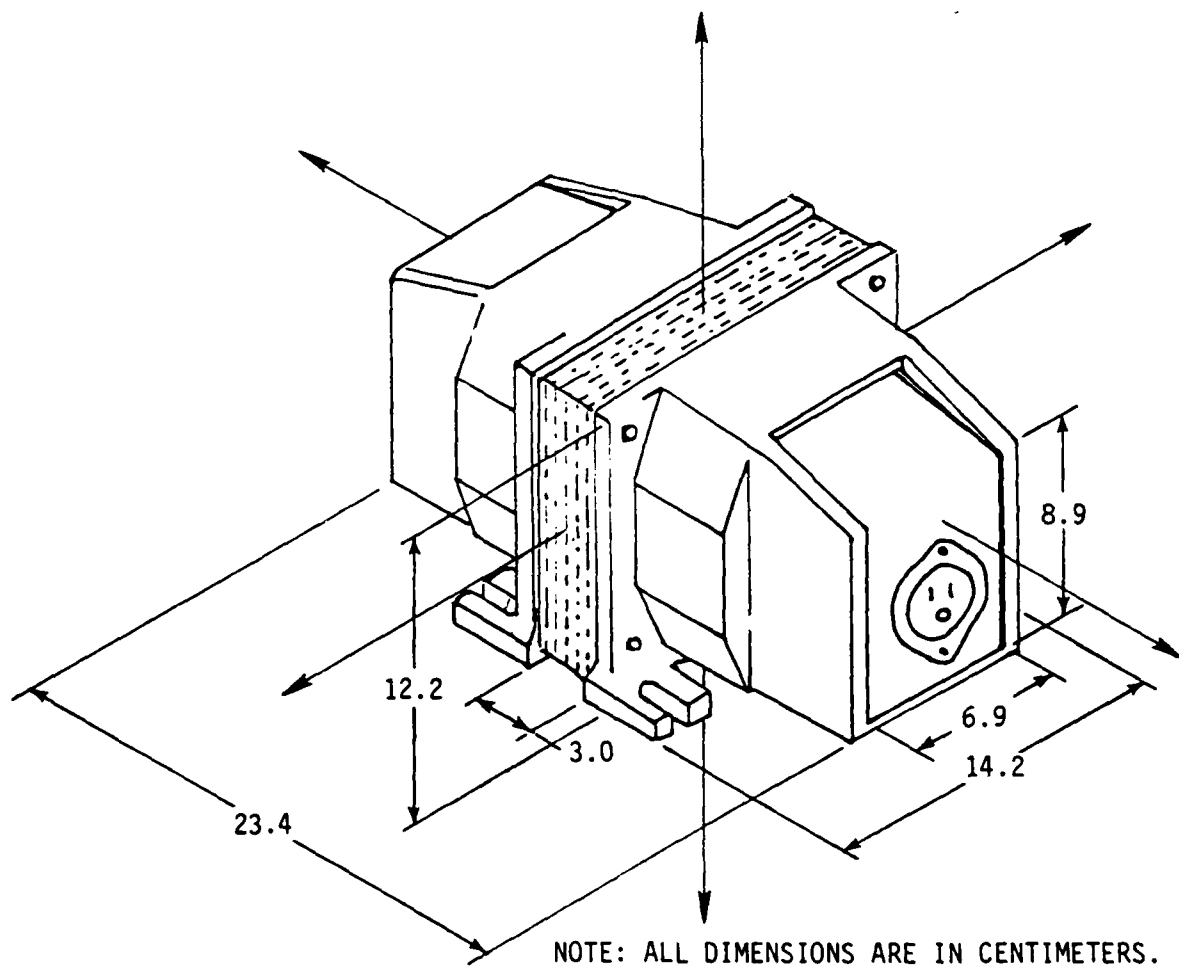


Figure 1. Deltec Corporation DT25T5 200 W Transformer Shown in Relation to a Coordinate System Referenced to its Symmetry Axes

TM 801173

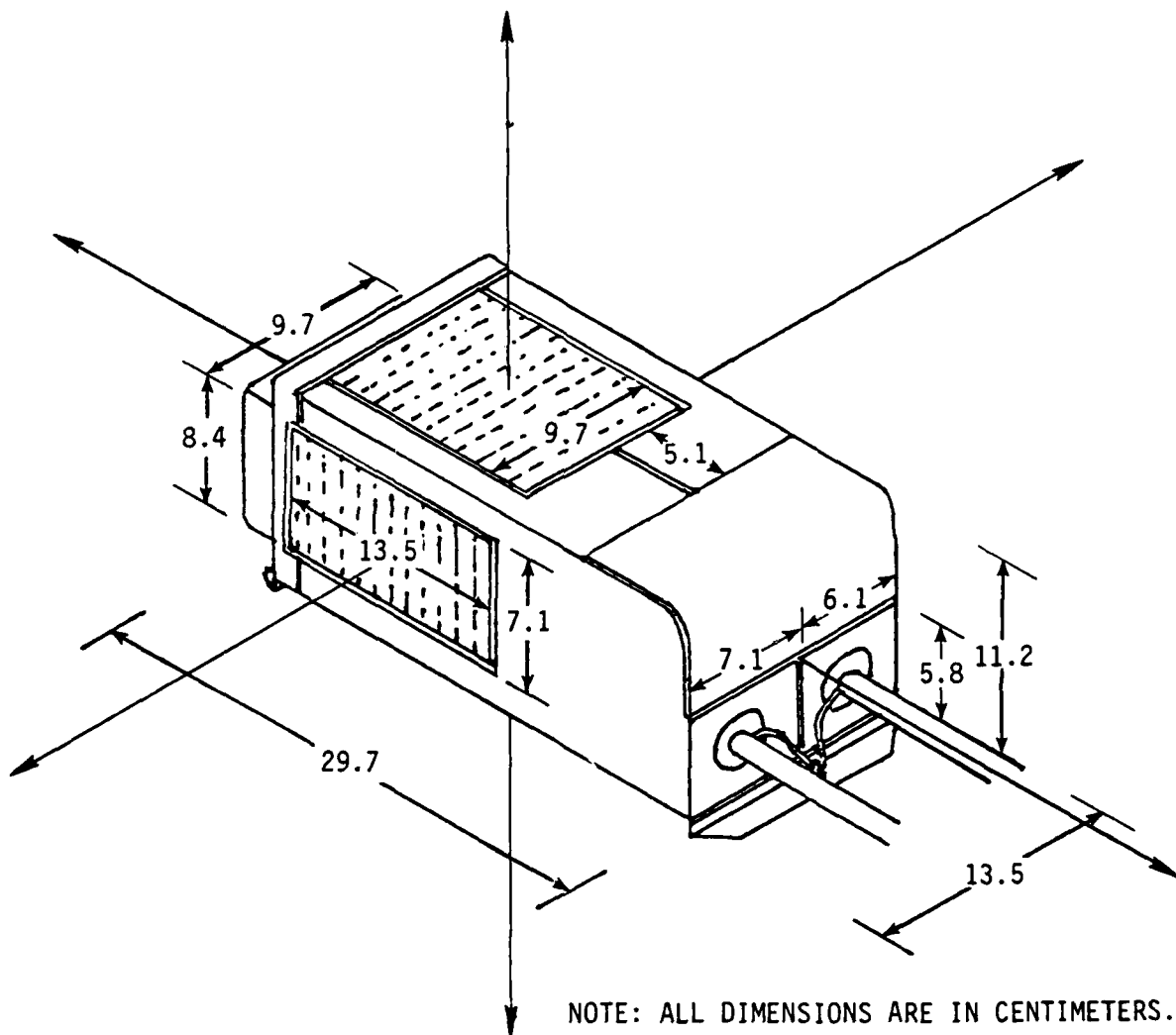


Figure 2. General Electric 9T51Y13 3 kVA Transformer Shown in Relation to a Coordinate System Referenced to its Symmetry Axes

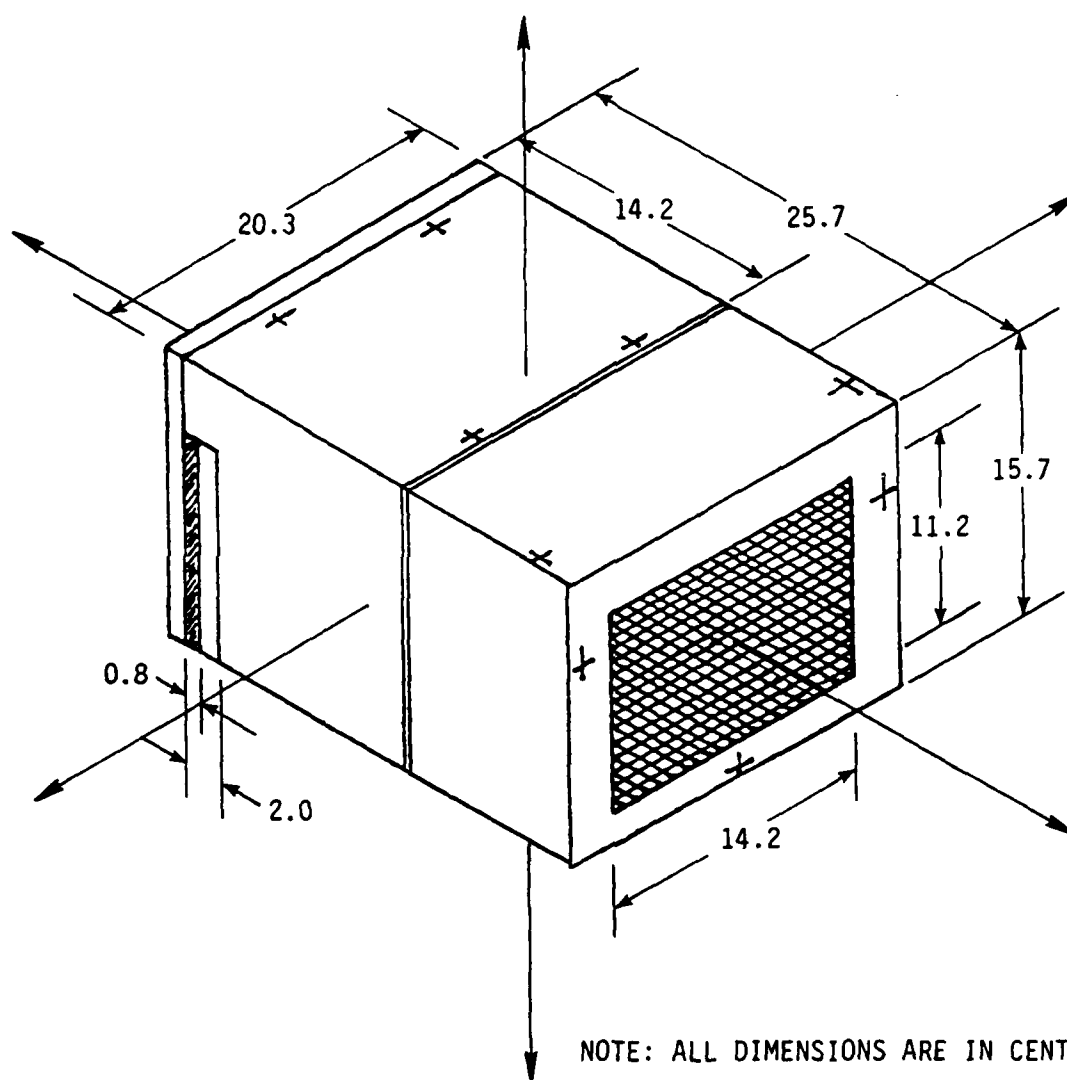


Figure 3. Jefferson Electric 5 kVA Transformer, Serial 12438, Shown in Relation to a Coordinate System Referenced to its Symmetry Axes

TM 801173

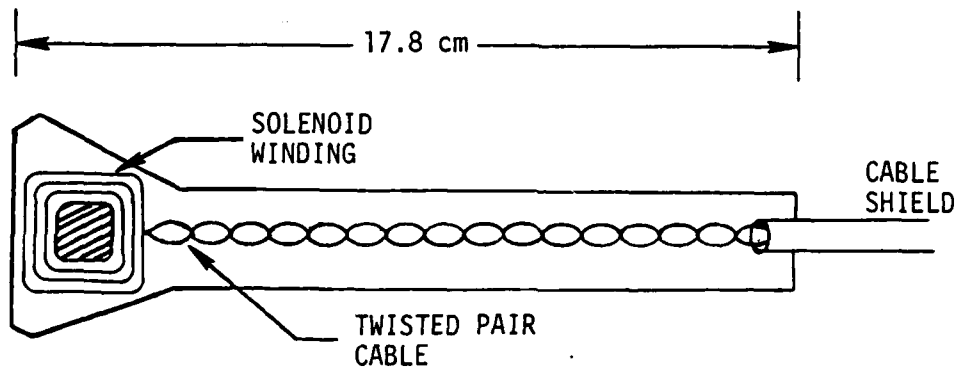


Figure 4. Horizontal Section of the Test Probe Showing Some Construction Details

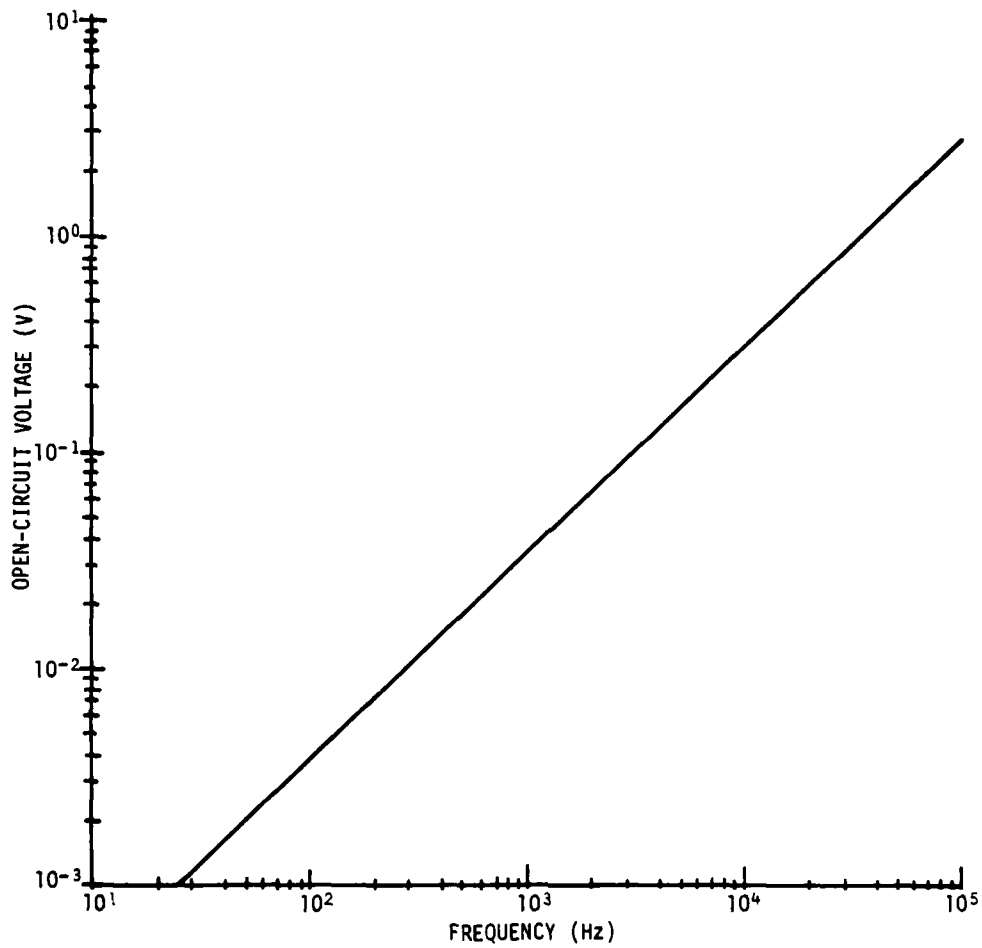


Figure 5. Series-Induced Open-Circuit Probe Voltage for a 1-Gauss Magnetic Field at Frequencies Up to 100 kHz

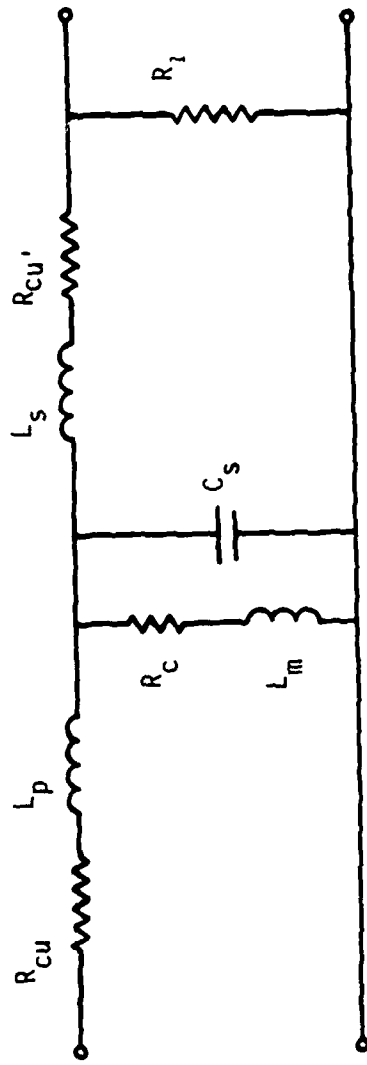


Figure 6. Approximate Transformer Equivalent Circuit  
for a Turns Ratio ( $n$ ) of 1:1

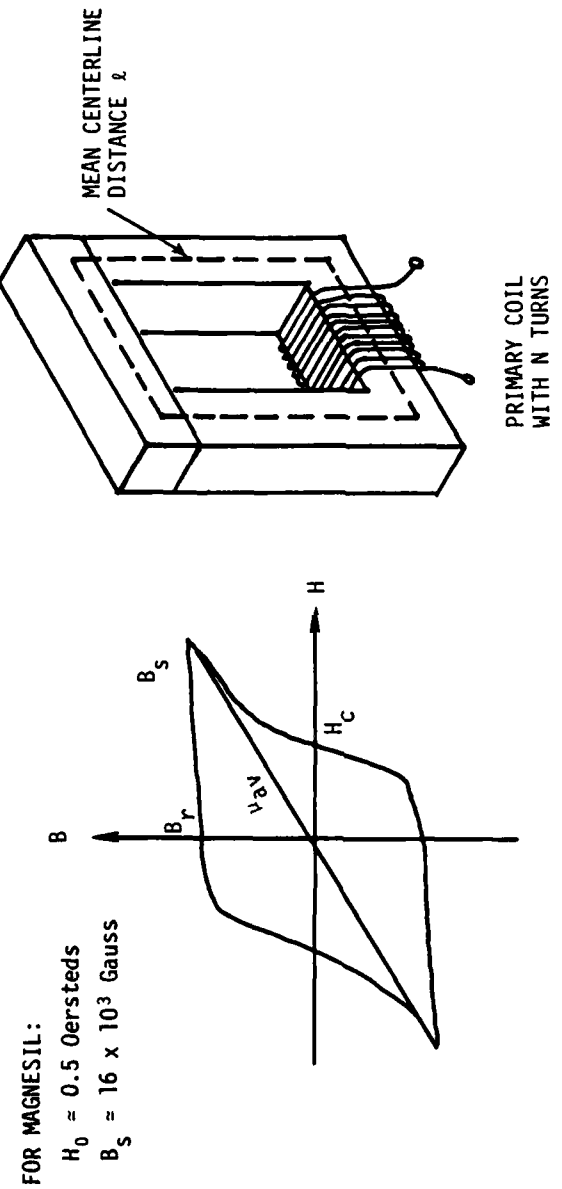


Figure 7a. Hysteresis Loop for a Typical Transformer Lamination Model

Figure 7. Hysteresis Loop for a Typical Transformer Lamination and Transformer Magnetizing Inductance Model

Figure 7b. Transformer Magnetizing Inductance Model

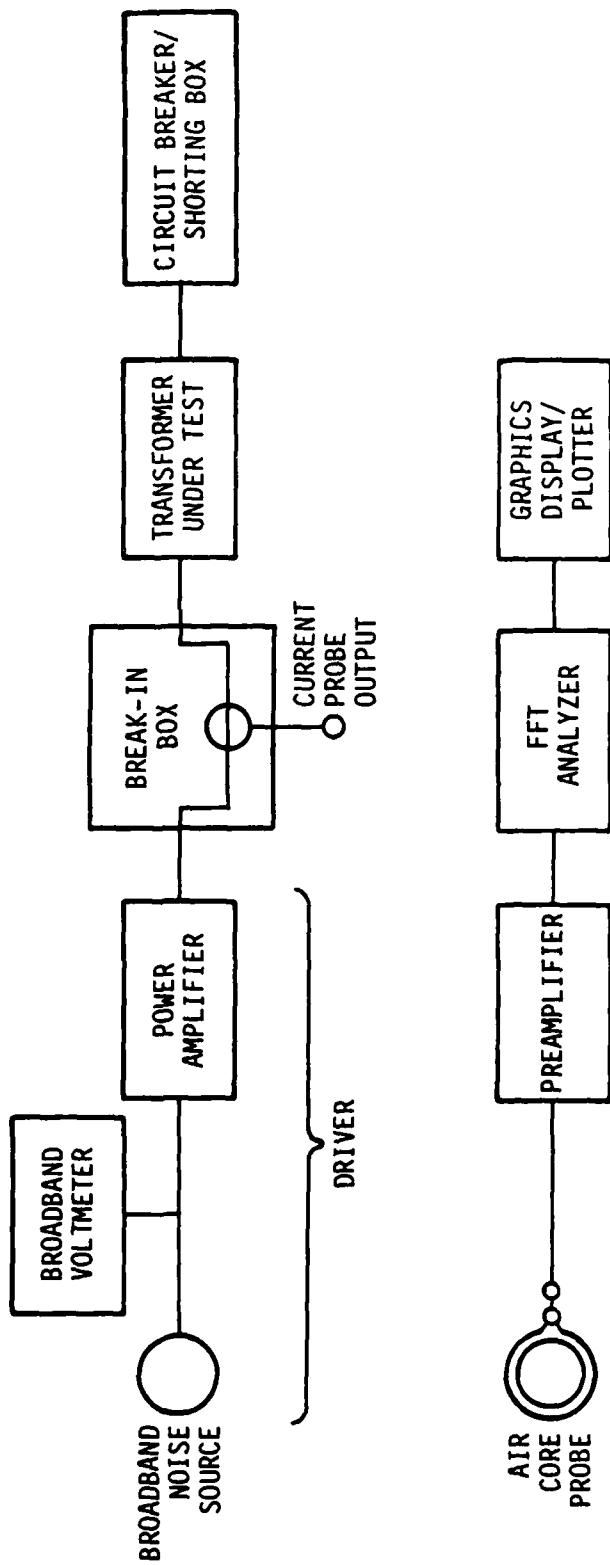


Figure 8. Block Diagram of Wide-Band Measurement System  
Used to Measure Transformer Magnetic Fields

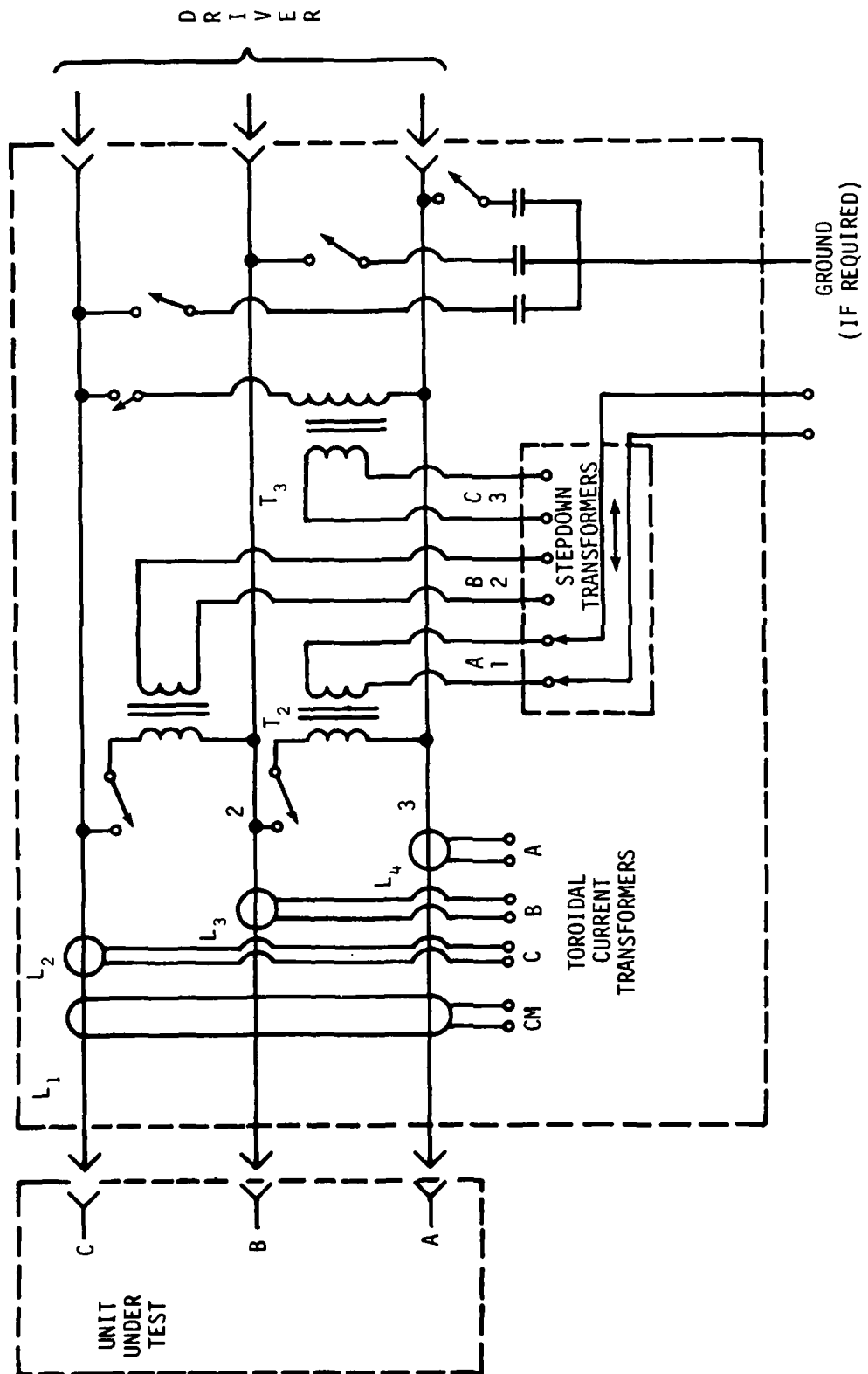


Figure 9. Circuit Diagram of Break-In Box Used in the Wide-Band Instrumentation System

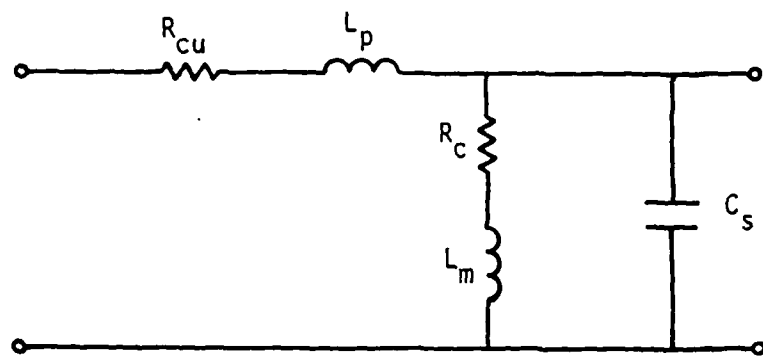


Figure 10a. Open-Circuited Secondary Winding

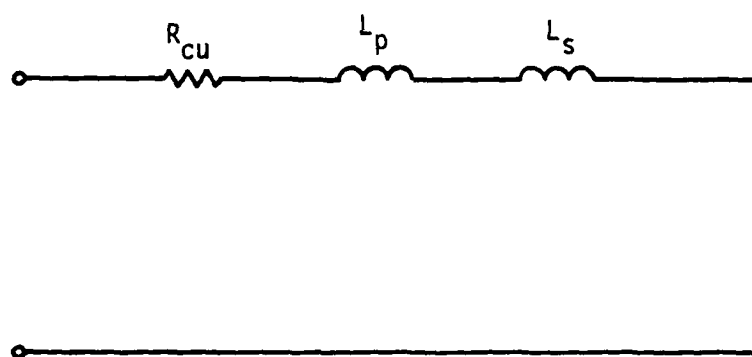


Figure 10b. Short-Circuited Secondary Winding

Figure 10. Approximate Transfer Equivalent Circuits With an  
Assumed Turns Ratio of Unity,  $n = 1:1$

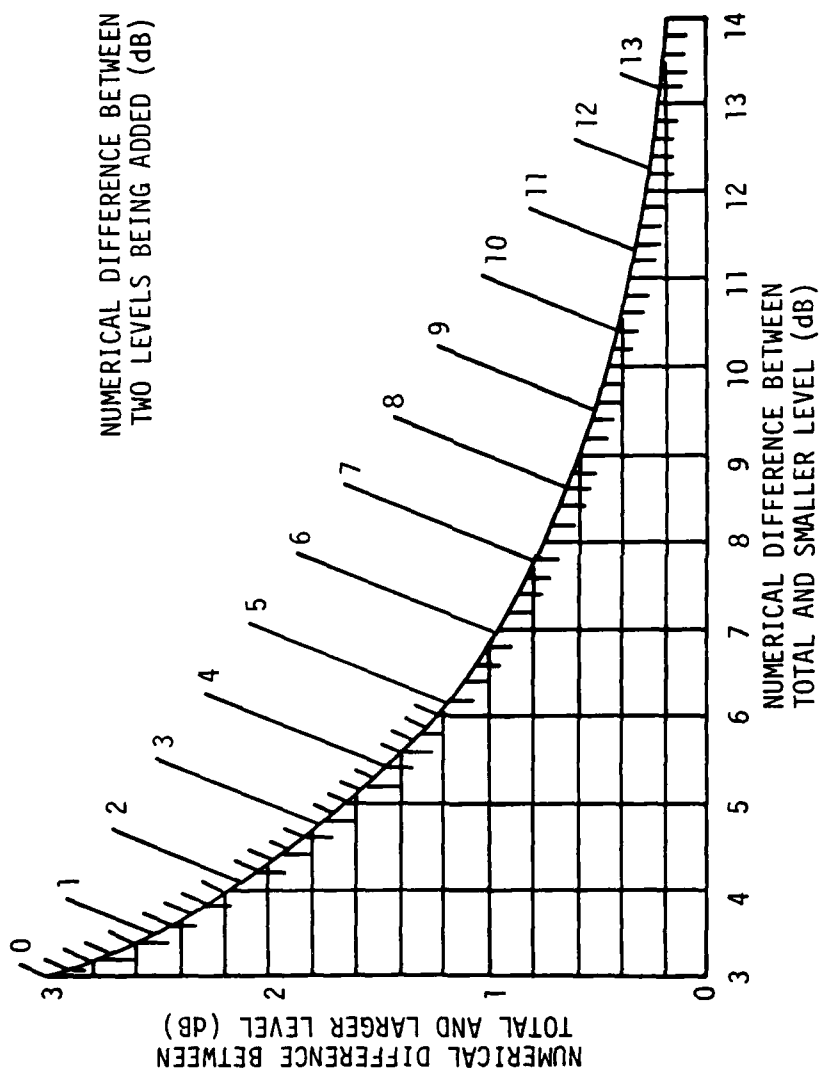


Figure 11. Diagram for Adding or Subtracting Decibels  
(Courtesy of General Radio Co., West Concord, MA)

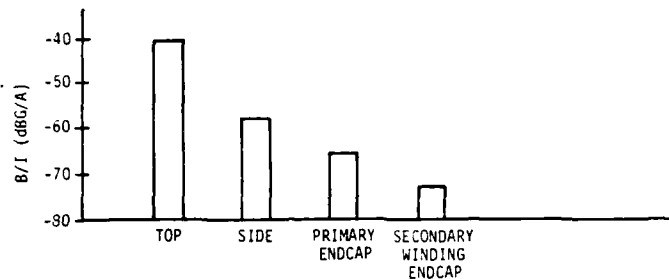


Figure 12a. Deltec DT25T5 200 W Transformer

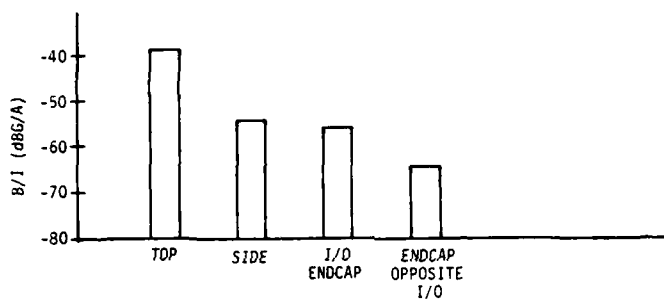


Figure 12b. GE 9T51Y13 2 kVA Transformer

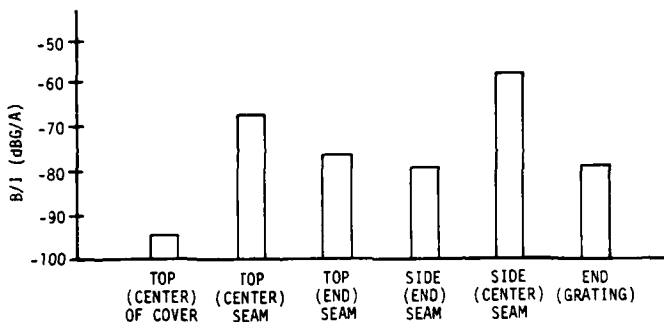


Figure 12c. Jefferson Electric 12438 5 kVA Transformer

Figure 12. Comparison of Flux Density at 25 kHz at Different Locations in the Leakage Field of Transformers Normalized to 1 A of Primary-Winding Current With a Short-Circuited Secondary Winding

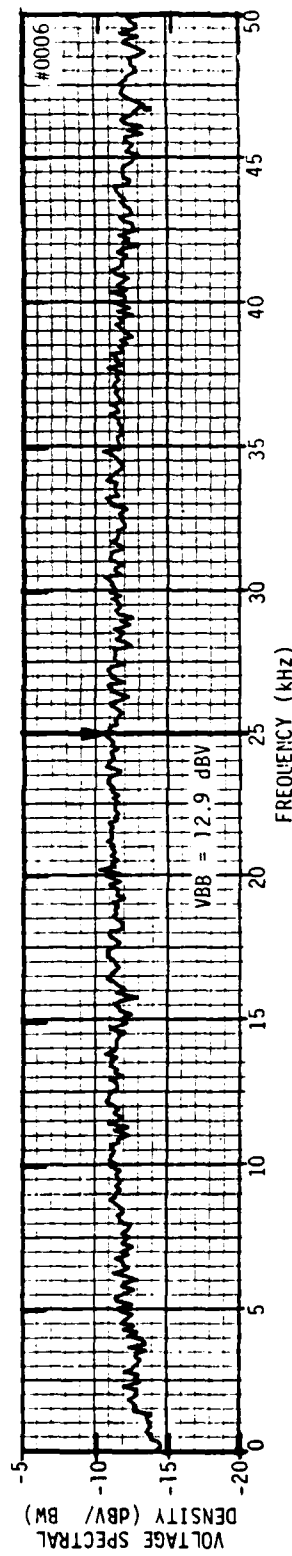


Figure 13a. Voltage Spectral Density at the Input (Primary) of a 200 W Deltec DT25T5 Transformer. The Wide-Band Input (0 - 50 kHz) Was Supplied by a Pseudorandom Noise Generator and a McIntosh Power-Amplifier Driver. The Transformer Secondary Was Shorted.

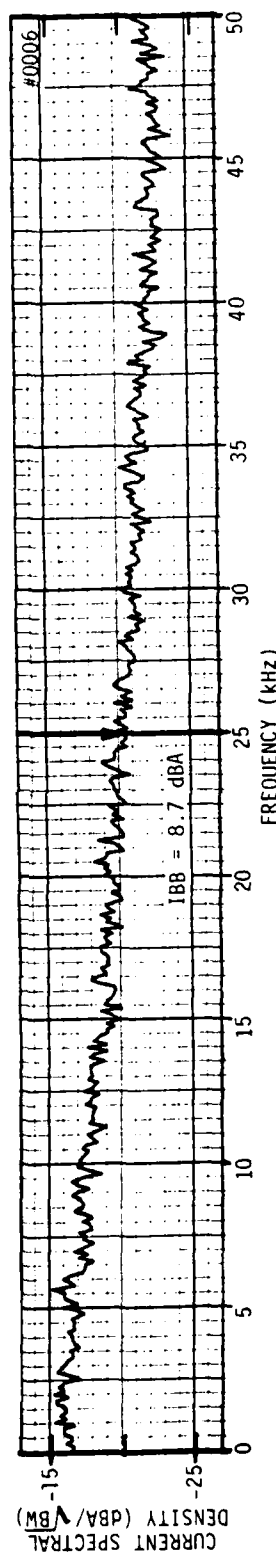


Figure 13b. Current Spectral Density at the Input (Primary Winding) of a 200 W Deltec DT25T5 Transformer for the Same Input Condition and Loading.

Figure 13. Input Voltage and Current Spectral Densities for a 200 W Transformer

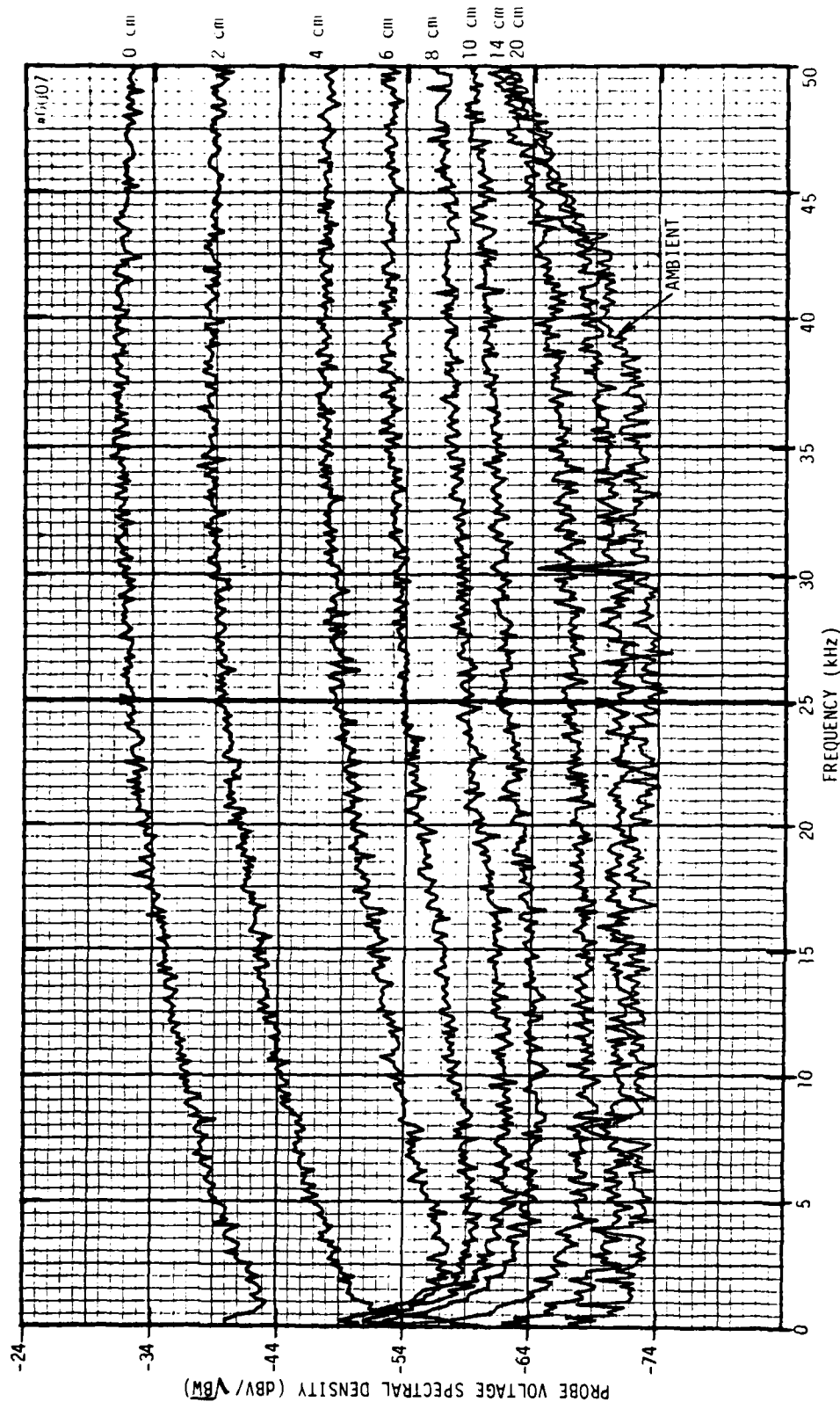


Figure 14. Probe Voltage Spectral Density (dBV/VBW) versus Frequency (kHz) Plots as a Function of Probe Distance From the Top Surface of the DT25T5 200 W Transformer as the Probe Was Moved Along the Vertical Coordinate Axis Shown in Figure 1

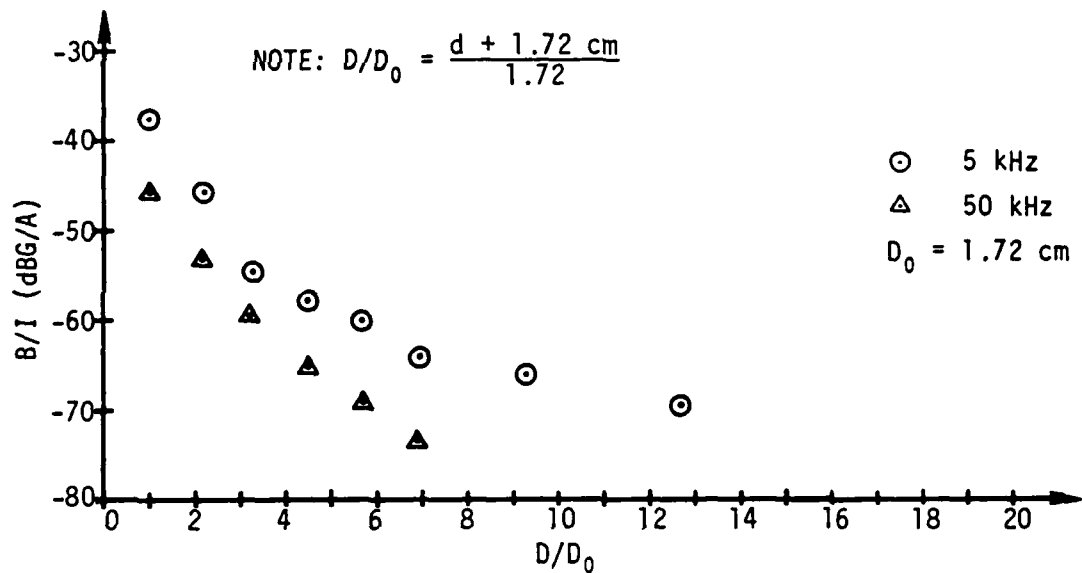


Figure 15a. The Perpendicular Component of Leakage Flux Density in Units of Decibels Relative to 1 Gauss Normalized to 1 A of Primary-Winding Current (B/I) for Frequencies of 5 and 50 kHz. B/I is Shown as a Function of the Probe Spacing Ratio,  $D/D_0$ . The Probe Was Located at the Top Surface of the DT25T5 Transformer Along the Vertical Coordinate Axis Shown in Figure 1.

Frequency (kHz)	d (cm)							
	0	2	4	6	8	10	14	20
15	-38.6	-45.6	-55.6	-60.6	-65.6	-67.6	-71.6	-74.6
25	-40.6	-47.7	-56.3	-61.5	-66.1	-70.3	-75.4	-78.1
35	-41	-48	-57	-62	-67	-70	-75	-83.4*

Figure 15b. B/I Versus Probe Spacing, d, at Frequencies Between the Limits of 5 and 50 kHz Shown Above.

Figure 15. Normalized Flux Density at the Top Surface of the 200 W Transformer (Center of Laminations)

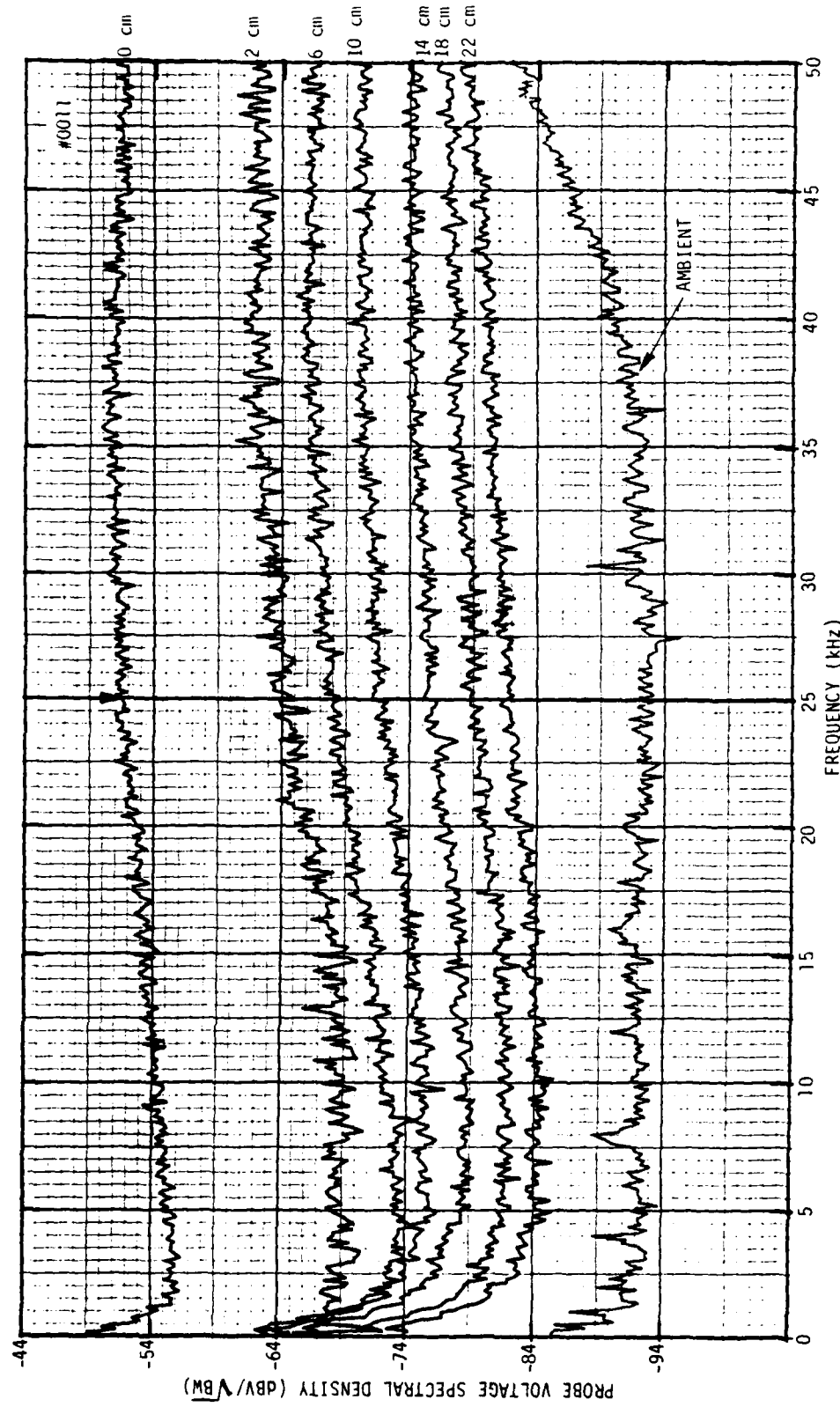


Figure 16. Probe Voltage Versus Frequency Plots as a Function of Probe Distance From the Top Surface of the DT25T5 Transformer as the Probe Was Moved Along a Vertical Axis Intersecting the Edge of the Lamination Stack

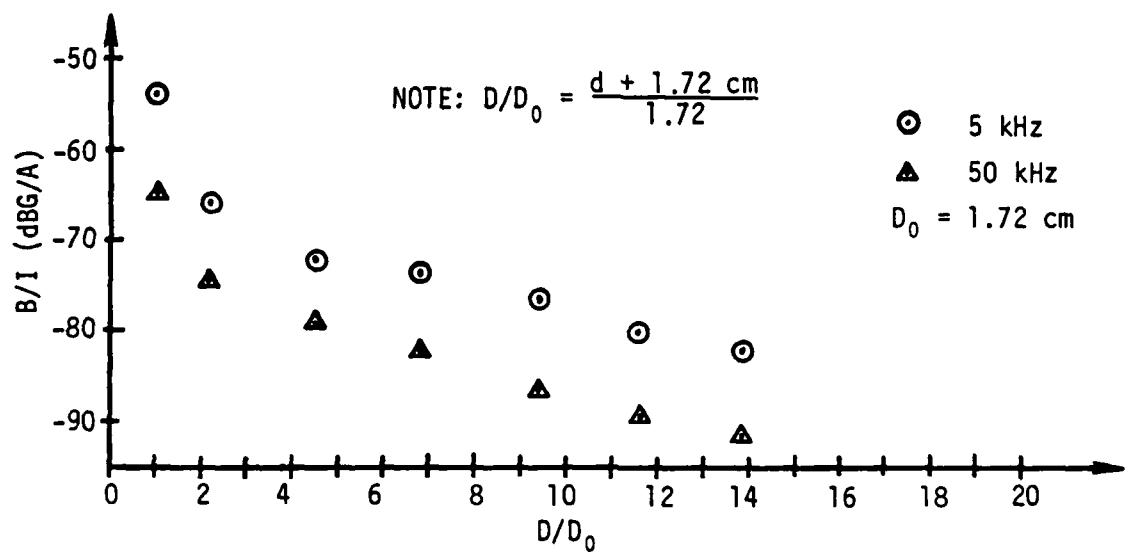


Figure 17a. The Perpendicular Component of Leakage Flux Density in Units of Decibels Relative to 1 Gauss Normalized to 1 A of Primary-Winding Current ( $B/I$ ) for Frequencies of 5 and 50 kHz.  $B/I$  is Shown as a Function of the Probe Spacing Ratio,  $D/D_0$ . The Probe Was Located at the Top Surface of the DT25T5 Transformer Along a Vertical Coordinate Axis Intersecting the Edge of the Lamination Stack.

Frequency (kHz)	$d$ (cm)						
	0	2	6	10	14	18	20
15	-57.6	-71.6	-75.1	-77.6	-81.6	-84.6	-87.6
25	-59.1	-71.7	-76.2	-78.7	-82.9	-86.6	-89.6
35	-60	-71	-75	-79.8	-84	-87.5	-89.8

Figure 17b.  $B/I$  Versus Probe Spacing,  $d$ , at Frequencies Between the Limits of 5 and 50 kHz Shown Above.

Figure 17. Normalized Flux Density at the Top Surface of the 200 W Transformer (Edge of Laminations)

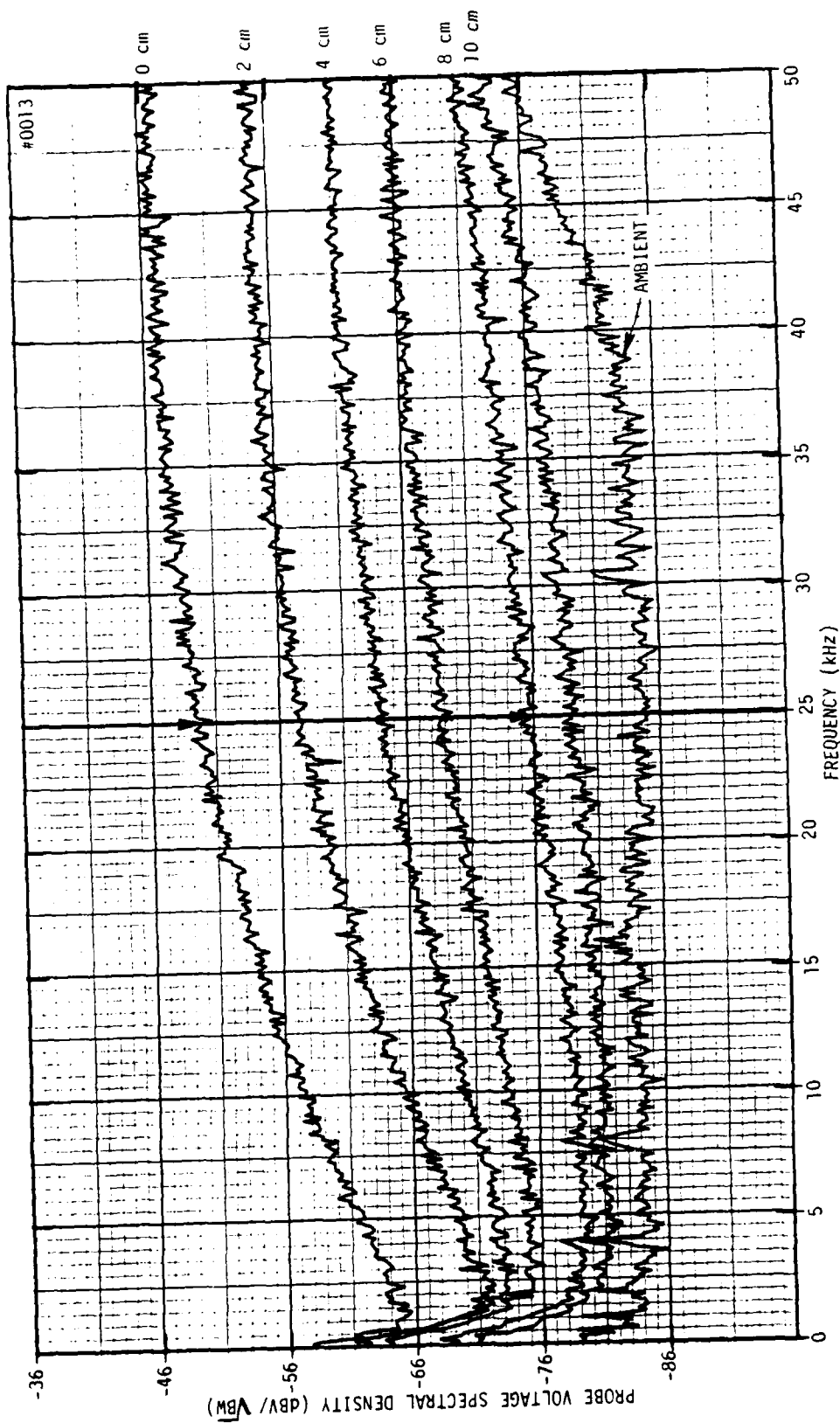


Figure 18. Probe Voltage Versus Frequency Plots as a Function of Probe Distance From the Side of the DT25T5 200 W Transformer as the Probe Was Moved Along the Horizontal Axis Shown in Figure 1

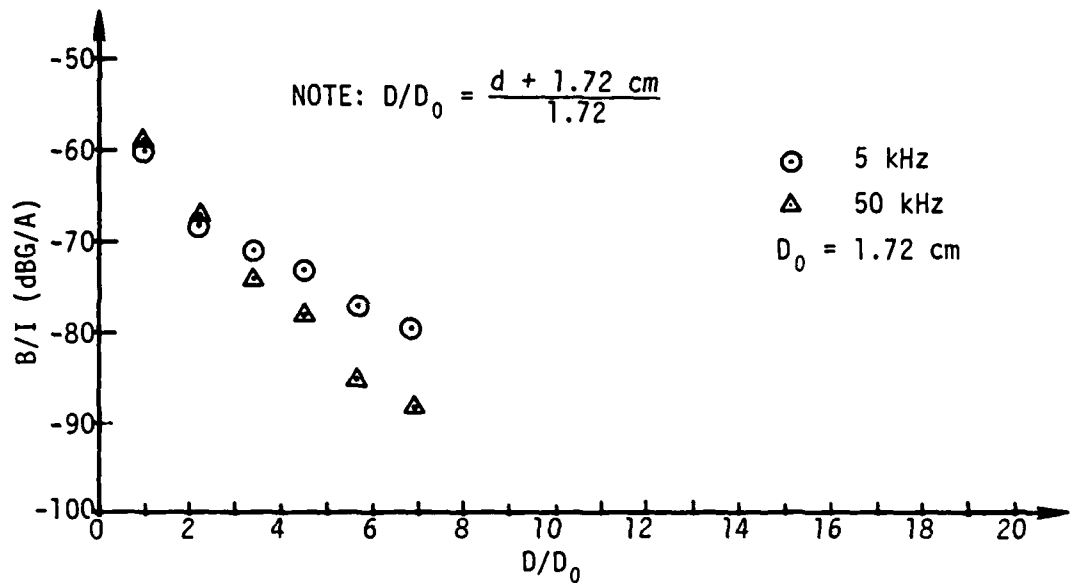


Figure 19a. The Perpendicular Component of Leakage Flux Density in Units of Decibels Relative to 1 Gauss Normalized to 1 A of Primary-Winding Current (B/I) for Frequencies of 5 and 50 kHz. B/I is Shown as a Function of the Probe Spacing Ratio,  $D/D_0$ . The Probe Was Located at the Side of the DT25T5 Transformer Along the Horizontal Coordinate Axis Shown in Figure 1.

Frequency (kHz)	d (cm)					
	0	2	4	6	8	10
15	-57.6	-65.6	-71.6	-75.6	-81.1	-83.6
25	-57.4	-65.5	-71.9	-76.7	-83.4	-86.5
35	-56.5	-65	-71	-76	-83	-86

Figure 19b. B/I Versus Probe Spacing,  $d$ , at Frequencies Between the Limits of 5 and 50 kHz Shown Above.

Figure 19. Normalized Flux Density at the Side of the 200 W Transformer

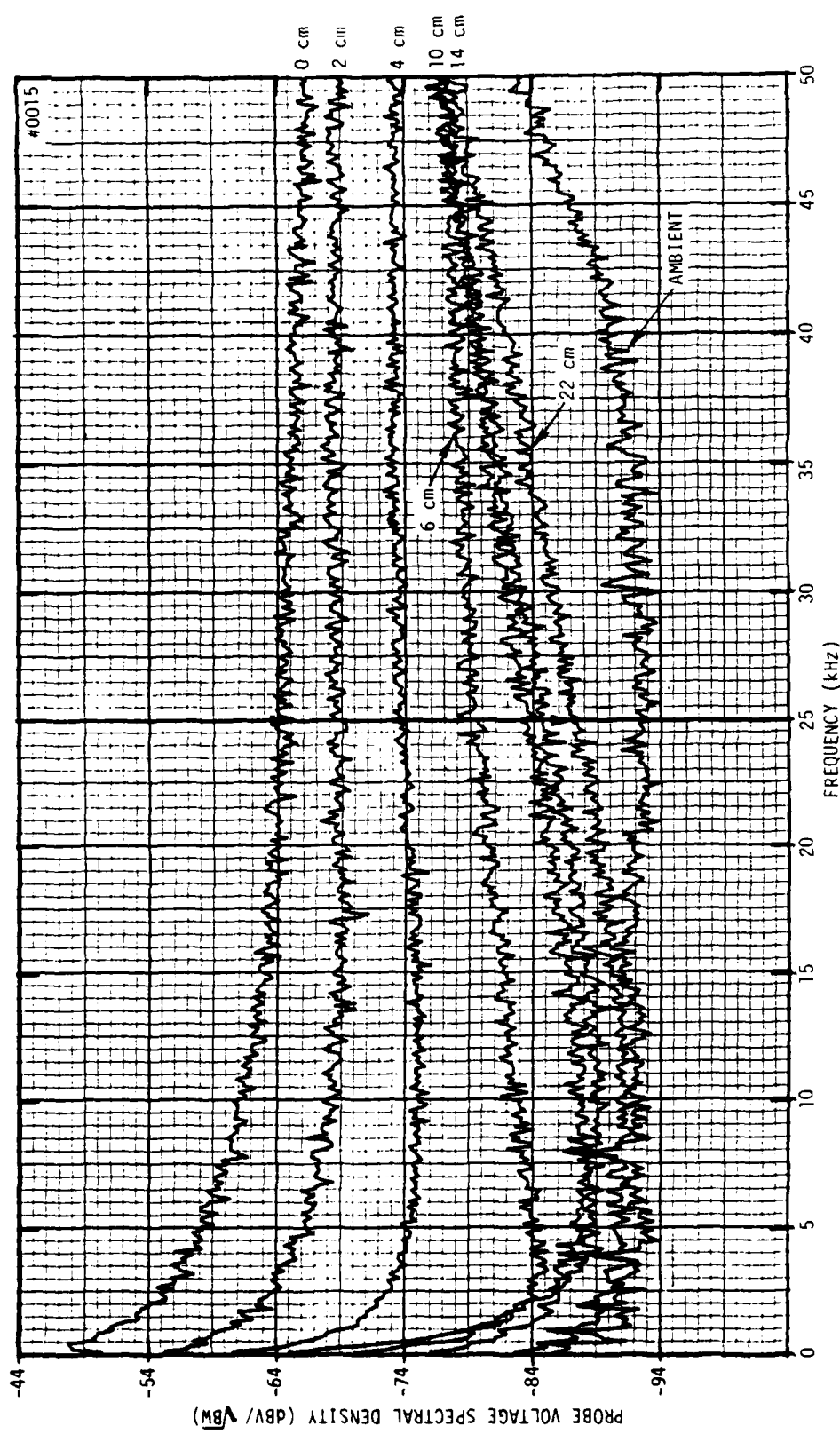


Figure 20. Probe Voltage Versus Frequency Plots as a Function of Probe Distance From the Primary-Side Endcap of the DT25T5 200 W Transformer as the Probe Was Moved Along the Horizontal Axis Intersecting the Endcap Shown in Figure 1

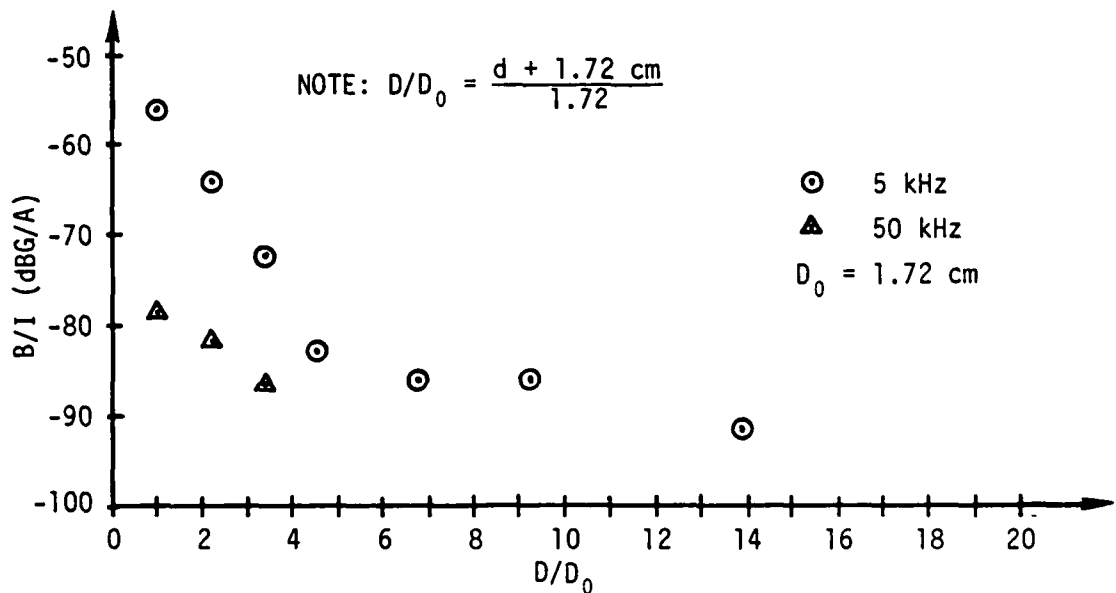


Figure 21a. The Perpendicular Component of Leakage Flux Density in Units of Decibels Relative to 1 Gauss Normalized to 1 A of Primary-Winding Current ( $B/I$ ) for Frequencies of 5 and 50 kHz.  $B/I$  is Shown as a Function of the Probe Spacing Ratio,  $D/D_0$ . The Probe Was Located at the Primary Endcap of the DT25T5 Transformer Along the Horizontal Coordinate Axis Shown in Figure 1.

Frequency (kHz)	$B/I$ (dBG/A)						
	0	2	4	6	10	14	22
15	-66.6	-72.1	-78.6	-85.6	-90.6	-91.6	-93.6
25	-72.6	-76.5	-80.5	-87.3	-90.7	-92.5	-94.6
35	-74	-77.5	-82	-87	-91	-90.5	-93

Figure 21b.  $B/I$  Versus Probe Spacing,  $d$ , at Frequencies Between the Limits of 5 and 50 kHz Shown Above.

Figure 21. Normalized Flux Density at the Primary Endcap of the 200 W Transformer

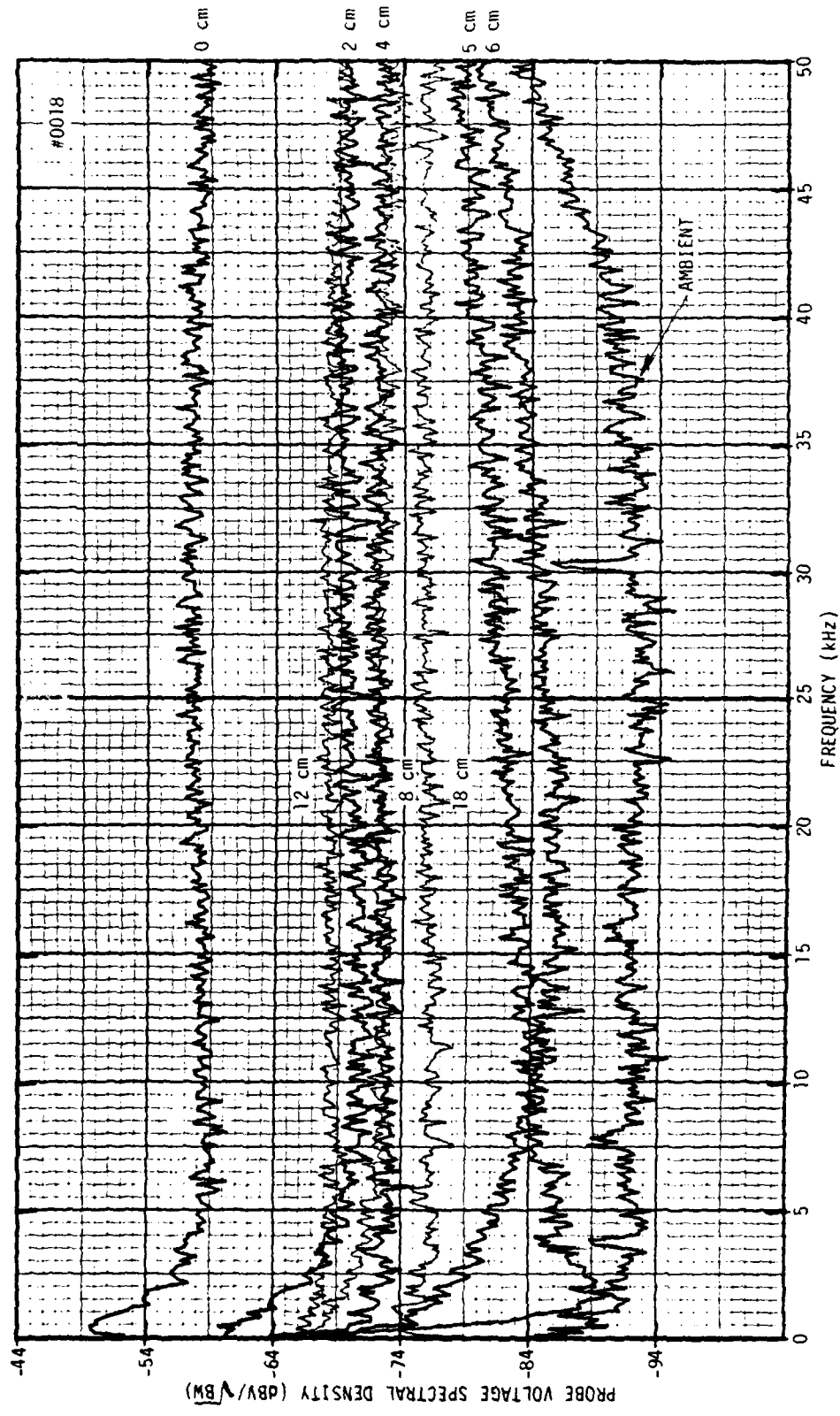


Figure 22. Probe Voltage Spectral Density (dBV/VBW) versus Frequency (kHz) plots for various probe distances from the secondary side endcap of the DT25T5 200 W Transformer

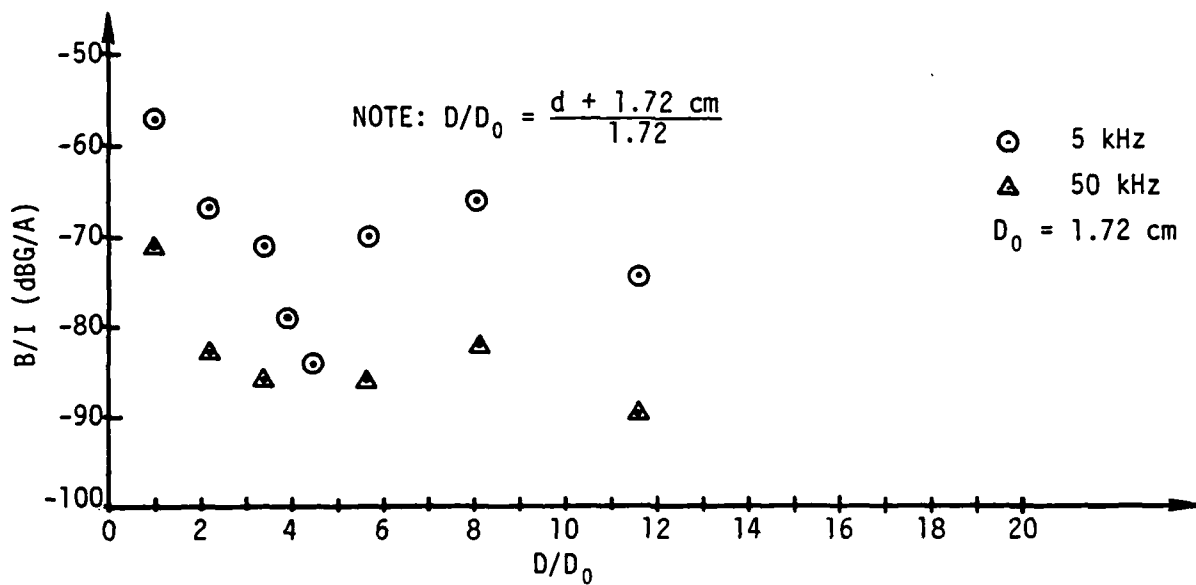


Figure 23a. The Perpendicular Component of Leakage Flux Density in Units of Decibels Relative to 1 Gauss Normalized to 1 A of Primary-Winding Current (B/I) for Frequencies of 5 and 50 kHz. B/I is Shown as a Function of the Probe Spacing Ratio,  $D/D_0$ . The Probe Was Located at the Secondary Side Endcap of the DT25T5 Transformer Along the Vertical Coordinate Axis Shown in Figure 1.

Frequency (kHz)	d (cm)							
	0	2	4	5	6	8	12	18
15	-61.6	-74.1	-76.1	-86.6	-89.6	-76.6	-72.6	-79.6
25	-66.2	-77.4	-79	-88.8	-92.1	-80	-76.1	-82.6
35	-66	-78	-82	-89	-93	-82	-77	-84

Figure 23b. B/I Versus Probe Spacing, d, at Frequencies Between the Limits of 5 and 50 kHz Shown Above.

Figure 23. Normalized Flux Density at the Secondary Endcap of the 200 W Transformer

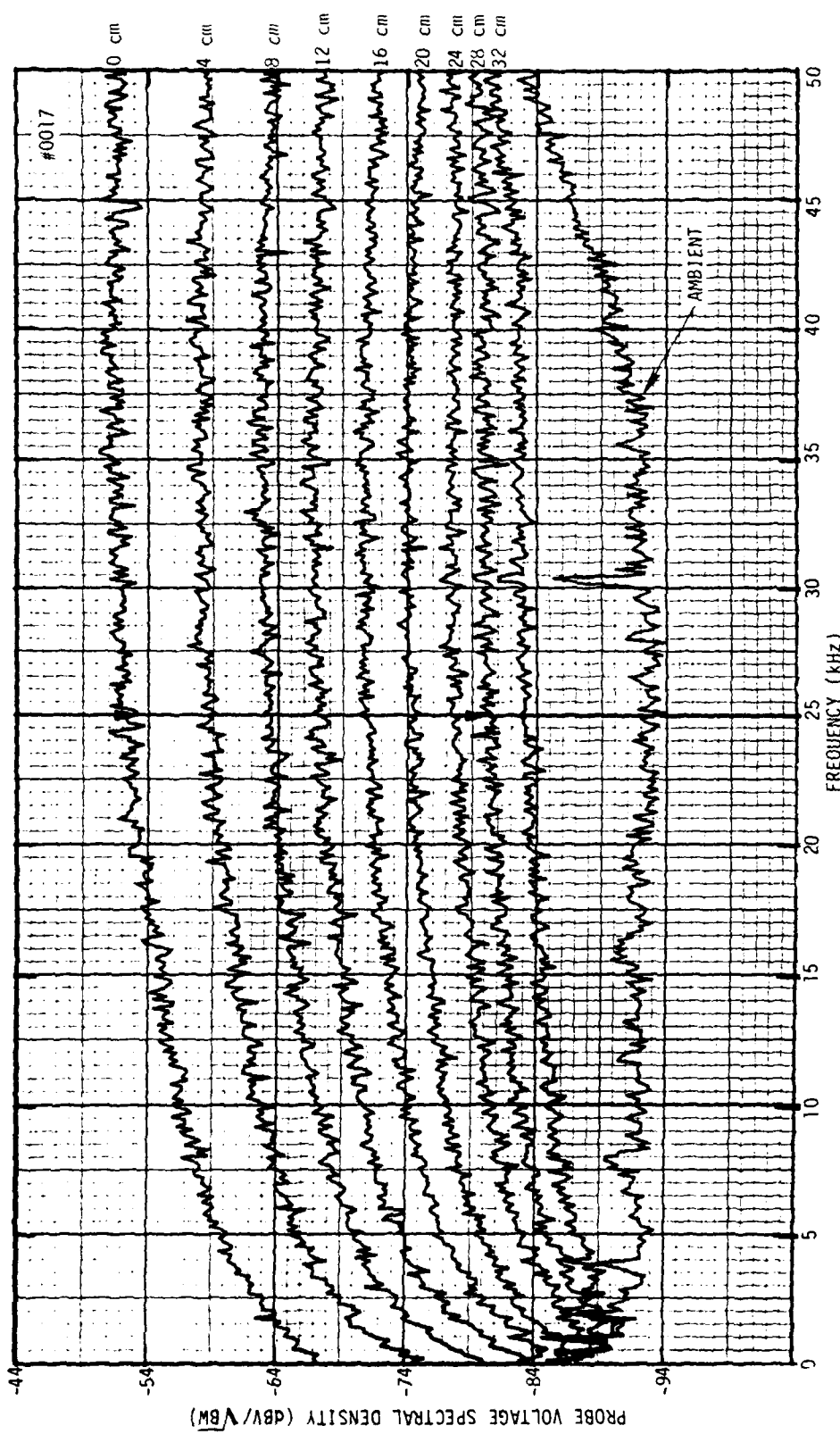


Figure 24. Probe Voltage Versus Frequency Plots as a Function of Probe Distance  
From the Secondary Side Endcap of the DT25T5 200 W  
Transformer (Open-Circuited Secondary)

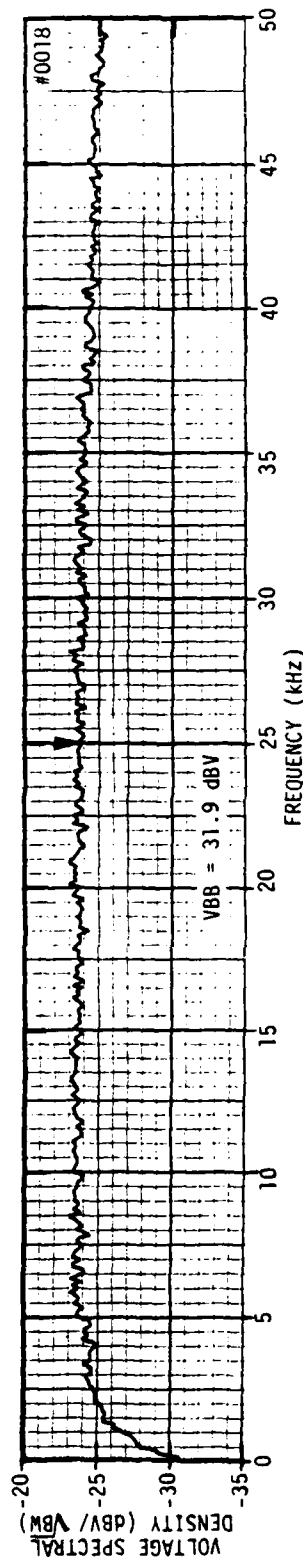


Figure 25a. Voltage Spectral Density at the Input (Primary Winding) of a 3 kVA GE 9T51Y13 Transformer. The Wide-Band Input (0 - 50 kHz) Was Supplied by a Pseudorandom Noise Generator and a McIntosh Power-Amplifier Driver. The Transformer Secondary Was Shorted.

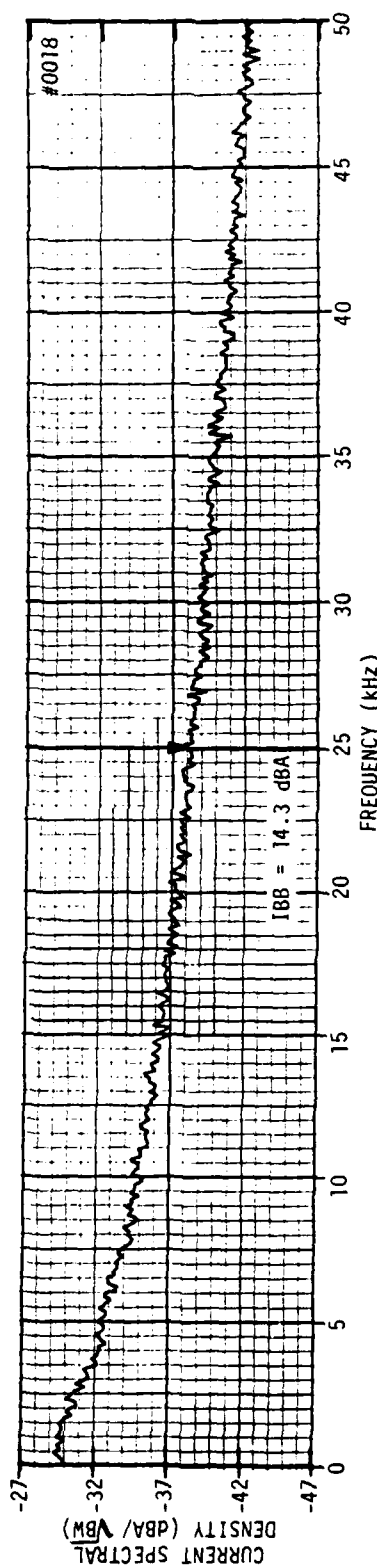


Figure 25b. Current Spectral Density at the Input (Primary Winding) of a 3 kVA GE 9T51Y13 Transformer for the Same Input Condition and Loading.

Figure 25. Input Voltage and Current Spectral Densities for a 3 kVA Transformer

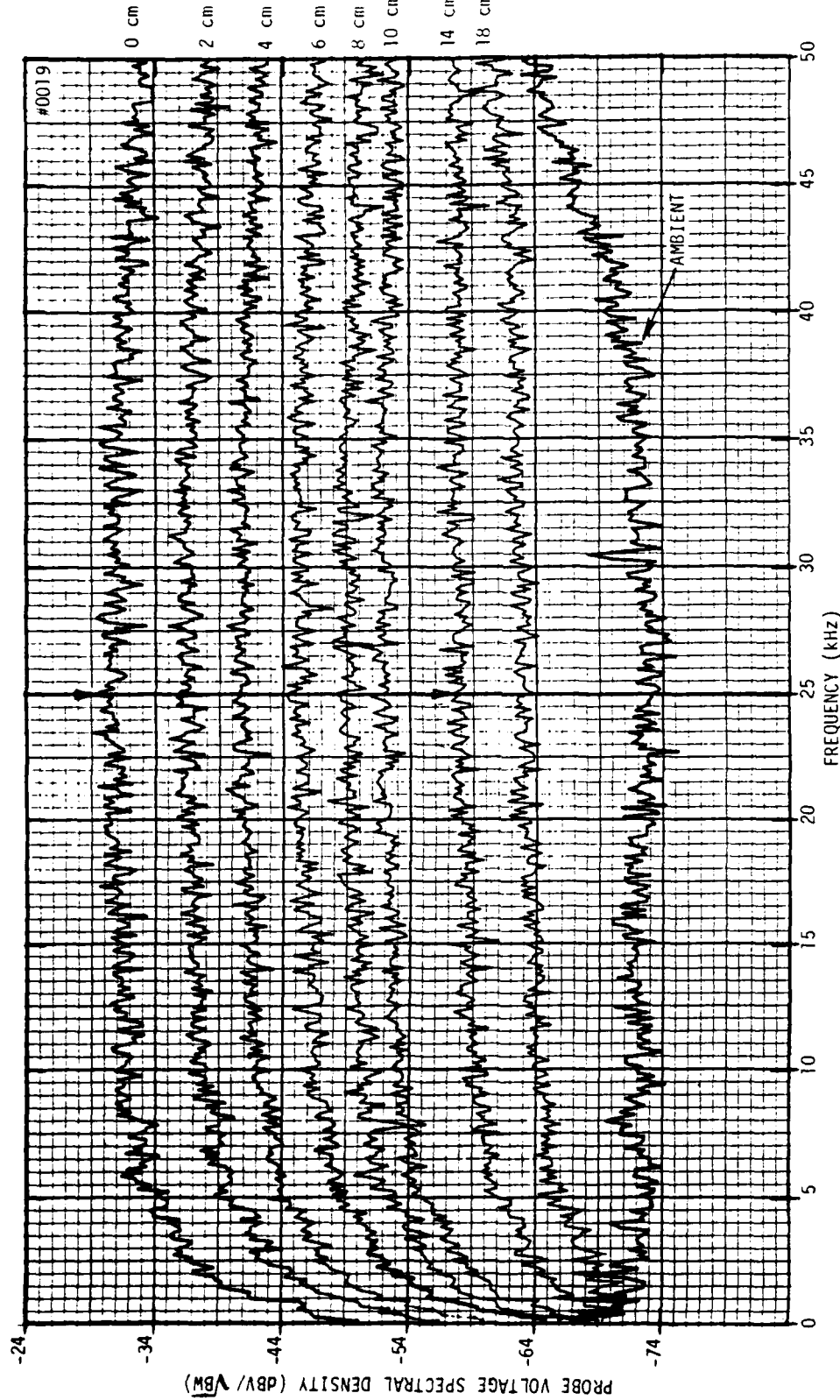


Figure 26. Probe Voltage Versus Frequency Plots as a Function of Probe Distance From the Top Surface of a 3 kVA GE 9T51Y13 Transformer as the Probe Was Moved Along a Vertical Axis Intersecting the Narrow Seam in the Transformer Cover Shown in Figure 2

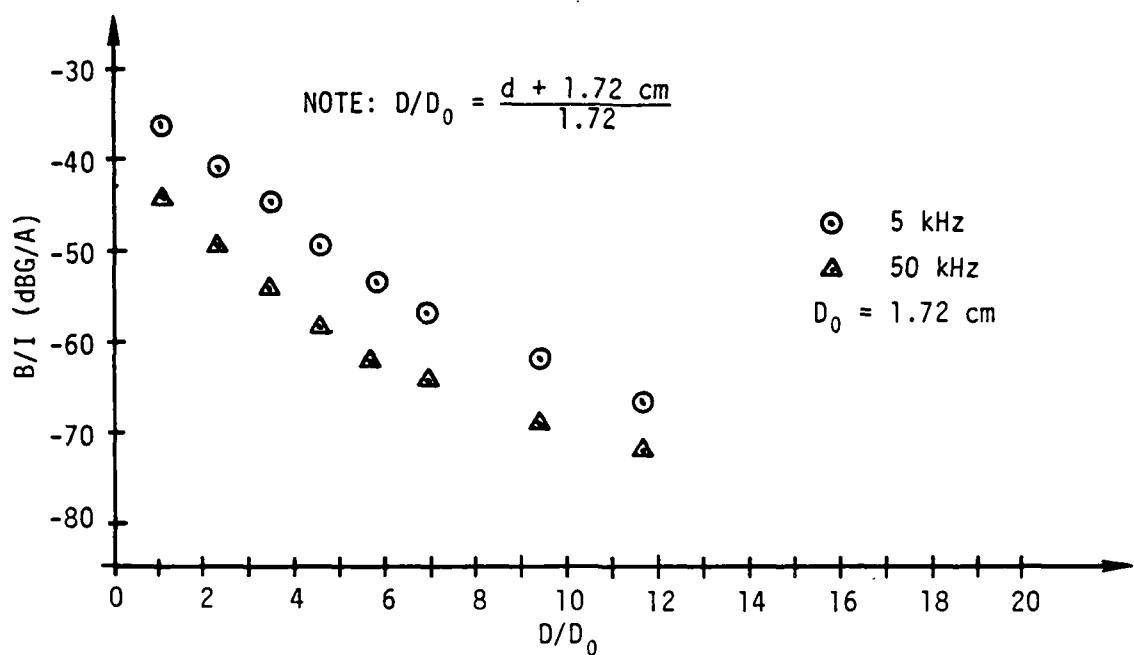


Figure 27a. The Perpendicular Component of Leakage Flux Density in Units of Decibels Relative to 1 Gauss Normalized to 1 A of Primary-Winding Current ( $B/I$ ) for Frequencies of 5 and 50 kHz.  $B/I$  is Shown as a Function of the Probe Spacing Ratio,  $D/D_0$ . The Probe Was Located Over the Seam in the Top Surface of the GE 9T51Y13 Transformer Along a Vertical Axis Shown in Figure 2.

Frequency (kHz)	$d$ (cm)							
	0	2	4	6	8	10	14	18
15	-38.6	-43.6	-47.6	-53.1	-57.6	-59.1	-65.6	-70.6
25	-39	-47.5	-50.6	-53.9	-57.8	-61.6	-69.4	-73.5
35	-42.1	-48.1	-52.1	-56.1	-60.1	-62.6	-69.6	-73.6

Figure 27b.  $B/I$  Versus Probe Spacing,  $d$ , at Frequencies Between the Limits of 5 and 50 kHz Shown Above.

Figure 27. Normalized Flux Density at the Top Surface of the 3 kVA Transformer Above the Narrow Seam in the Cover

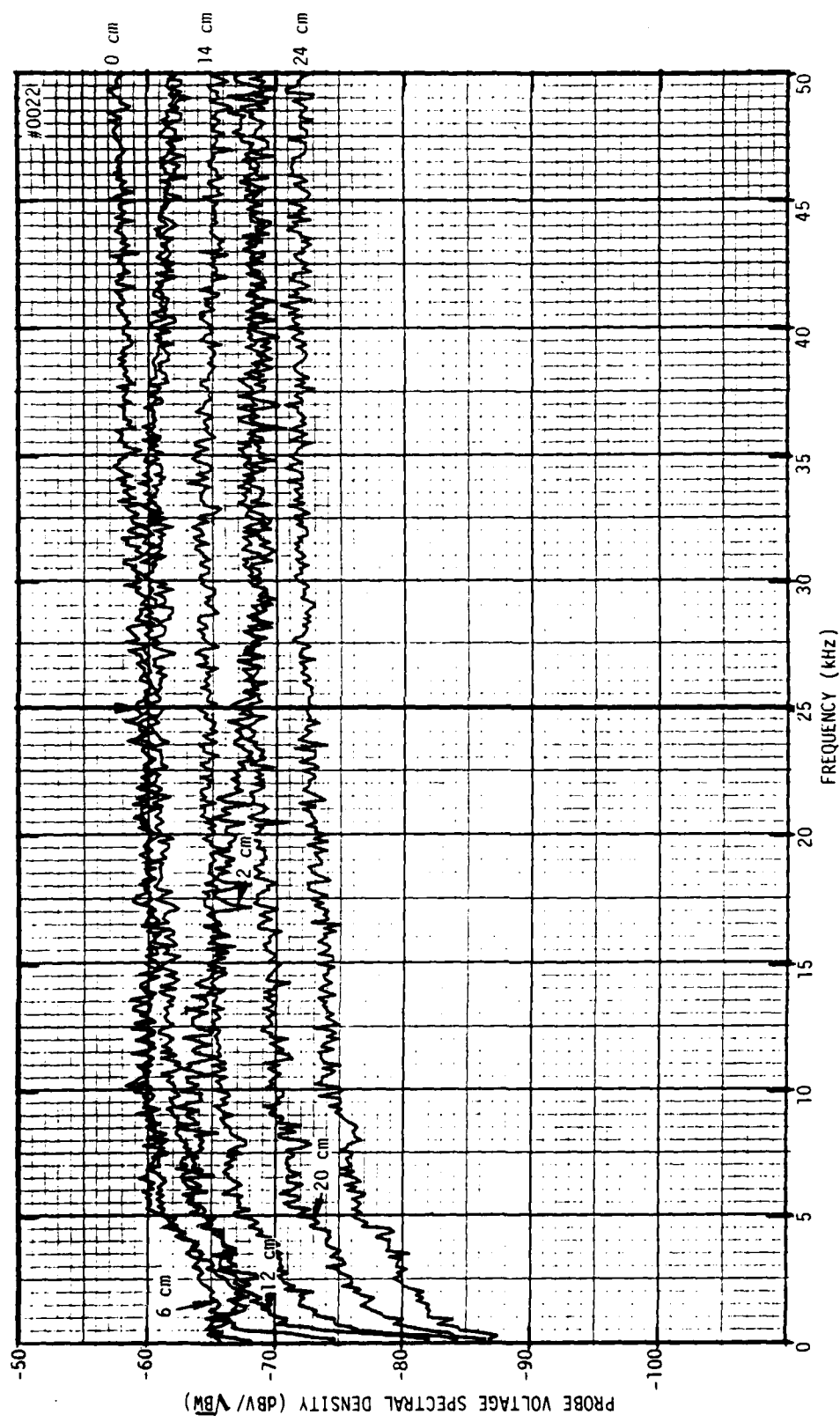


Figure 28. Probe Voltage Versus Frequency Plots as a Function of Probe Distance From the Top Surface of a 3 kVA GE 9T51Y13 Transformer as the Probe Was Moved Along a Vertical Axis Intersecting the Center of the Lamination Stack Shown in Figure 2

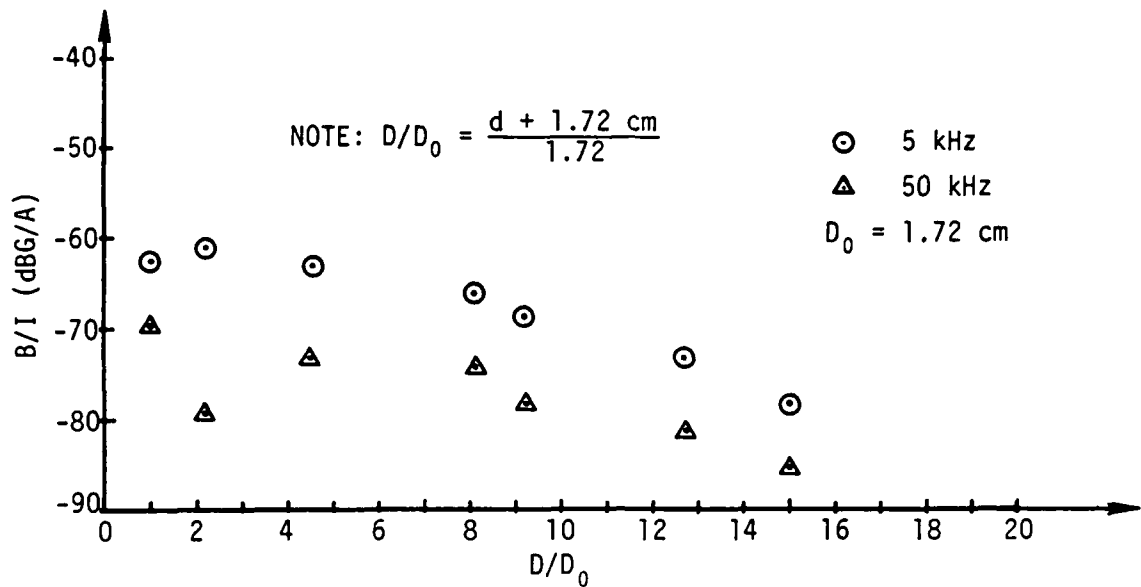


Figure 29a. The Perpendicular Component of Leakage Flux Density in Units of Decibels Relative to 1 Gauss Normalized to 1 A of Primary-Winding Current ( $B/I$ ) for Frequencies of 5 and 50 kHz.  $B/I$  is Shown as a Function of the Probe Spacing Ratio,  $D/D_0$ . The Probe Was Located at the Top Surface of the GE 9T51Y13 Transformer Along the Coordinate Axis Shown in Figure 2.

Frequency (kHz)	$d$ (cm)						
	0	2	6	12	14	20	24
15	-67.1	-71.6	-66.6	-68.1	-71.6	-76.6	-80.6
25	-68.7	-76.4	-69.7	-70.7	-73.7	-77.2	-82.2
35	-69.6	-80.1	-71.1	-72.1	-75.1	-78.6	-82.1

Figure 29b.  $B/I$  Versus Probe Spacing,  $d$ , at Frequencies Between the Limits of 5 and 50 kHz Shown Above.

Figure 29. Normalized Flux Density at the Top Surface of the 3 kVA Transformer Above the Center of the Lamination Stack

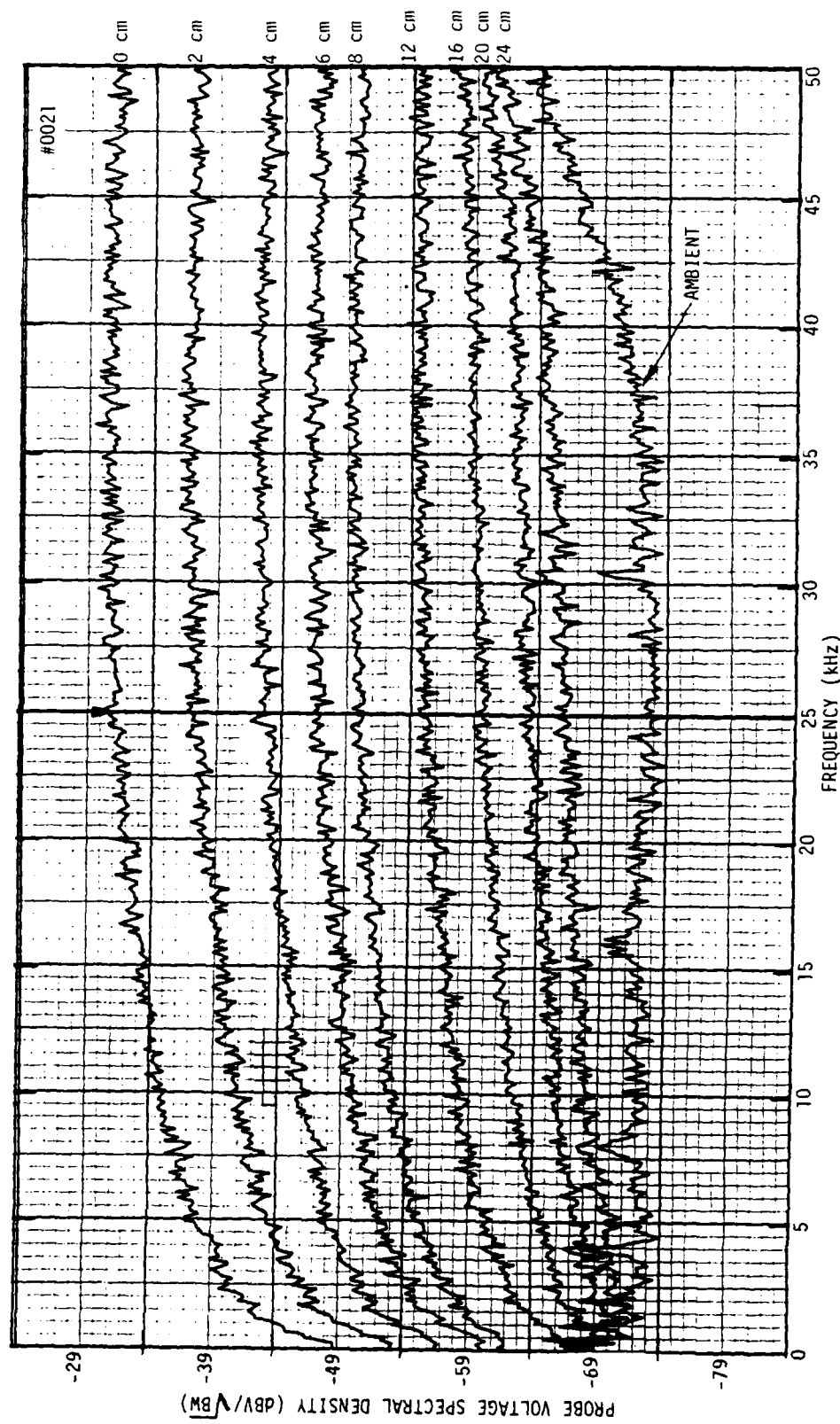


Figure 30. Probe Voltage Versus Frequency Plots as a Function of Probe Distance From the Top Surface of a 3 kVA GE 9T51Y13 Transformer (Open-Circuited Secondary)

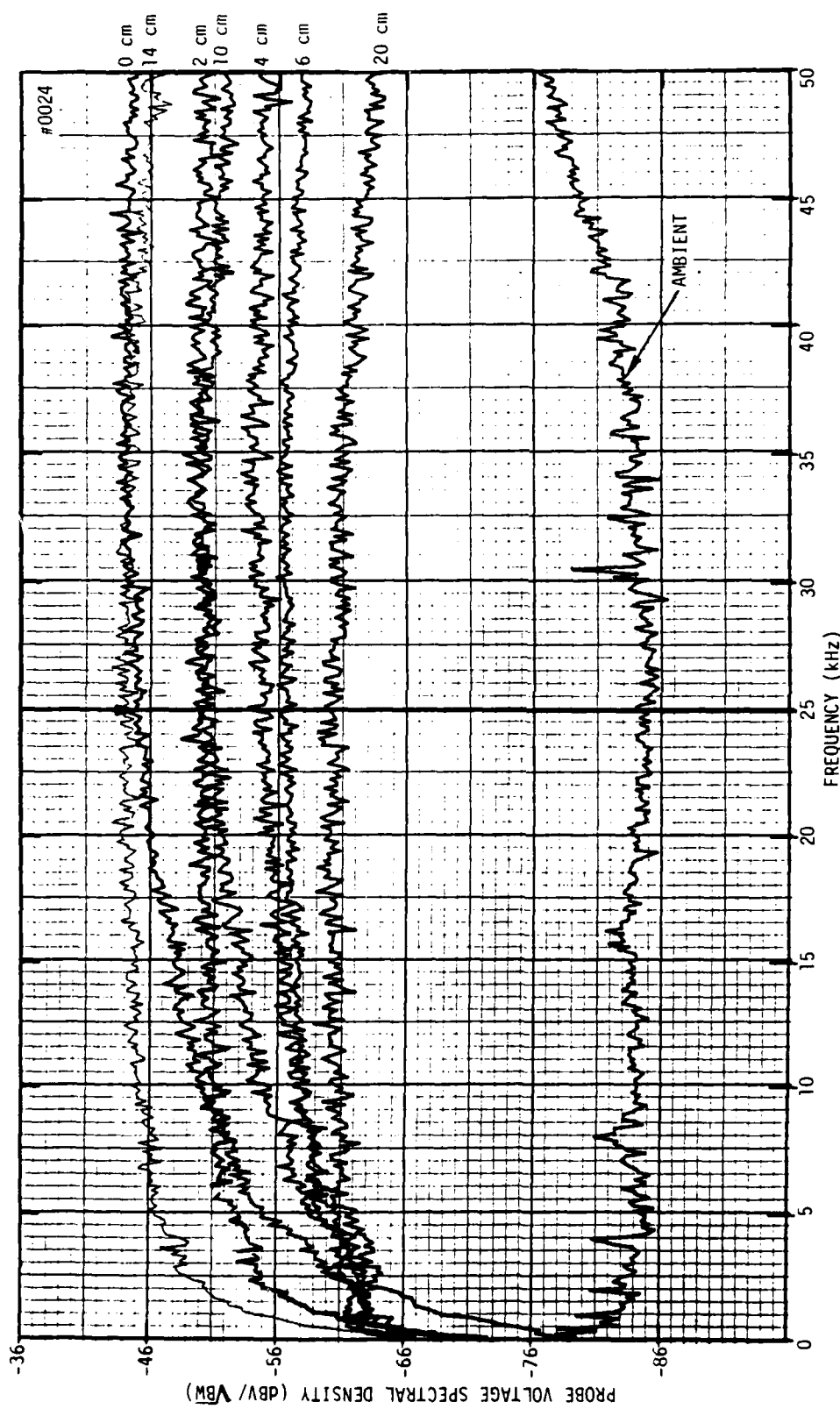


Figure 31. Probe Voltage Versus Frequency Plots as a Function of Probe Distance From the Side of the 3 kVA GE 9T51Y13 Transformer as the Probe Was Moved Along the Horizontal Axis Shown in Figure 2

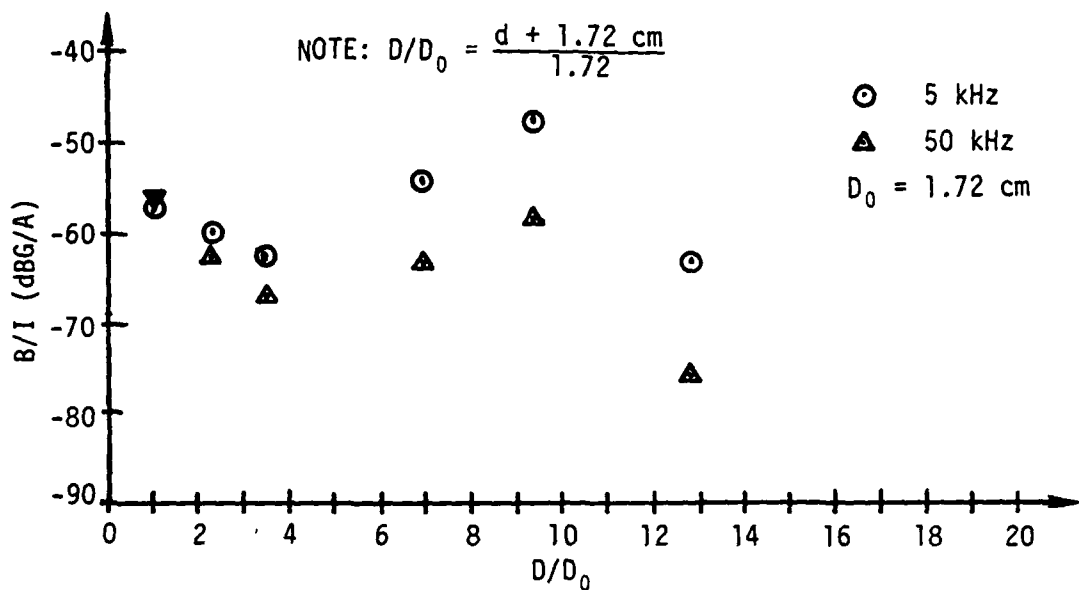


Figure 32a. The Perpendicular Component of Leakage Flux Density in Units of Decibels Relative to 1 Gauss Normalized to 1 A of Primary-Winding Current ( $B/I$ ) for Frequencies of 5 and 50 kHz.  $B/I$  is Shown as a Function of the Probe Spacing Ratio,  $D/D_0$ . The Probe Was Located at the Side of the GE 9T51Y13 Transformer Along the Horizontal Coordinate Axis Shown in Figure 2.

Frequency (kHz)	$B/I$ (dBG/A)					
	0	2	4	10	14	20
15	-54.6	-60.6	-62.6	-57.6	-51.6	-66.6
25	-54.6	-60.1	-63.8	-59.7	-53.7	-69.7
35	-55.1	-61.1	-65.1	-61.1	-55.1	-73.1

Figure 32b.  $B/I$  Versus Probe Spacing,  $d$ , at Frequencies Between the Limits of 5 and 50 kHz Shown Above.

Figure 32. Normalized Flux Density at the Side of the 3 kVA Transformer

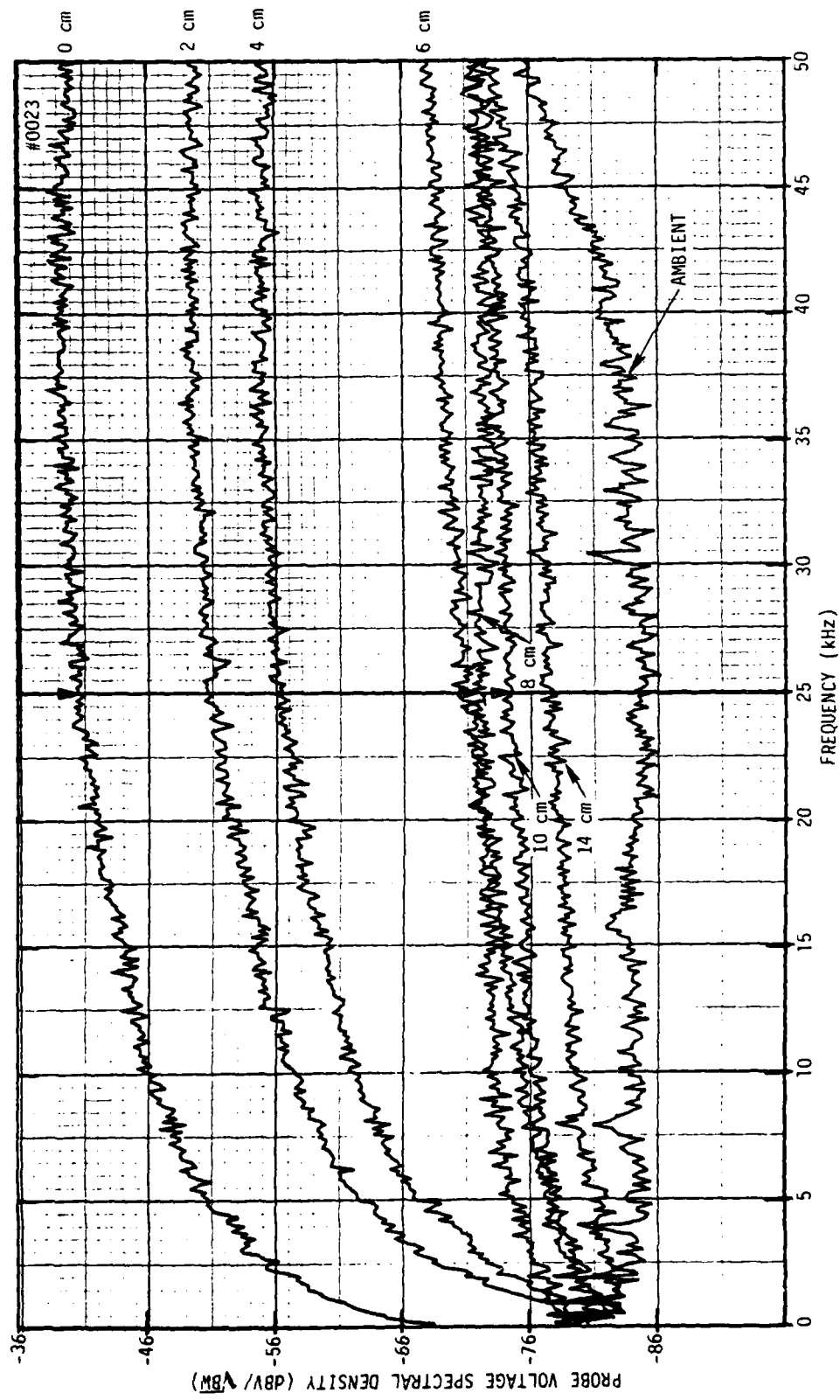


Figure 33. Probe Voltage Versus Frequency Plots as a Function of Probe Distance From the Side of a 3 kVA GE 9T51Y13 Transformer (Open-Circuited Secondary)

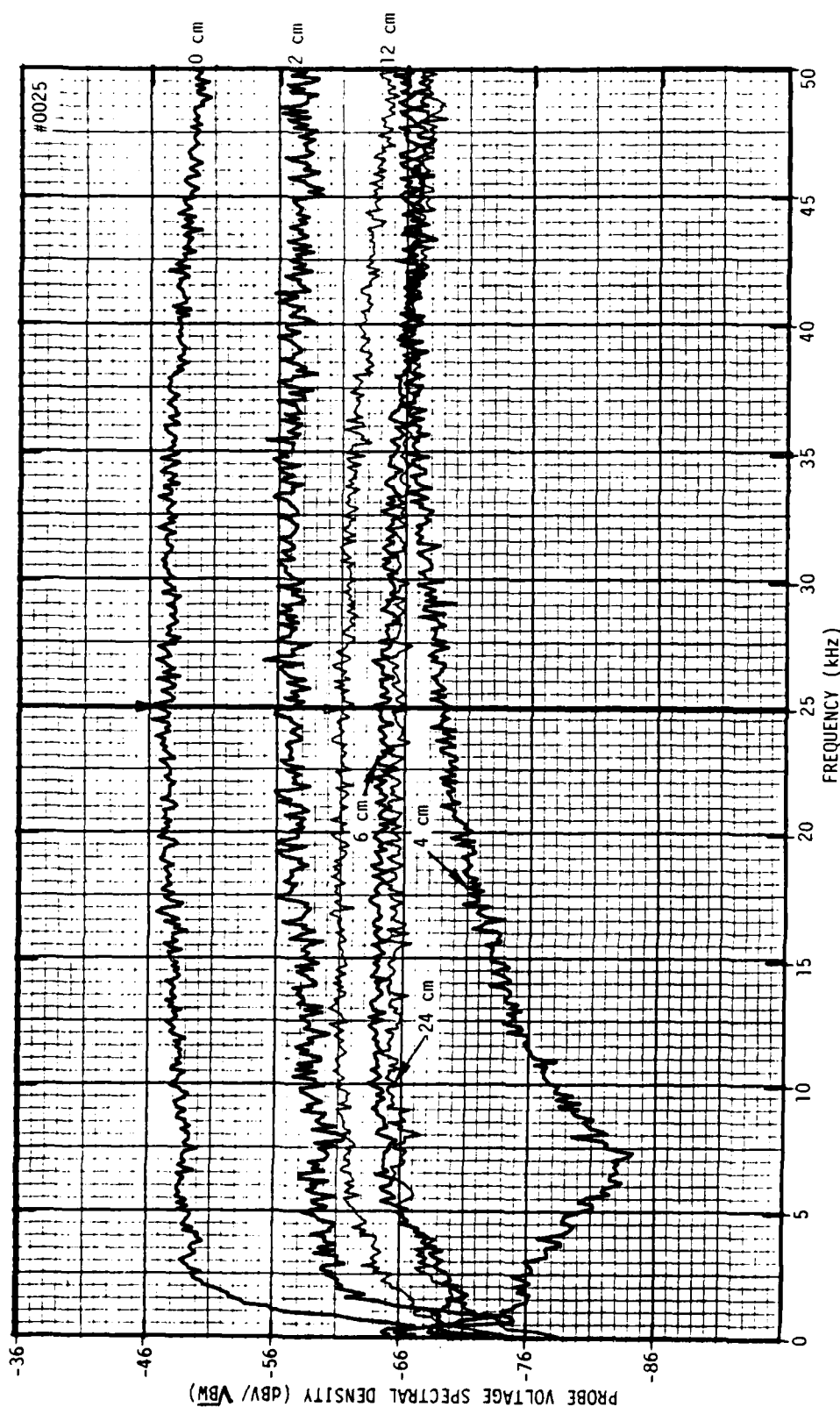


Figure 34. Probe Voltage Versus Frequency Plots as a Function of Probe Distance From the I/O Endcap of a 3 kVA GE 9T51Y13 Transformer as the Probe Was Moved Along the Horizontal Axis Shown in Figure 2

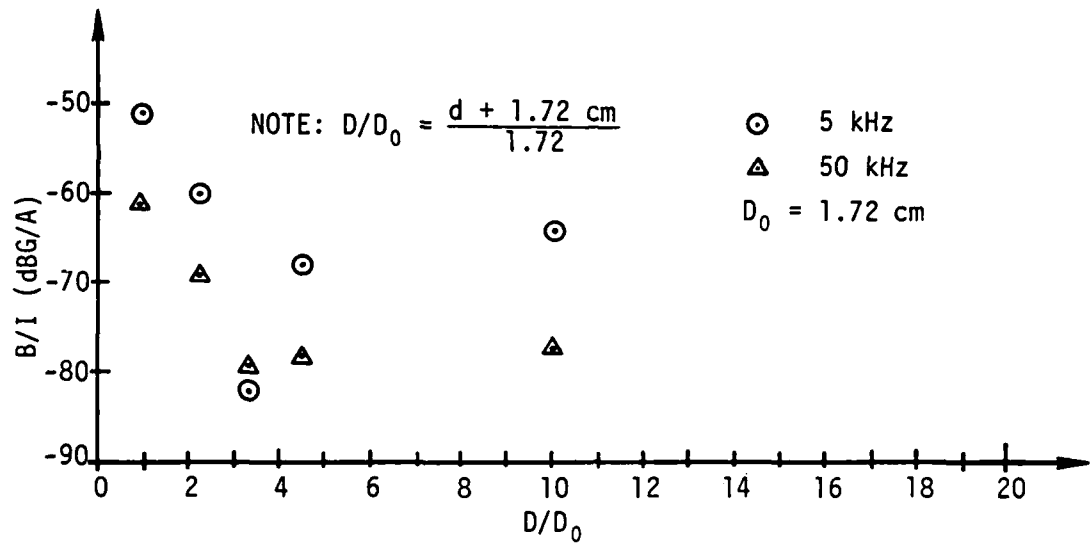


Figure 35a. The Perpendicular Component of Leakage Flux Density in Units of Decibels Relative to 1 Gauss Normalized to 1 A of Primary-Winding Current ( $B/I$ ) for Frequencies of 5 and 50 kHz.  $B/I$  is Shown as a Function of the Probe Spacing Ratio,  $D/D_0$ . The Probe Was Located at the I/O Endcap of the GE 9T51Y13 Transformer Along the Horizontal Coordinate Axis Shown in Figure 2.

Frequency (kHz)	$d$ (cm)				
	0	2	4	6	12
15	-54.6	-64.6	-79.6	-70.6	-68.1
25	-56.2	-67.6	-79.4	-73.7	-70.7
35	-59.1	-68.1	-78.1	-76.1	-72.6

Figure 35b.  $B/I$  Versus Probe Spacing,  $d$ , at Frequencies Between the Limits of 5 and 50 kHz Shown Above.

Figure 35. Normalized Flux Density at the I/O Endcap of the 3 kVA Transformer

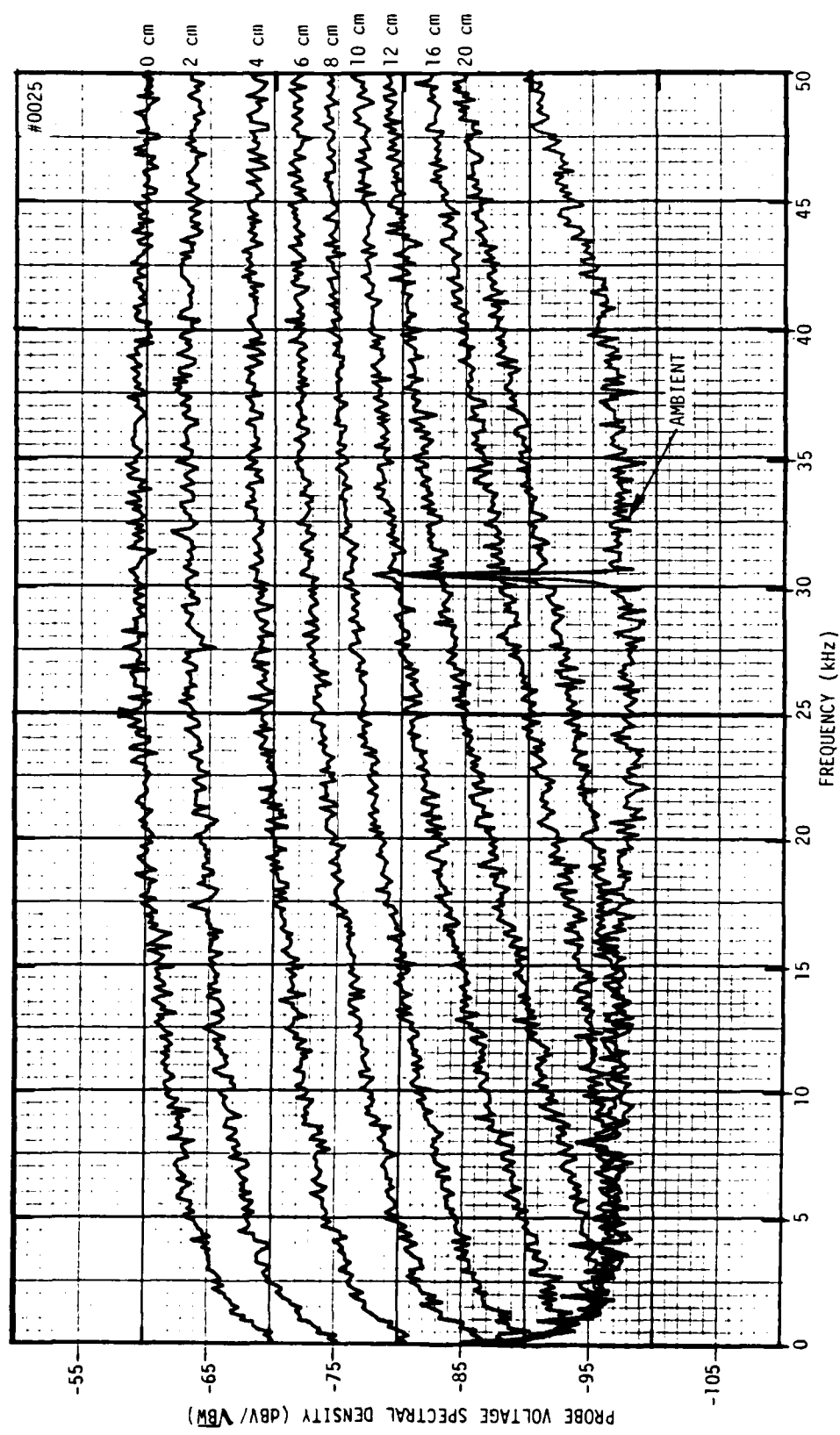


Figure 36. Probe Voltage Versus Frequency Plots as a Function of Probe Distance From the I/O Endcap of a 3 kVA GE 9T51Y13 Transformer (Open-Circuited Secondary)

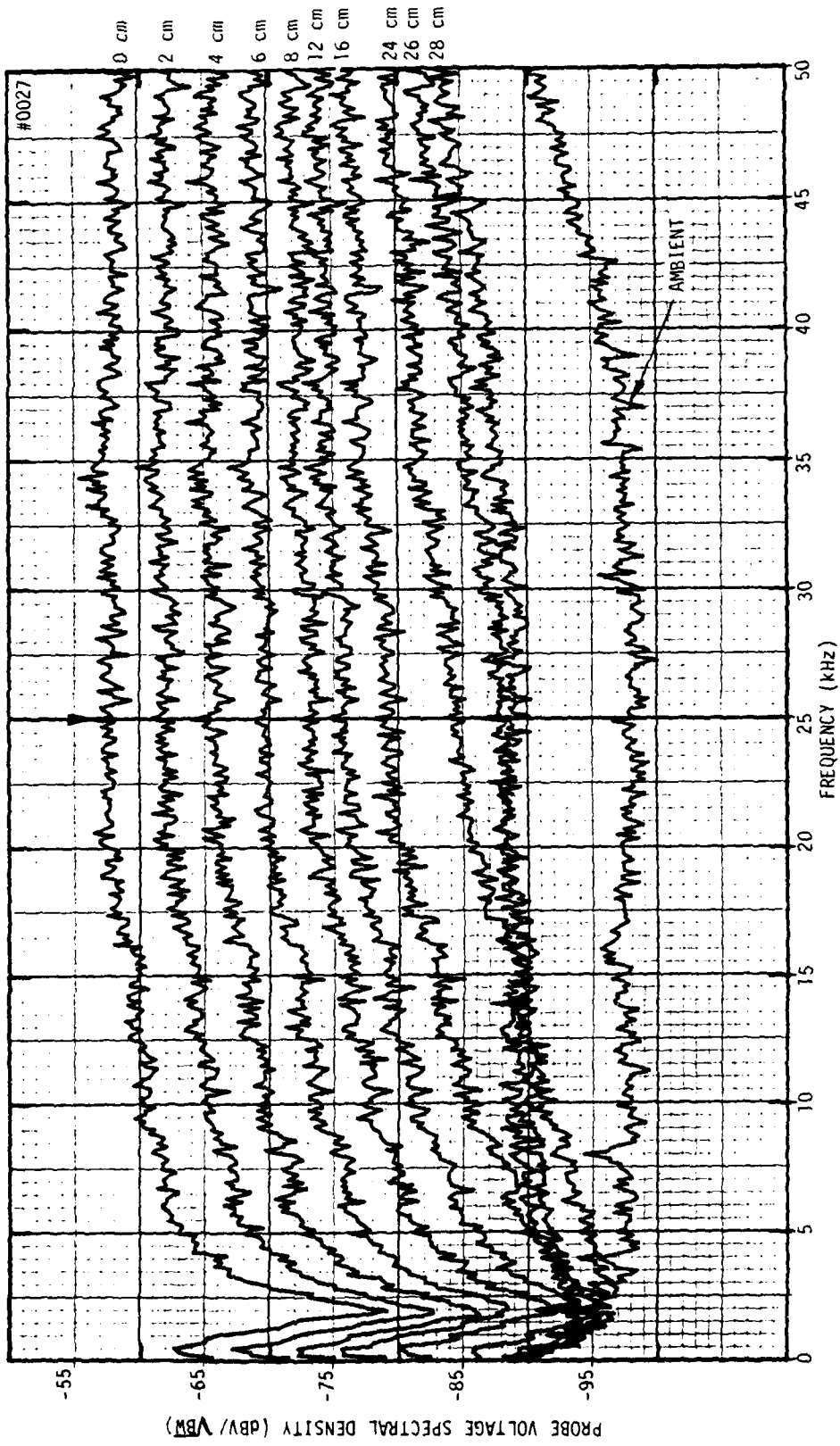


Figure 37. Probe Voltage Versus Frequency plots as a Function of Probe Distance From the Endcap Opposite the I/O Endcap of the 3 kVA GE 9T51Y13 Transformer as the Probe Was Moved Along the Horizontal Axis Shown in Figure 2

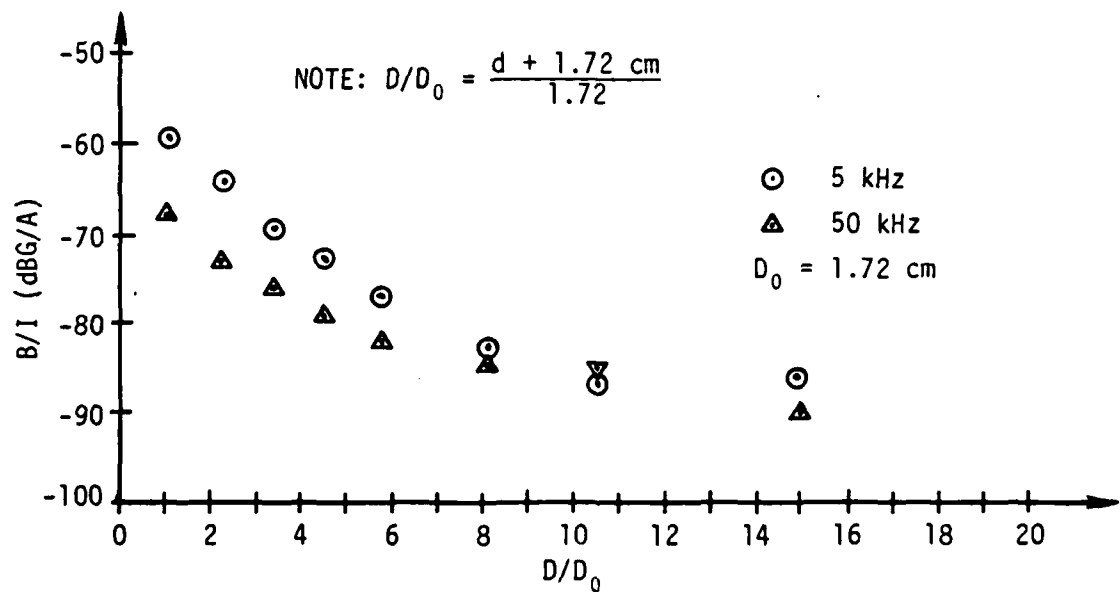


Figure 38a. The Perpendicular Component of Leakage Flux Density in Units of Decibels Relative to 1 Gauss Normalized to 1 A of Primary-Winding Current ( $B/I$ ) for Frequencies of 5 and 50 kHz.  $B/I$  is Shown as a Function of the Probe Spacing Ratio,  $D/D_0$ . The Probe Was Located at the Endcap Opposite the I/O Endcap of the GE 9T51Y13 Transformer Along the Horizontal Coordinate Axis Shown in Figure 2.

Frequency (kHz)	$B/I$ (dBG/A)							
	0	2	4	6	8	12	16	24
15	-64.2	-68.2	-72.7	-76.2	-80.2	-83.2	-87.2	-93.2
25	-64.3	-68.9	-72.0	-77.1	-80.6	-83.2	-86.2	-92
35	-68.1	-72.1	-76.1	-79.6	-83.1	-85.6	-88.1	-92.6

Figure 38b.  $B/I$  Versus Probe Spacing,  $d$ , at Frequencies Between the Limits of 5 and 50 kHz Shown Above.

Figure 38. Normalized Flux Density at the Endcap Opposite the I/O Endcap of the 3 kVA Transformer

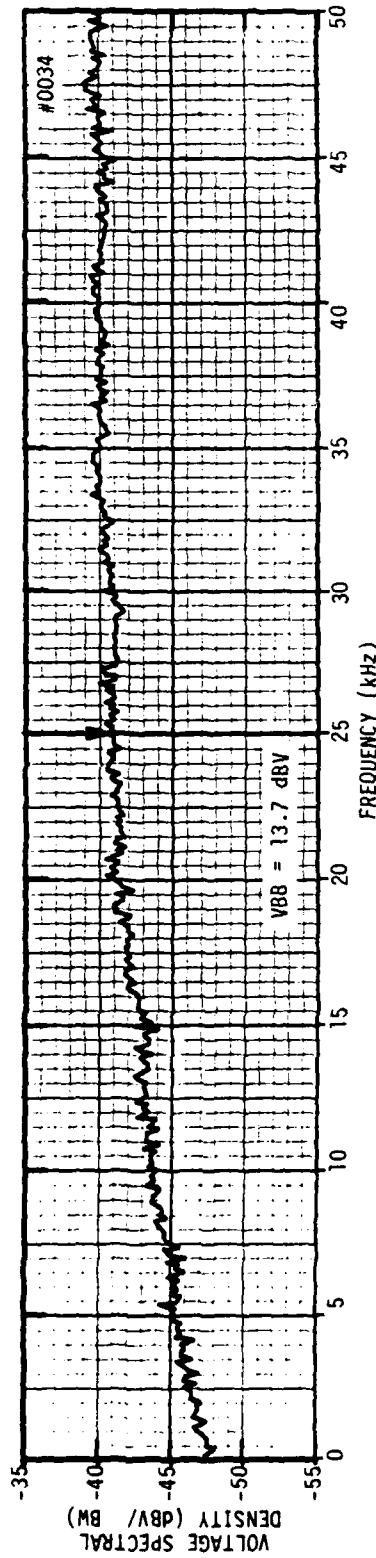


Figure 39a. Voltage Spectral Density at the Input (Primary Winding) of a 5 kVA Jefferson Electric 12438 Transformer. The Wide-Band Input (0 - 50 kHz) Was Supplied by a Pseudorandom Noise Generator and a McIntosh Power-Amplifier Driver. The Transformer Secondary Was Shorted.

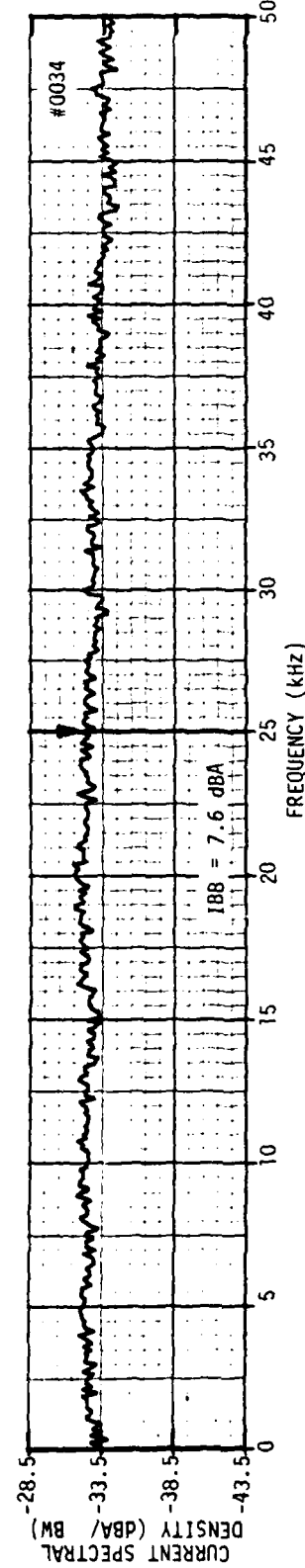


Figure 39b. Current Spectral Density at the Input (Primary Winding) of a 5 kVA Jefferson Electric 12438 Transformer for the Same Input Condition and Loading.

Figure 39. Input Voltage and Current Spectral Densities for a 5 kVA Transformer

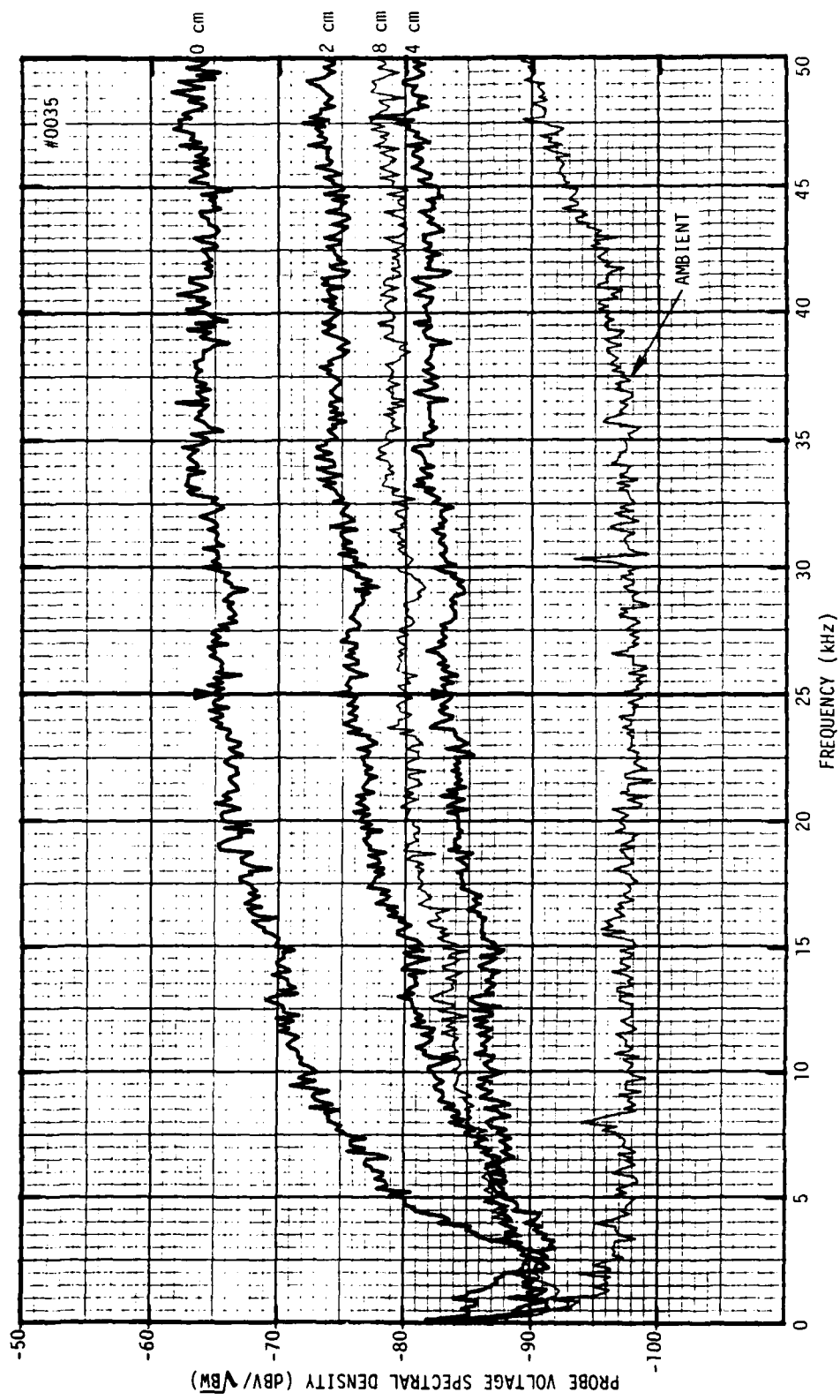


Figure 40. Probe Voltage Spectral Density (dBV/Hz) Versus Frequency (kHz) Plots as a Function of Probe Distance From the Top Surface of the Jefferson Electric 12438 Transformer as the Probe Was Moved Along a Vertical Axis Intersecting the Center of the Seam Nearest the Endcap Shown in Figure 3

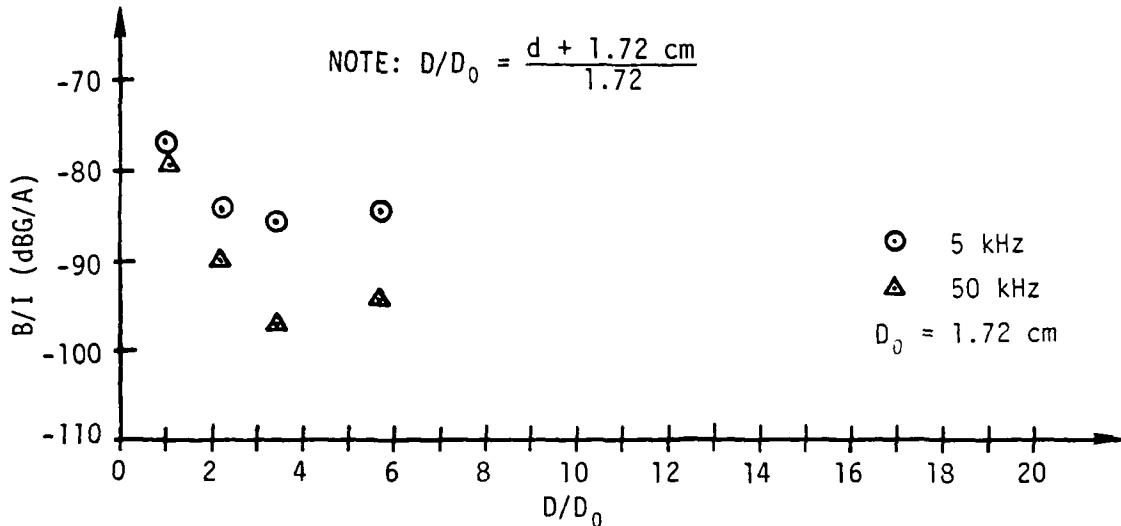


Figure 41a. The Perpendicular Component of Leakage Flux Density in Units of Decibels Relative to 1 Gauss Normalized to 1 A of Primary-Winding Current (B/I) for Frequencies of 5 and 50 kHz. B/I is Shown as a Function of the Probe Spacing Ratio,  $D/D_0$ . The Probe Was Located at the Top Surface of the Jefferson Electric 12438 Transformer Along a Vertical Axis Intersecting the Center of the Seam Nearest the Endcap Shown in Figure 3.

Frequency (kHz)	d (cm)			
	0	2	4	8
15	-76.6	-87.6	-93.6	-90.6
25	-76.1	-85.2	-94.6	-90.2
35	-77.9	-87.6	-95.6	-92.6

Figure 41b. B/I Versus Probe Spacing, d, at Frequencies Between the Limits of 5 and 50 kHz Shown Above.

Figure 41. Normalized Flux Density at the Top Surface of the 5 kVA Transformer Above the Seam Nearest the Endcap

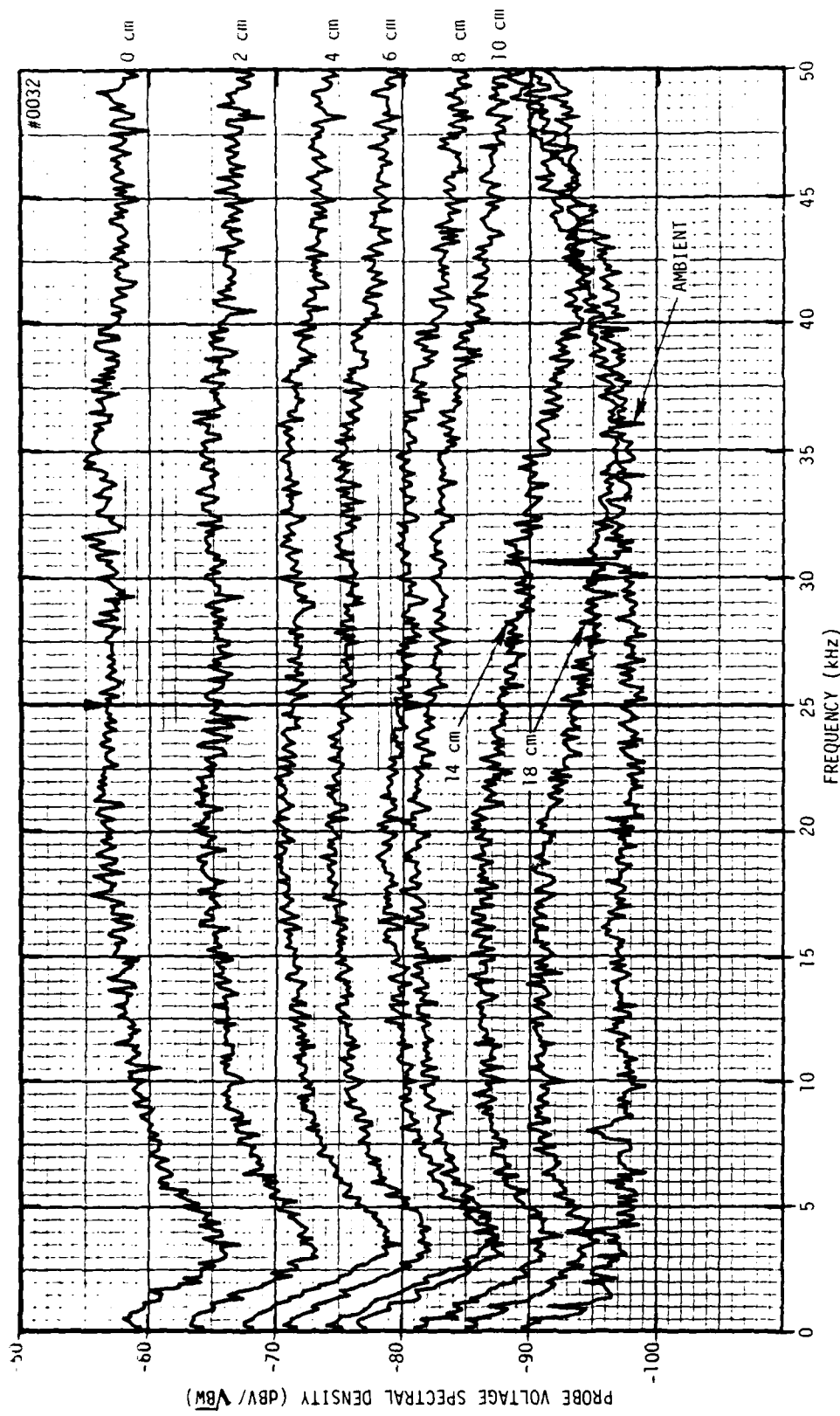


Figure 42. Probe Voltage Spectral Density as a Function of Probe Distance From the Top Surface of the Jefferson Electric 12438 Transformer as the Probe Was Moved Along a Vertical Axis Intersecting the Center of the Seam Nearest the Endcap (Open-Circuited Secondary)

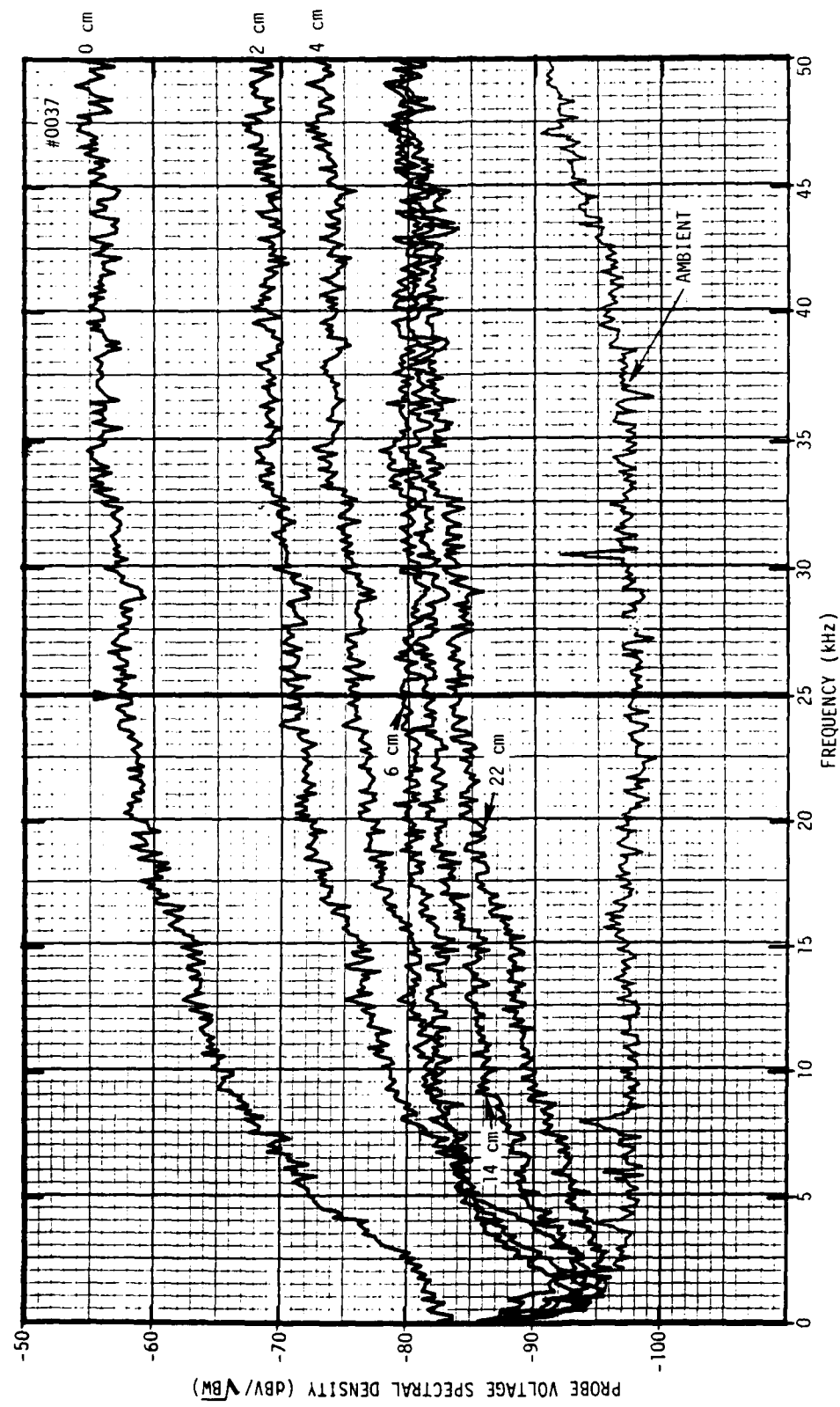


Figure 43. Probe Voltage Versus Frequency Plots as a Function of Probe Distance From the Top Surface of the Jefferson Electric 12438 Transformer as the Probe Was Moved Along a Vertical Axis Intersecting the Center of the Seam Nearest the Center of the Case Shown in Figure 3

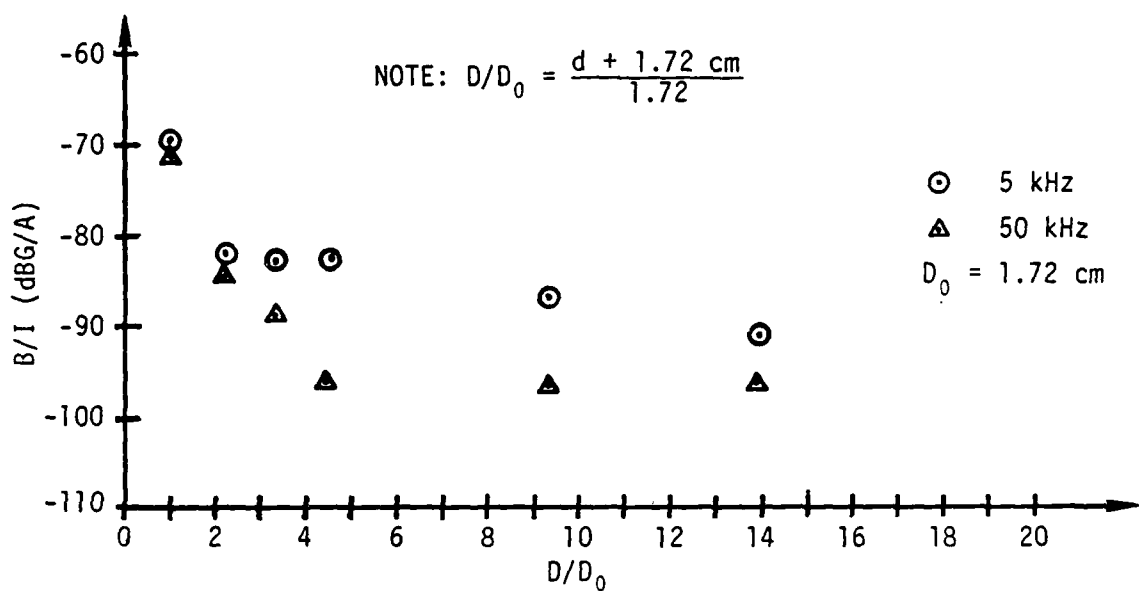


Figure 44a. The Perpendicular Component of Leakage Flux Density in Units of Decibels Relative to 1 Gauss Normalized to 1 A of Primary-Winding Current ( $B/I$ ) for Frequencies of 5 and 50 kHz.  $B/I$  is Shown as a Function of the Probe Spacing Ratio,  $D/D_0$ . The Probe Was Located at the Top Surface of the Jefferson Electric 12438 Transformer Along a Vertical Axis Intersecting the Center of the Seam Nearest the Center of the Case Shown in Figure 3.

Frequency (kHz)	$B/I$ (dBG/A)					
	0	2	4	6	14	22
15	-70.2	-83.1	-87.1	-89.6	-92.6	-94.6
25	-68.2	-81.6	-86.6	-90.5	-92.3	-95.2
35	-69.6	-82.6	-87.6	-93.1	-94.4	-96.4

Figure 44b.  $B/I$  Versus Probe Spacing,  $d$ , at Frequencies Between the Limits of 5 and 50 kHz Shown Above.

Figure 44. Normalized Flux Density at the Top Surface of the 5 kVA Transformer Above the Seam Nearest the Center of the Case

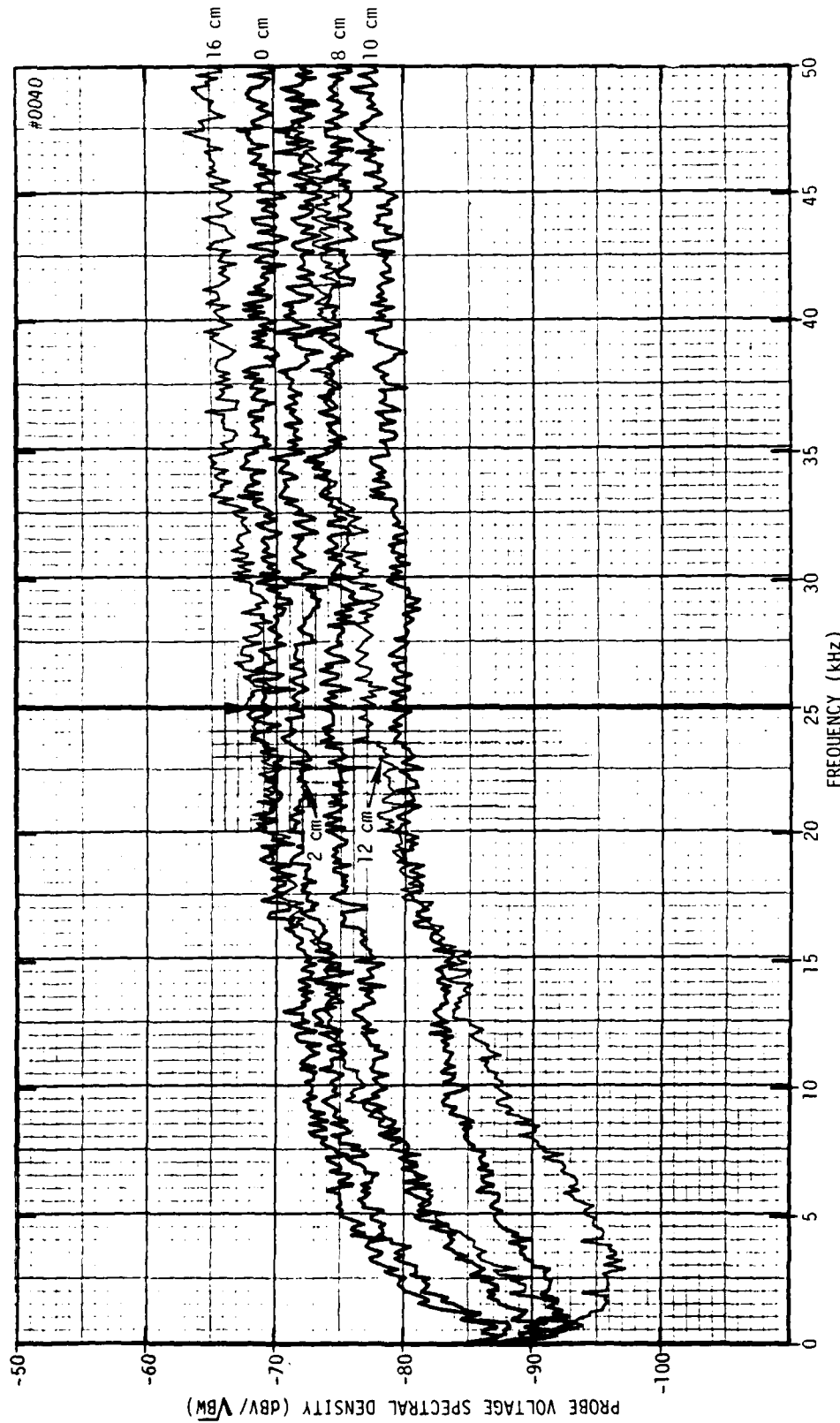


Figure 45. Probe Voltage Versus Frequency Plots as a Function of Probe Distance From the Side of the Jefferson Electric 12438 Transformer as the Probe Was Moved Along the Horizontal Axis Shown in Figure 3

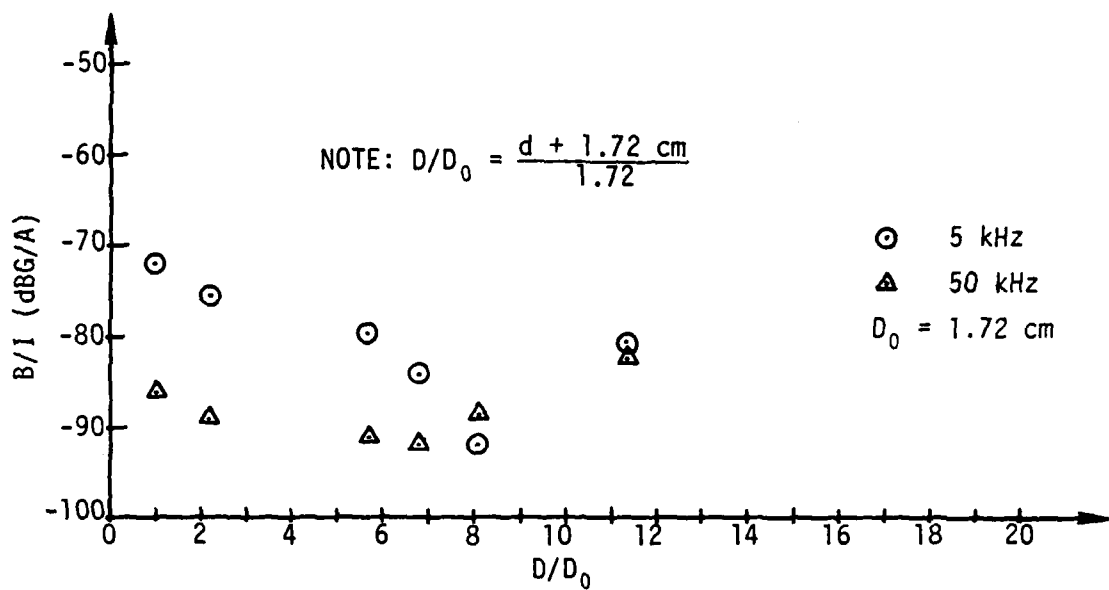


Figure 46a. The Perpendicular Component of Leakage Flux Density in Units of Decibels Relative to 1 Gauss Normalized to 1 A of Primary-Winding Current (B/I) for Frequencies of 5 and 50 kHz. B/I is Shown as a Function of the Probe Spacing Ratio,  $D/D_0$ . The Probe Was Located at the Side of the Jefferson Electric 12438 Transformer Along the Horizontal Coordinate Axis Shown in Figure 3.

Frequency (kHz)	B/I (dBG/A)					
	0	2	8	10	12	16
15	-79.1	-80.8	-84.1	-90.1	-90.6	-81.1
25	-79	-82.4	-84.7	-89.6	-87.2	-79
35	-82.1	-84.6	-87.4	-92.2	-88.3	-79.7

Figure 46b. B/I Versus Probe Spacing, d, at Frequencies Between the Limits of 5 and 50 kHz Shown Above.

Figure 46. Normalized Flux Density at the Side of the 5 kVA Transformer

TM 801173

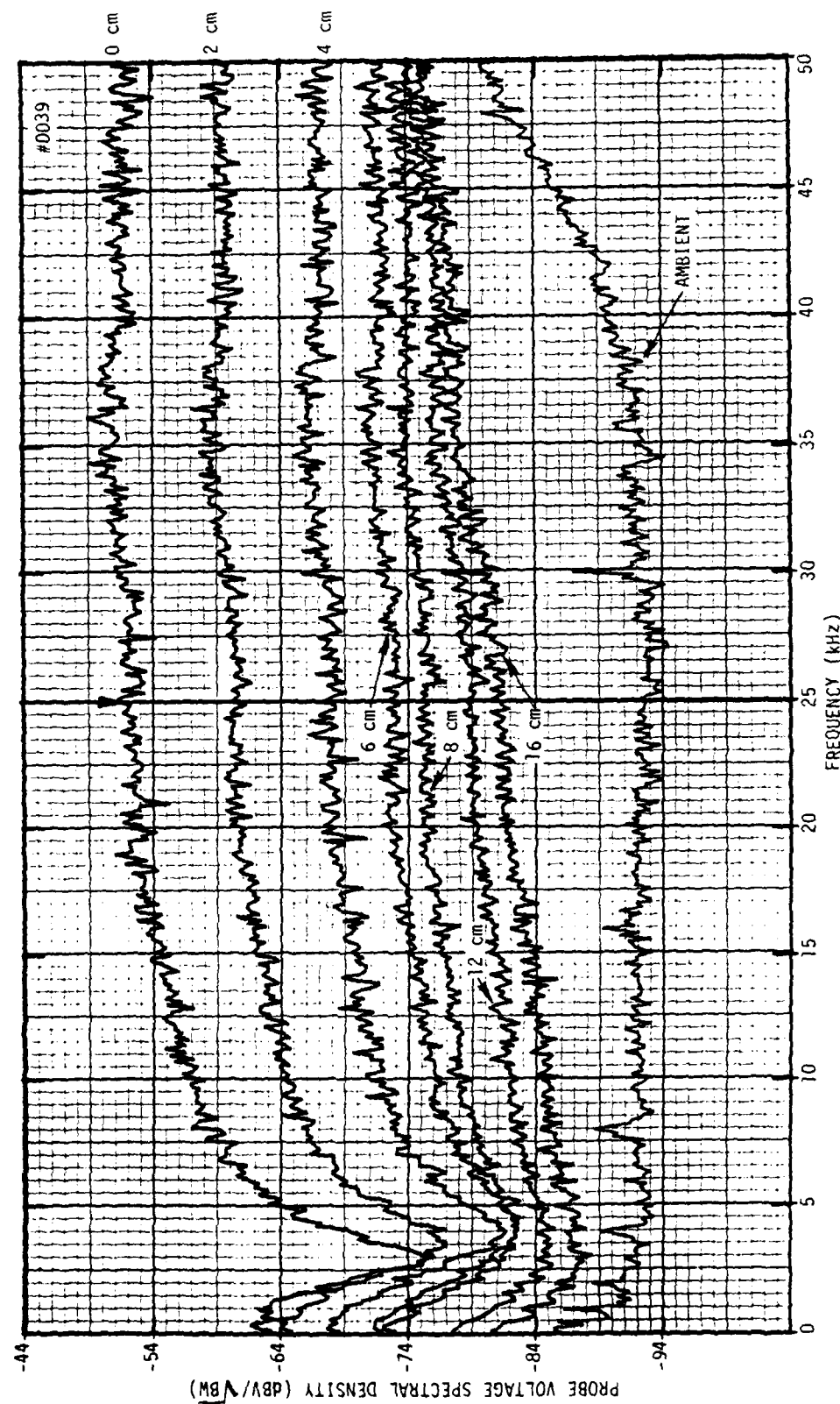


Figure 47. Probe Voltage Versus Frequency Plots as a Function of Probe Distance From the Side of the Jefferson Electric 12438 Transformer (Open-Circuited Secondary)

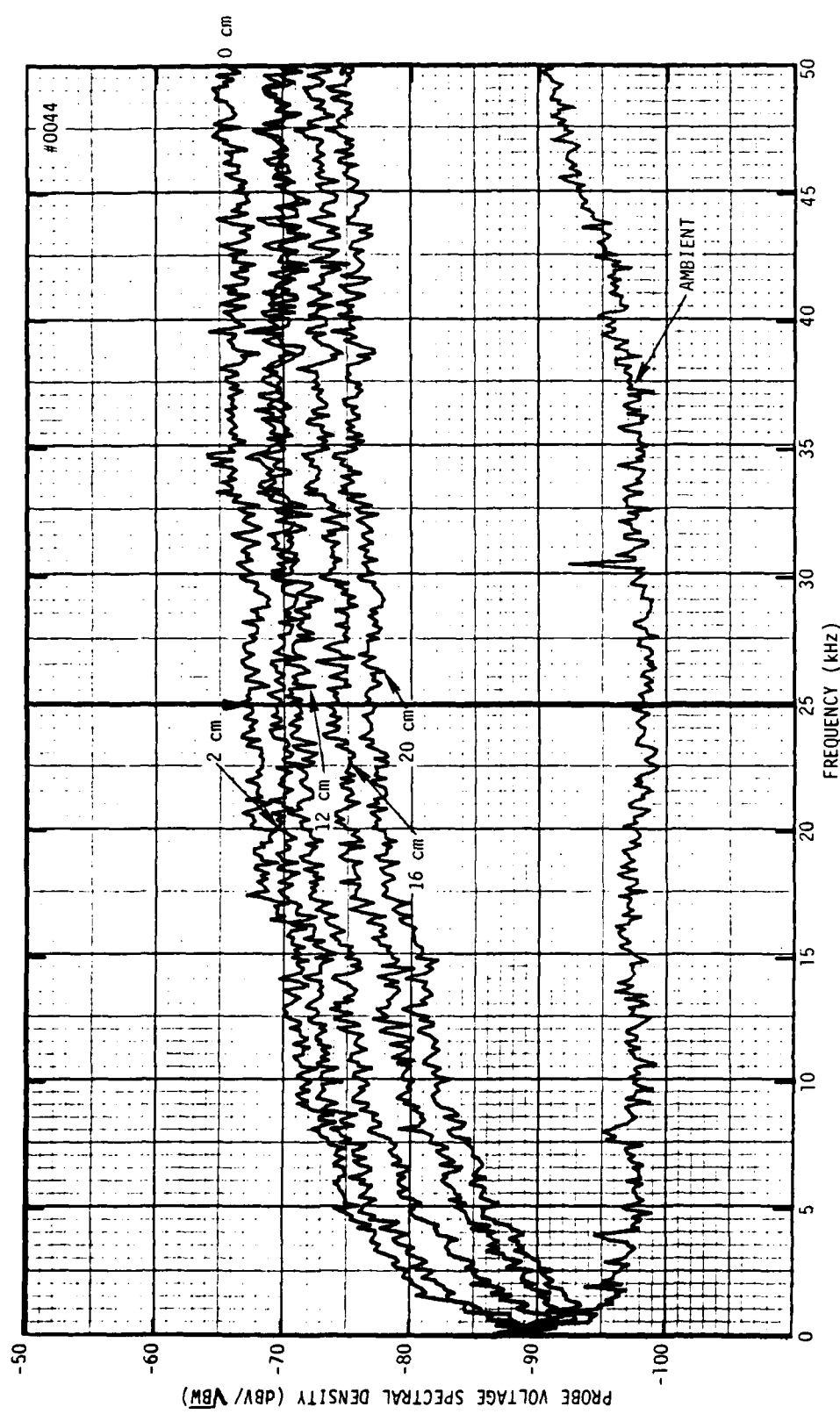


Figure 48. Probe Voltage Versus Frequency Plots as a Function of Probe Distance From the Endcap of the Jefferson Electric 12438 Transformer (Side With Open Grating) Shown in Figure 3

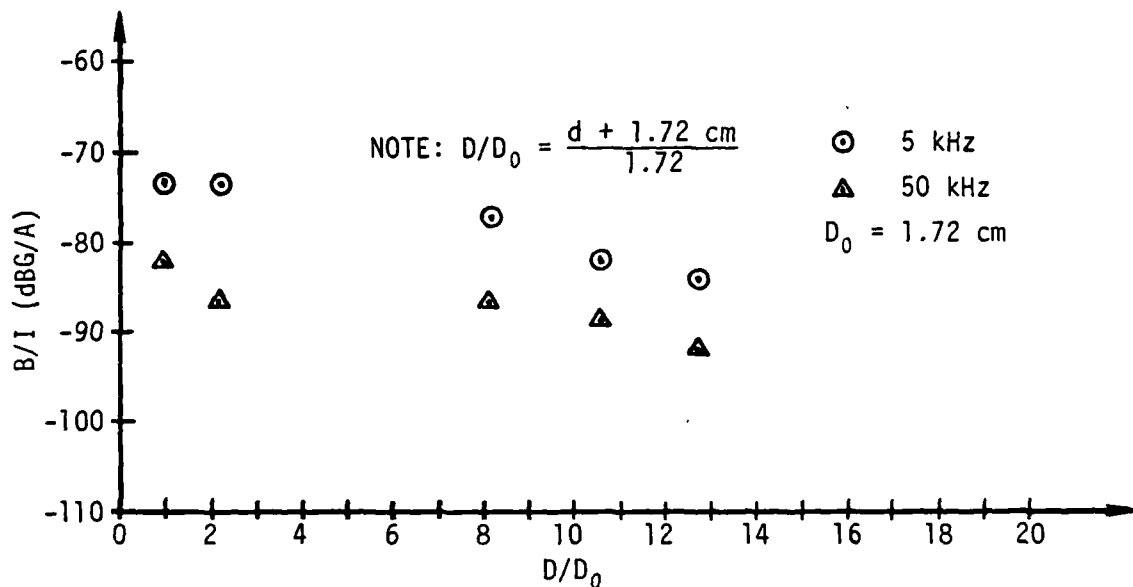


Figure 49a. The Perpendicular Component of Leakage Flux Density in Units of Decibels Relative to 1 Gauss Normalized to 1 A of Primary-Winding Current ( $B/I$ ) for Frequencies of 5 and 50 kHz.  $B/I$  is Shown as a Function of the Probe Spacing Ratio,  $D/D_0$ . The Probe Was Located at the Endcap of the Jefferson Electric 12438 Transformer (Side With Open Grating) Shown in Figure 3.

Frequency (kHz)	$B/I$ (dBG/A)				
	0	2	12	16	20
15	-77.8	-80.6	-81.9	-85.0	-87.5
25	-78.2	-79.7	-82.9	-84.6	-88.7
35	-79.6	-82.6	-83.6	-86.6	-88.6

Figure 49b.  $B/I$  Versus Probe Spacing,  $d$ , at Frequencies Between the Limits of 5 and 50 kHz Shown Above.

Figure 49. Normalized Flux Density at the Endcap (Open Grating) of the 5 kVA Transformer

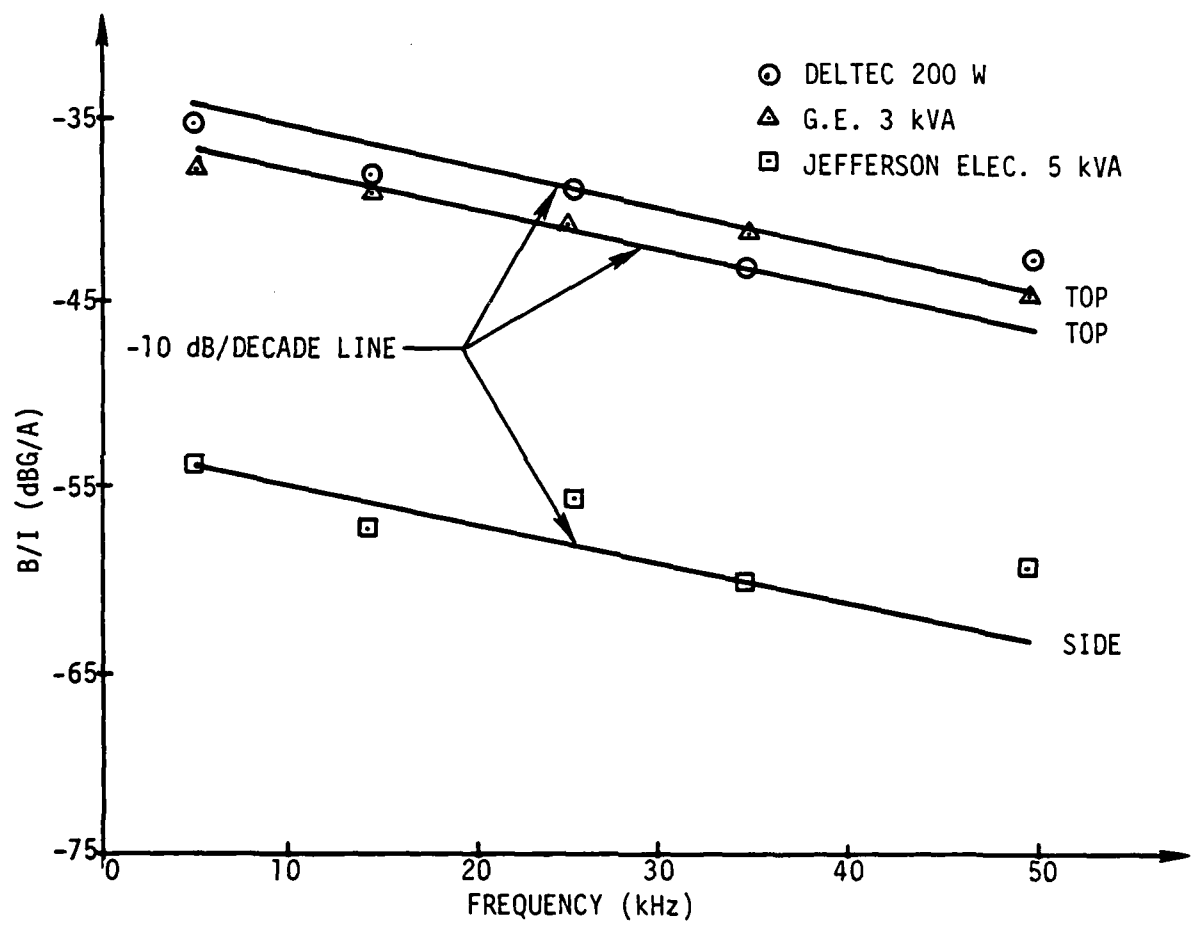


Figure 50. Comparison of the Maximum Leakage Flux Density From a 200 W, a 3 kVA, and a 5 kVA Transformer in Units of Decibels Relative to 1 Gauss Normalized to 1 A of Primary-Winding Current ( $B/I$ ) Versus Frequency With the Location of the Respective Transformer Surface Identified at the Right

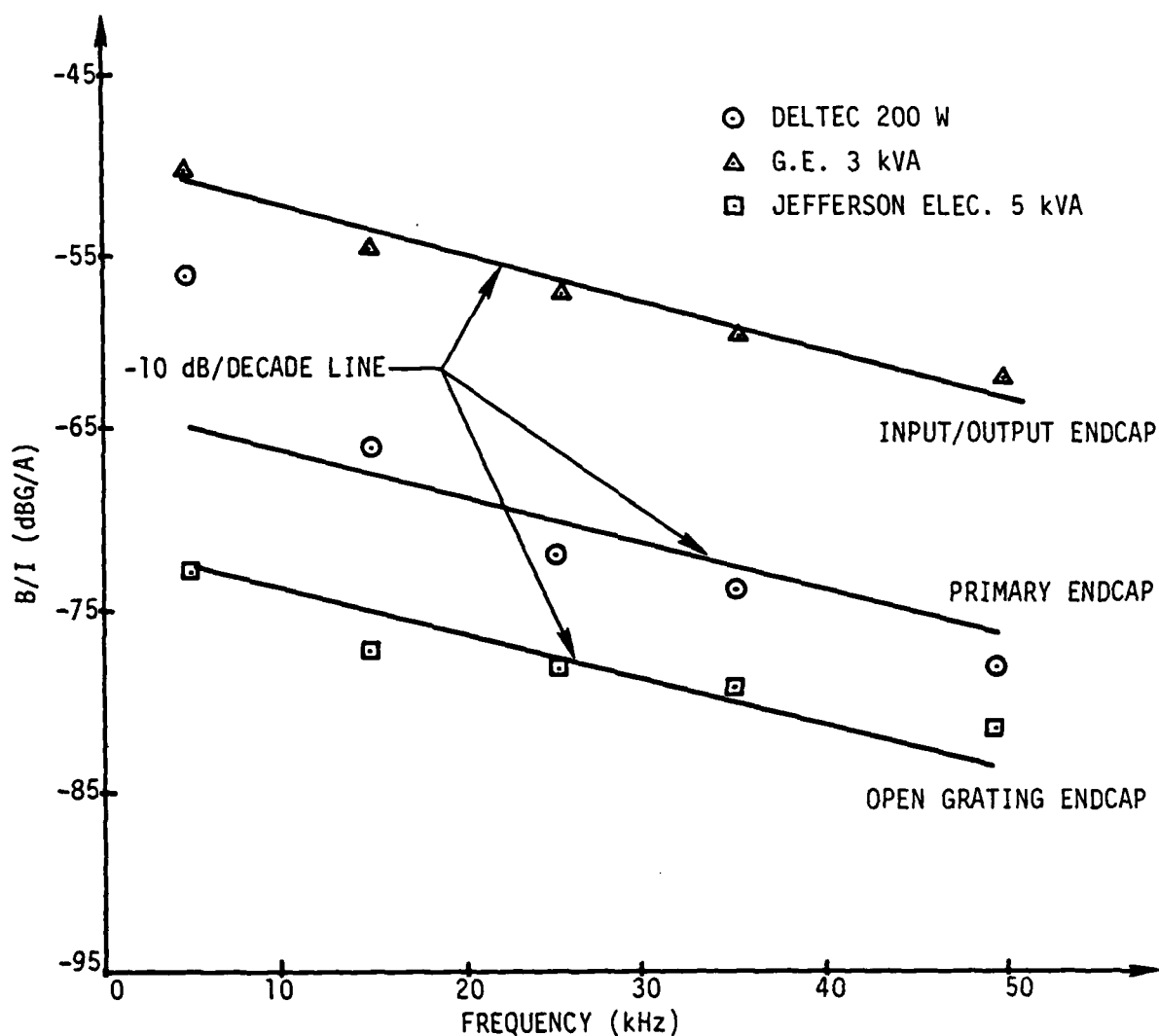


Figure 51. Comparison of the Leakage Flux Density From a 200 W, a 3 kVA, and a 5 kVA Transformer in Units of Decibels Relative to 1 Gauss Normalized to 1 A of Primary-Winding Current ( $B/I$ ) Versus Frequency With the Location of the Respective Transformer Surface Identified at the Right

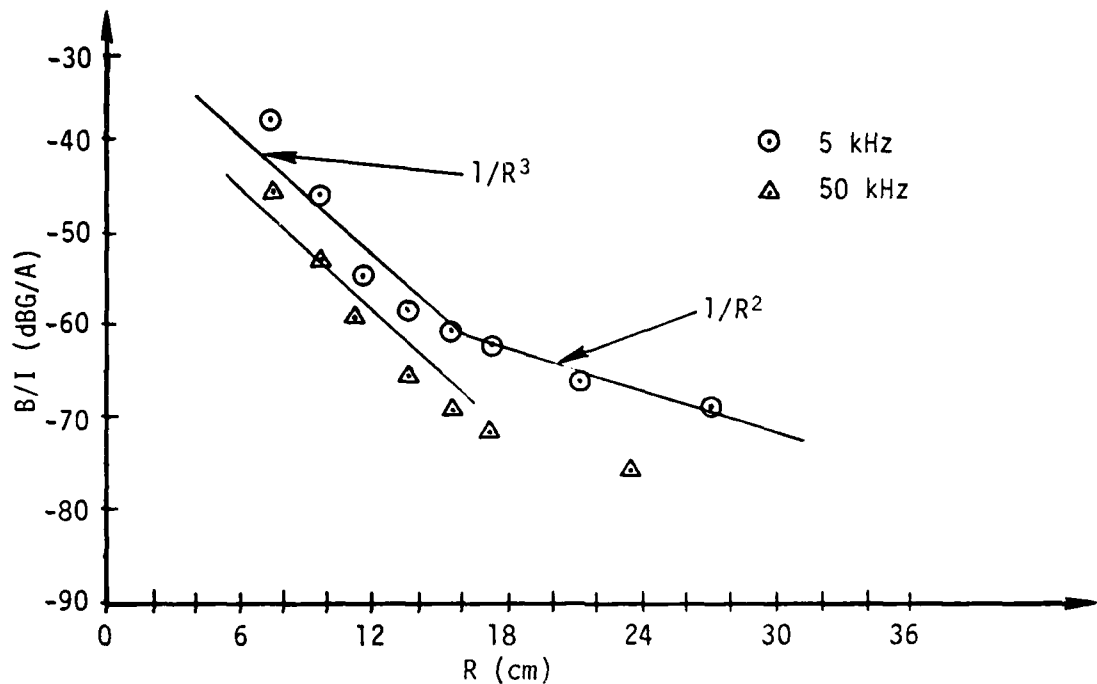


Figure 52a. The Leakage Flux Density at the Top Surface of a 200 W Deltec DT25T5 Transformer. B/I is in Units of Decibels Relative to 1 Gauss Normalized to 1 A of Primary Current. B/I is Shown as a Function of the Probe Spacing Measured From the Center of the Transformer, R, at Frequencies of 5 and 50 kHz.

Frequency (kHz)	B/I (dBG/A)							
	7.8	9.8	11.8	13.8	15.8	17.8	21.8	27.8
15	-38.6	-45.6	-55.6	-60.6	-65.6	-67.6	-71.6	-74.6
25	-40.6	-47.7	-56.3	-61.5	-66.1	-70.3	-75.4	-78.1
35	-41	-48	-57	-62	-67	-70	-75	

Figure 52b. B/I Versus Probe Spacing, R, at Frequencies Between the Limits of 5 and 50 kHz Shown Above.

Figure 52. Normalized Flux Density at the Top Surface of a 200 W Transformer Versus Spacing

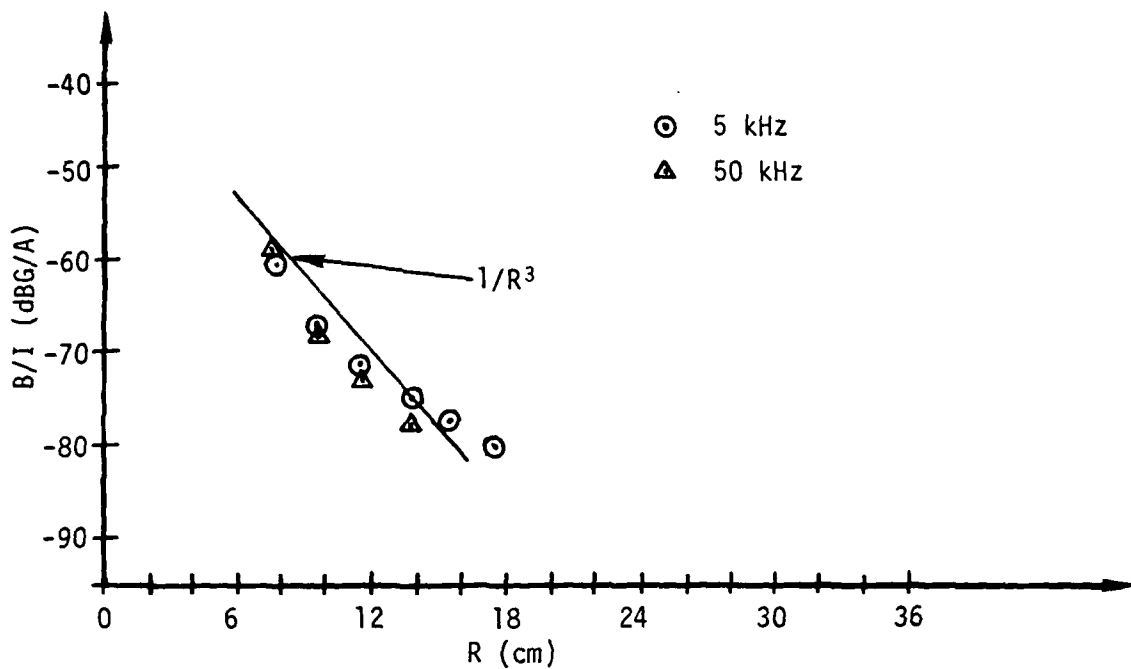


Figure 53a. The Leakage Flux Density at a Side Surface of a 200 W Deltec DT25T5 Transformer.  $B/I$  is in Units of Decibels Relative to 1 Gauss Normalized to 1 A of Primary Current.  $B/I$  is Shown as a Function of the Probe Spacing Measured From the Center of the Transformer,  $R$ , at Frequencies of 5 and 50 kHz.

Frequency (kHz)	$B/I$ (dBG/A)					
	7.8	9.8	11.8	13.8	15.8	17.8
15	-57.6	-65.6	-71.6	-75.6	-81.1	-83.6
25	-57.4	-65.5	-71.9	-76.7	-83.4	-86.5
35	-56.5	-65	-71	-76	-83	-86

Figure 53b.  $B/I$  Versus Probe Spacing,  $R$ , at Frequencies Between the Limits of 5 and 50 kHz Shown Above.

Figure 53. Normalized Flux Density at the Side of a 200 W Transformer Versus Spacing

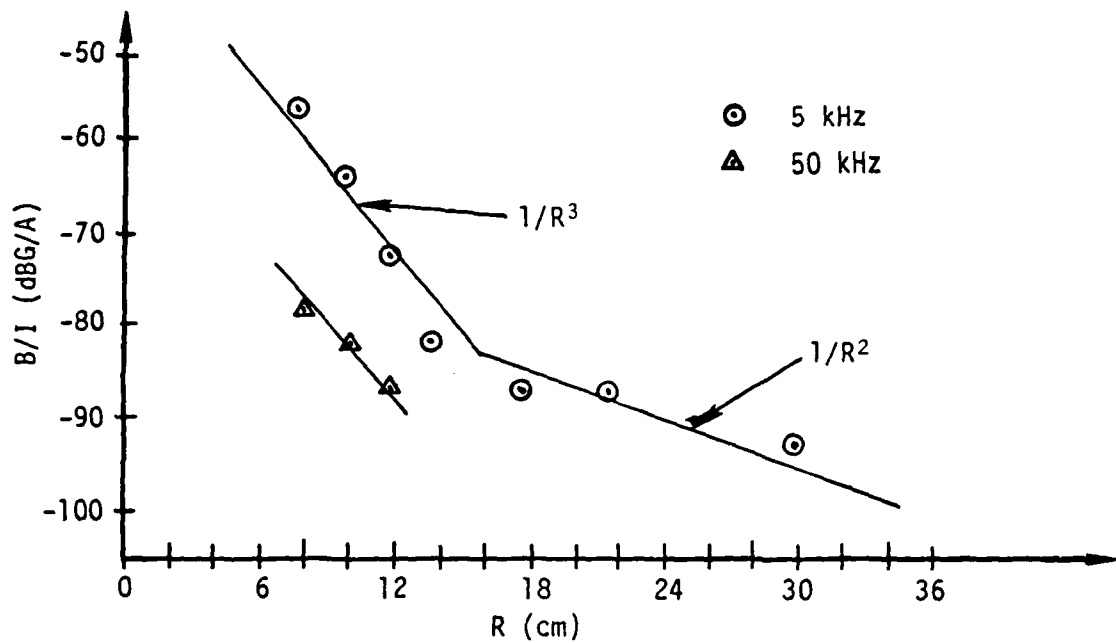


Figure 54a. The Leakage Flux Density at the Primary Endcap of a 200 W Deltec DT25T5 Transformer. B/I is in Units of Decibels Relative to 1 Gauss Normalized to 1 A of Primary Current. B/I is Shown as a Function of the Probe Spacing Measured From the Center of the Transformer, R, at Frequencies of 5 and 50 kHz.

Frequency (kHz)	B/I (dBG/A)						
	7.8	9.8	11.8	13.8	17.8	21.8	29.8
15	-66.6	-72.1	-78.6	-85.6	-90.6	-91.6	-93.6
25	-72.6	-76.5	-80.5	-87.3	-90.7	-92.5	-94.6
35	-74	-77.5	-82	-87	-91	-90.5	-93

Figure 54b. B/I Versus the Probe Spacing, R, at Frequencies Between the Limits of 5 and 50 kHz Shown Above.

Figure 54. Normalized Flux Density at the Primary Endcap of a 200 W Transformer Versus Spacing

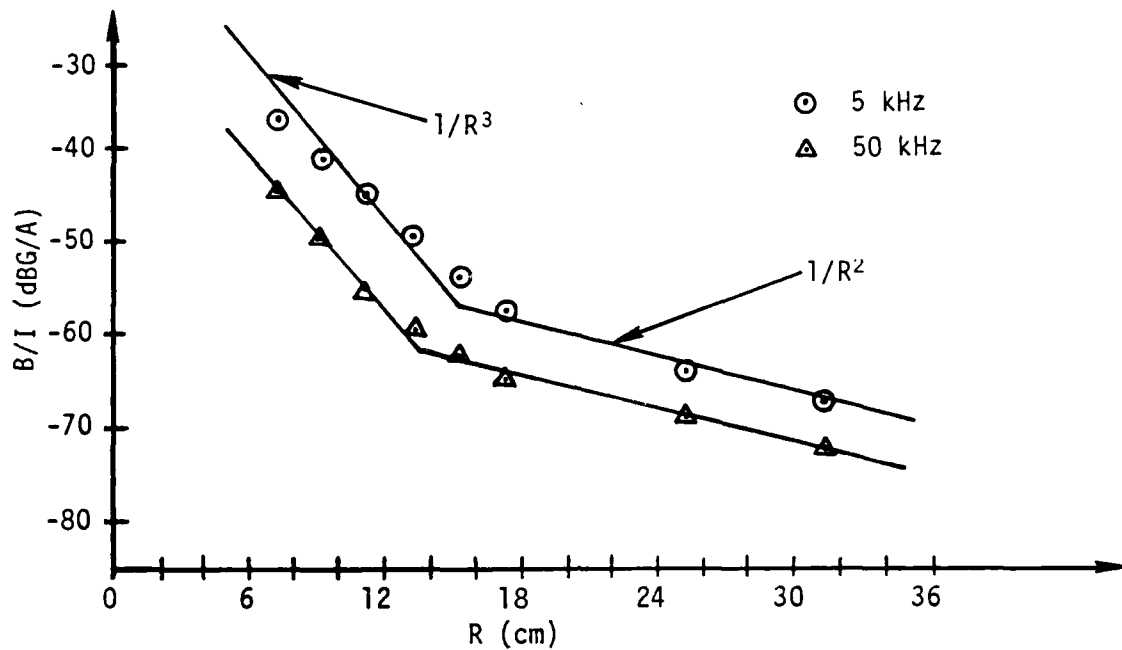


Figure 55a. The Leakage Flux Density at the Top Surface Seam of a 3 kVA GE 9T51Y13 Transformer.  $B/I$  is in Units of Decibels Relative to 1 Gauss Normalized to 1 A of Primary Current.  $B/I$  is Shown as a Function of the Probe Spacing Measured From the Center of the Transformer,  $R$ , at Frequencies of 5 and 50 kHz.

Frequency (kHz)	$B/I$ (dBG/A)							
	$R$ (cm)							
	7.3	9.3	11.3	13.3	15.3	17.3	21.3	25.3
15	-38.6	-43.6	-47.6	-53.1	-57.6	-59.1	-65.6	-70.6
25	-39	-47.5	-50.6	-53.9	-57.8	-61.6	-69.4	-73.5
35	-42.1	-48.1	-52.1	-56.1	-60.1	-62.6	-69.6	-73.6

Figure 55b.  $B/I$  Versus Probe Spacing,  $R$ , at Frequencies Between the Limits of 5 and 50 kHz Shown Above.

Figure 55. Normalized Flux Density at the Top Surface Seam of a 3 kVA Transformer Versus Spacing

AD-A103 824      NAVAL UNDERWATER SYSTEMS CENTER NEWPORT RI      F/G 20/14  
SHIPBOARD POWERLINE TRANSFORMERS: H EMISSION CHARACTERISTICS, E--ETC(U)  
JAN 81 L J DALSASS  
UNCLASSIFIED      NUSC-TM-801173

NL

2 OF 2  
AD 4  
107824

END  
DATE  
FILED  
10-8-1  
DTIC

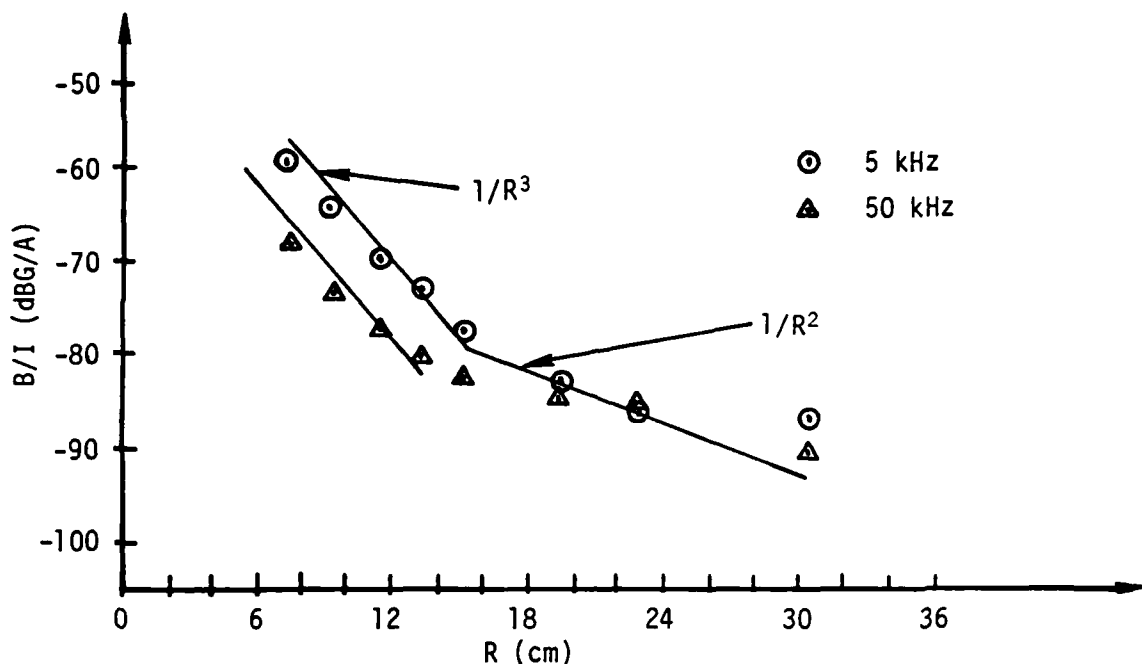


Figure 56a. The Leakage Flux Density at the Endcap Opposite the I/O Endcap of a 3 kVA GE 9T51Y13 Transformer. B/I is in Units of Decibels Relative to 1 Gauss Normalized to 1 A of Primary Current. B/I is Shown as a Function of the Probe Spacing Measured From the Center of the Transformer, R, at Frequencies of 5 and 50 kHz.

Frequency (kHz)	B/I (dBG/A)							
	R (cm)							
	7.3	9.3	11.3	13.3	15.3	19.3	23.3	31.3
15	-64.2	-68.2	-72.7	-76.2	-80.2	-83.2	-87.2	-93.2
25	-64.3	-68.9	-72.0	-77.1	-80.6	-83.2	-86.2	-92
35	-68.1	-72.1	-76.1	-79.6	-83.1	-85.6	-88.1	-92.6

Figure 56b. B/I Versus Probe Spacing, R, at Frequencies Between the Limits of 5 and 50 kHz Shown Above.

Figure 56. Normalized Flux Density at the Endcap Opposite the I/O Endcap of the 3 kVA Transformer Versus Spacing

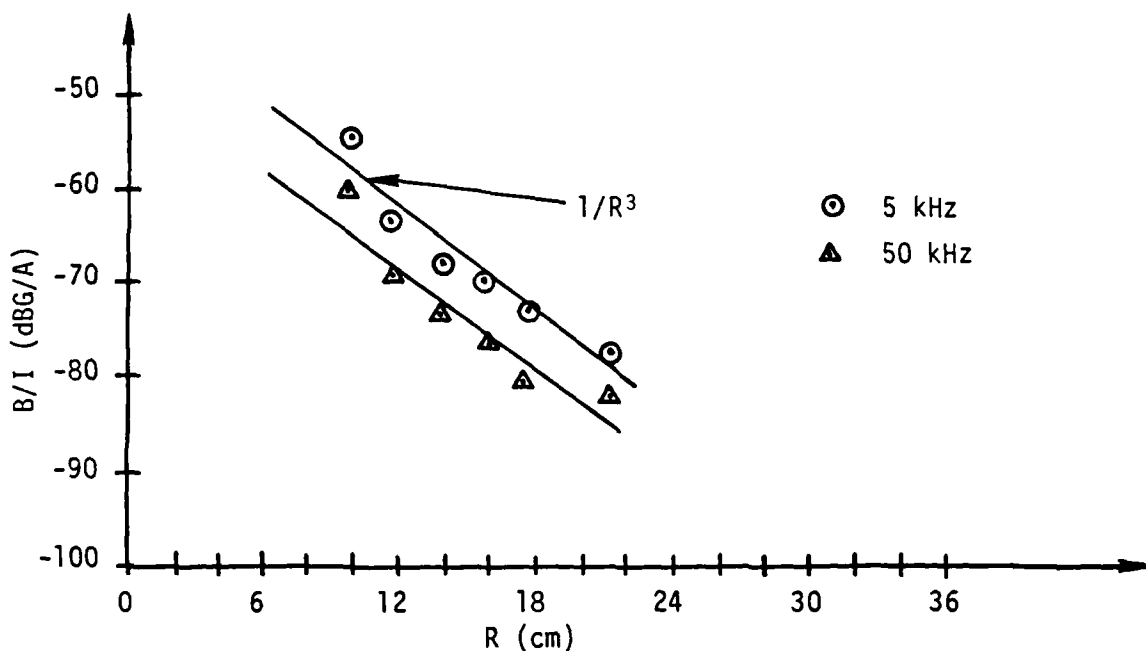


Figure 57a. The Leakage Flux Density at the Side Surface of a 5 kVA Jefferson Electric 12438 Transformer.  $B/I$  is in Units of Decibels Relative to 1 Gauss Normalized to 1 A of Primary Current.  $B/I$  is Shown as a Function of the Probe Spacing Measured From the Center of the Transformer,  $R$ , at Frequencies of 5 and 50 kHz.

Frequency (kHz)	$B/I$ (dBG/A)					
	9.6	11.6	13.6	15.6	17.6	21.6
15	-57.6	-64.6	-69.6	-73.6	-77.6	-80.6
25	-56.9	-63.9	-69.7	-72.8	-77.9	-79.6
35	-58.3	-65.4	-70.6	-74.6	-78.6	-80.6

Figure 57b.  $B/I$  Versus Probe Spacing,  $R$ , at Frequencies Between the Limits of 5 and 50 kHz Shown Above.

Figure 57. Normalized Flux Density at the Side of the 5 kVA Transformer Versus Spacing

REFERENCES

1. A. E. Fitzgerald and C. Kingsley, Electrical Machinery, McGraw-Hill Book Company, Inc., NY, 1952, p. 650.
2. K. Henney, Radio Engineering Handbook, McGraw-Hill Book Company, Inc., NY, 1959, pp. 17-49.
3. "The Effect of Nickel Content on Magnetic and Expansion Properties of High Nickel-Iron Alloys," Technical Note, Carpenter Technology Corporation.
4. "Magnetic Laminations," Catalog ML-303S, Magnetics, Inc.
5. F. E. Terman, Radio Engineers Handbook, McGraw-Hill Book Company, Inc., NY, pp. 99-101.
6. "Fast Fourier Transforms and its Application to Digital Filtering and Spectral Analysis," IEEE Transactions on Audio and Electroacoustics, vol. AU-15, no. 2, June 1967.
7. "Instruction Manual for the Model 446 FFT Spectrum Analyzer," Nicolet Scientific Co.
8. "Systems Electromagnetic Compatibility Evaluation," Report 74-03, University of Pennsylvania, 31 August 1973, p. 30.
9. S. Shenfeld, Prediction of Coupling, Shielding, and Grounds for Low-Frequency Fields, "NUSC Technical Report 4051, Naval Underwater Systems Center, New London, CT, 2 April 1971.

LEAKAGE REACTANCE TRANSFORMER TESTS

1. REVIEW TRANSFORMER LEAKAGE REACTANCE SPECIFICATION STANDARDS;  
LEAKAGE REACTANCE TEST PROCEDURES (IEEE, COMMERCIAL, MILITARY)
2. CONDUCT LEAKAGE REACTANCE SCREEN ROOM TESTS ON 50W TO 5 KVA XFMRS
3. CORRELATE MEASUREMENTS IN (2) WITH RADIATED EMISSION MODELS
4. TEST XFMRS OF GIVEN POWER RATING IN THE 5 TO 15% IMPEDANCE RANGE MAY  
REQUIRE PURCHASE IF NOT LOCALLY AVAILABLE.
5. ATTEMPT TO CONSTRUCT RADIATED EMISSION MODELS WHICH ACCOUNT FOR LEAKAGE  
REACTANCE VARIATIONS FROM:
  - a. NAME PLATE INFORMATION IF AVAILABLE (POSSIBLE WITH LARGE DISTRIBUTION  
TYPE XFMRS)
  - b. CLASS SPECIFICATIONS

Enclosure (3) to NUSC Ltr. Ser. 1343-197

- TRANSFORMER EMI MODEL TASK: REMAINING WORK
- O EXAMINE DISTANCE MODELS FOR 50W to 5 KVA TRANSFORMERS WITH RESPECT TO:
- a. AXIS TRANSLATION CORRECTION METHOD (to locate dipole center)
  - b. SOLENOID METHOD ( $\vec{H}$ -vs -distance)
- O COMMENCE WORK TO DEFINE THE EFFECTS ON MODELS OF:
- a. LEAKAGE REACTANCE VARIATIONS AMONG TRANSFORMER CLASSES:
    - i.e., ISOLATION, DISTRIBUTION STEP UP/STEP DOWN
  - b. CORE DESIGN (SHELL/CORE)
  - c. LOADING
  - d. SATURATION
  - e. SHIELDING (MODERATE/HEAVY)
  - f. FREQUENCY RANGE: 60 Hz/400 Hz to 1 kHz
  - g. TRANSITION FROM LOW FREQ. TO 5 kHz

Enclosure (2) to NUSC Ltr. Ser. 1343-197

